12-2007

Optimal Sizing and Location of Static and Dynamic Reactive Power Compensation

Wenjuan Zhang
University of Tennessee - Knoxville

To the Graduate Council:

I am submitting herewith a dissertation written by Wenjuan Zhang entitled "Optimal Sizing and Location of Static and Dynamic Reactive Power Compensation." I have examined the final electronic copy of this dissertation for form and content and recommend that it be accepted in partial fulfillment of the requirements for the degree of Doctor of Philosophy, with a major in Electrical Engineering.

Leon M. Tolbert, Major Professor

We have read this dissertation and recommend its acceptance:

Fangxing Li, Jack S. Lawler, Suzanne M. Lenhart

Accepted for the Council:

Carolyn R. Hodges

Vice Provost and Dean of the Graduate School

(Original signatures are on file with official student records.)

To the Graduate Council:

I am submitting herewith a dissertation written by Wenjuan Zhang entitled "Optimal Sizing and Location of Static and Dynamic Reactive Power Compensation." I have examined the final electronic copy of this dissertation for form and content and recommend that it be accepted in partial fulfillment of the requirements for the degree of Doctor of Philosophy, with a major in Electrical Engineering.

Leon M. Tolbert
Major Professor

We have read this dissertation
and recommend its acceptance:

Fangxing Li

Jack S. Lawler

Suzanne M. Lenhart

Accepted for the Council:

Carolyn Hodges

Vice Provost and Dean
of the Graduate School

(Original signatures are on file with official student records.)

OPTIMAL SIZING AND LOCATION OF STATIC AND DYNAMIC REACTIVE POWER COMPENSATION

A Dissertation
Presented for the
Doctor of Philosophy Degree
The University of Tennessee, Knoxville

Wenjuan Zhang
December 2007

ACKNOWLEDGEMENTS

There are many people who deserve my sincerest thanks for supporting me to finish this dissertation. I sincerely thank my advisor, Dr. Leon M. Tolbert and my co-advisor, Dr. Fangxing Li for their continuous academic advice, financial support, and understanding in the past years. What I learned from their guidance is not only on research and academic progress. I don't know how I can ever repay them.

I have been fortunate to have had an excellent thesis committee. I sincerely thank Dr. Jack S. Lawler and Dr. Suzanne M. Lenhart for their support and comments on my research. In addition, I would also like to thank John D. Kueck for giving me an opportunity to work on an Oak Ridge National Laboratory (ORNL) project.

I also appreciate the collaboration from my colleagues in the Power Engineering Laboratory at the University of Tennessee including Huijuan Li, Rui Bo, Surin Khomfoi, Faisal Kahn, Yan Xu, Zhong Du, Kaiyu Wang, Mengwei Li, Weston Johnson, Jeremy Campbell, and Ben Sooter for helping me with school related works and for making me familiar with American culture.

This work is supported in part by the National Science Foundation under Contract NSF ECS-0093884 and Oak Ridge National Laboratory under Contract 4000041689.

Finally, I would like to thank my parents and all other family members for giving me tremendous support and understanding. It is their love that makes me more confident and makes my life more meaningful.

ABSTRACT

The key of reactive power planning (RPP), or Var planning, is the optimal allocation of reactive power sources considering location and size. Traditionally, the locations for placing new Var sources were either simply estimated or directly assumed. Recent research works have presented some rigorous optimization-based methods in RPP. Different constraints are the key of various optimization models, identified as Optimal Power Flow (OPF) model, Security Constrained OPF (SCOPF) model, and Voltage Stability Constrained OPF model (VSCOPF).

First, this work investigates the economic benefits from local reactive power compensation including reduced losses, shifting reactive power flow to real power flow, and increased transfer capability. Then, the benefits in the three categories are applied to Var planning considering different locations and amounts of Var compensation in an enumeration method, but many OPF runs are needed.

Then, the voltage stability constrained OPF (VSCOPF) model with two sets of variables is used to achieve an efficient model. The two sets of variables correspond to the "normal operating point (o)" and "collapse point (*)" respectively. Finally, an interpolation approximation method is adopted to simplify the previous VSCOPF model by approximating the TTC function, therefore, eliminating the set of variables and constraints related to the "collapse point". In addition, interpolation method is compared with the least square method in the literature to show its advantages. It is also interesting to observe that the test results from a seven-bus system show that it is not always economically efficient if Var compensation increases continuously.

TABLE OF CONTENTS

LIST OF FIGURES

LIST OF TABLES

1 . INTRODUCTION

1.1 Deregulation leading to problems

When the creation, movement, and utilization of electrical power are discussed, they can be separated into three areas, which traditionally determined the way in which electric utility companies had been organized.

- Generation
- Transmission
- Distribution

With the ongoing deregulation of the electric utility industry in many countries, generation, transmission, and distribution are not provided by one company any more. Instead, generation functions have been separated from the transmission and distribution service in a deregulated market as mandated by the Federal Energy Regulatory Commission (FERC) under Order Number 889 [2].

Deregulation requires an open-access power delivery system, which enables power delivery within and between regions and facilitates access to interconnected competitive generations. Meanwhile, deregulation leads to little or no market-based incentives for transmission investment. At the same time, open transmission access has resulted in increased electric power transfers and the system operates closer and closer to its voltage stability limits. However, the existing system is not originally designed for open-access power delivery. System capacity has not kept pace with supply and demand. The permitting, siting, and construction of new transmission lines are difficult, expensive, time-consuming, and controversial in the long run.

Recent FERC study identified 16 major transmission bottlenecks in the U.S. for 2004 summer flow conditions [3]. These bottlenecks cost consumers over $1 billion in the past 2 summers, and it is estimated that $12.6 billion is needed to fix the identified bottlenecks.

Congestion and voltage instability problems are getting worse largely because the grid is continuously loaded more heavily. Reactive power compensation at key locations in the system is a viable solution to ease the problems, because it may increase the maximum transfer capability constrained by voltage stability. This is shown in Figure 1.1. This proposal will focus on finding the key locations with the consideration of both economic and technical benefits.

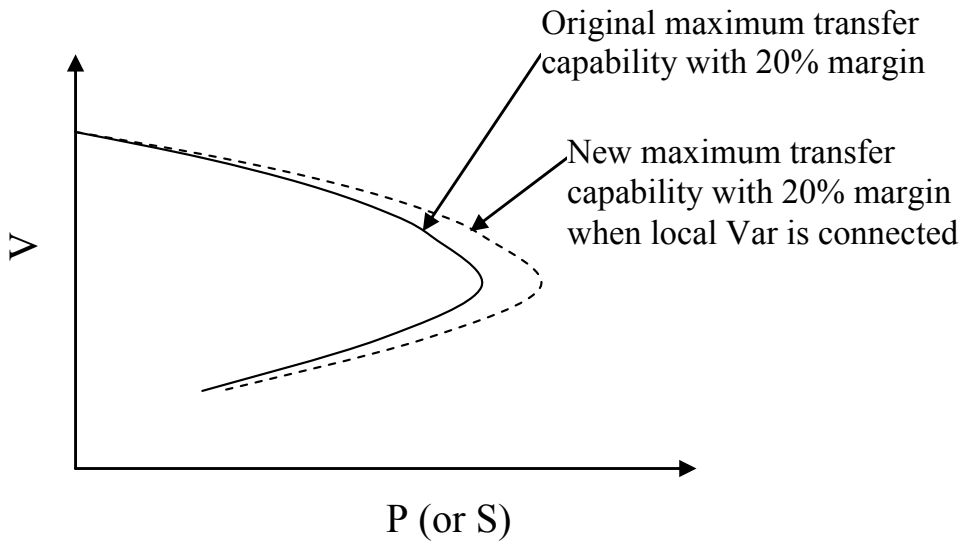

Figure 1.1. The original and new transfer capability considering a certain security margin.

1.2 Blackout reasons

Reactive power shortage and inadequate reactive power management are at the heart of the reliability problems of the electric power transmission, including unplanned and planned rolling power blackouts. Chebbo *et al.* [4] noted that the cause of the 1977 New York blackout was proved to have been a reactive power problem, and the 1987 Tokyo blackout was believed to be a consequence of a reactive power shortage and a voltage collapse during a summer peak load.

Reactive power is critical to affect voltage in electric power systems because deficiencies of reactive power cause voltages to fall, while excesses cause voltages to rise as shown in Figure 1.2 (a 7-bus case). Voltages that are too high or too low can result in increased power system losses, overheating of motors and other equipment, and system voltage collapse with consequent loss of customer load. Indeed, today the voltage/reactive problem is the single most frequent bulk system event causing customer outages.

However, the reactive power in US power systems was not very well planned and managed, as evidenced by the Great 2003 Blackout that occurred in northeastern US and Canada in August 2003. The official final report of the Blackout indicated that "deficiencies in corporate policies, lack of adherence to industry policies, and inadequate management of reactive power and voltage caused the blackout [5]."

Reactive power including its planning process has received tremendous interest and re-examination after the Blackout involving power utilities, independent system operators (ISOs), researchers, and the government. For example, various reactive power planning

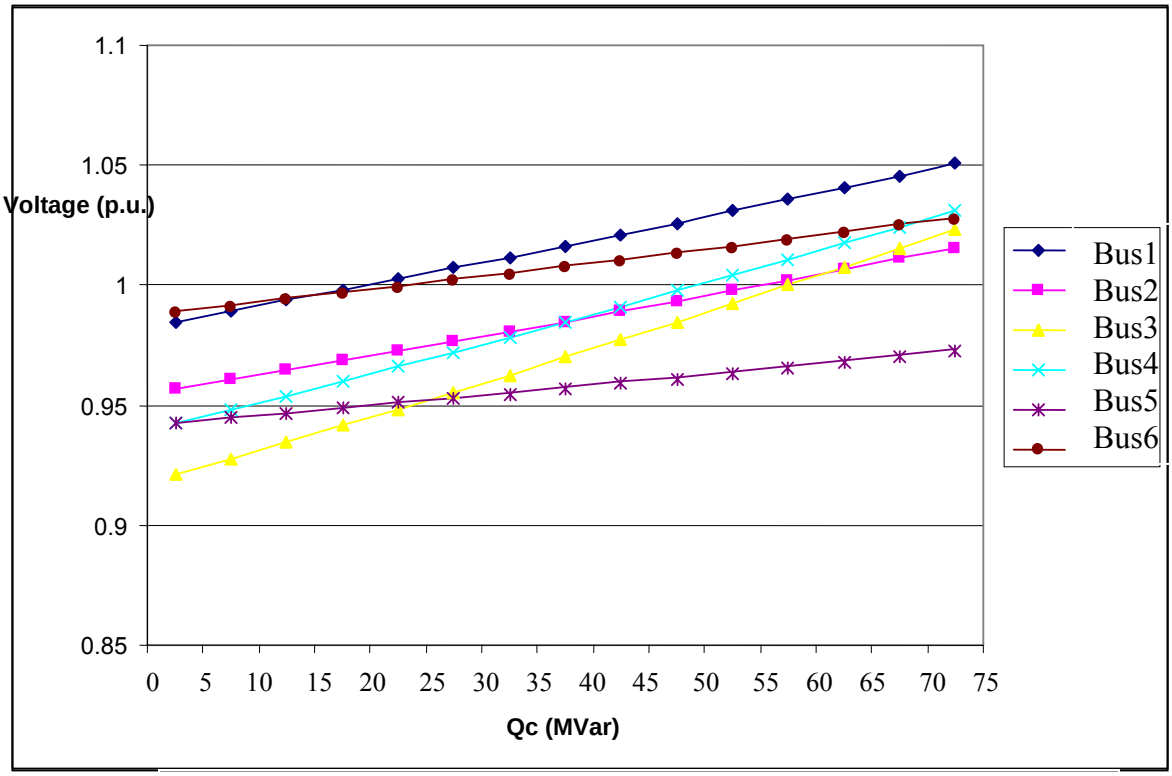

Figure 1.2. Reactive power compensation and all bus voltage relationship.

groups have been formed in ISOs. Also, the U.S. Department of Energy has funded a project at Oak Ridge National Laboratory to study Distributed Energy Resources for Reactive Power Compensation [6].

Consequently, an interesting question has been raised frequently by utility planners and manufacturers: where is the right location and what is the right amount of reactive power compensators that we should install considering technical and economic needs? In order to answer the above questions, it should be stated that optimal allocation of static and dynamic Var sources belongs to the Reactive Power Planning (RPP) or Var planning category. RPP deals with the decision on new Var source location and size to cover normal, as well as, contingency conditions. The planning process aims at providing the

system with efficient Var compensation to enable the system to be operated under a correct balance between security and economic concerns.

1.3 Why reactive power can not be shipped from far away?

ion line I^2X losses due to reactive power flow

When the reactive power is moved over a certain distance, reactive loss on the transmission line I^2X becomes a corresponding burden on the sending end as shown in Figure 1.3 (a). With an increase of the active power flow through a line, the line reactive power loss I^2X increases because the line current I becomes larger as shown in Figure 1.3 (b). In addition, I^2X increases with the square of the current flowing in the line as shown in the two circles of Figure 1.3 (c).

This is why the inadequate reactive power supply at the sending end may limit the active power transfer capability. Delivering reactive power to customers adds more current to the line as shown in Figure 1.3 (b) and also increases reactive losses. As a result, reactive power is preferred to be provided locally, which also induces the location question.

al I^2X at higher loading

The more heavily the line is loaded, the more reactive power is needed. Increasing the active power load pushes up the I^2X curve where even a small increase in current leads to great increase in the reactive losses as is compared in Figure 5 (c). For example, when a system is stressed, delivering 100 MVar to the receiving end may need 250 MVar at the sending end to accomplish that. That is partly the reason that one can not ship reactive power.

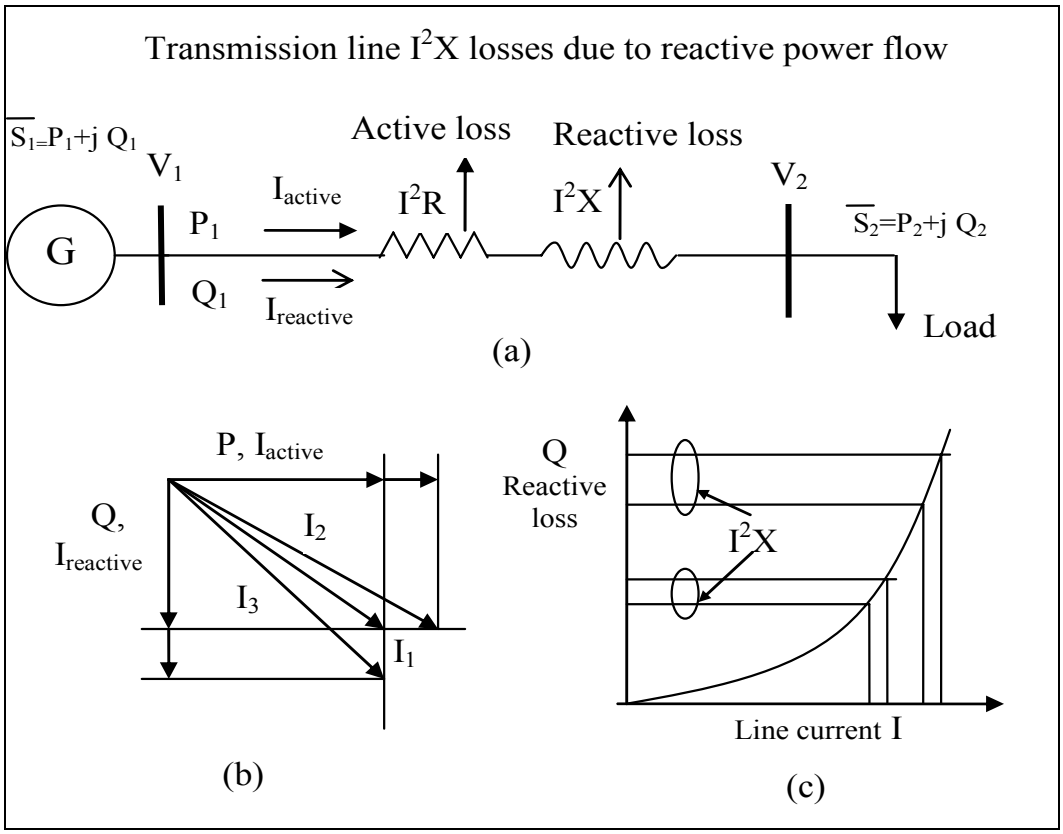

Figure 1.3. Transmission line I2X losses due to reactive power flow.

low voltage

When voltage drops, usually the generator active power output remains constant because generator governors make adjustments. Since the active power is the product of voltage and active current such as P=VI=1.0, any voltage drop results in an increase in active current to keep the constant power such as P=0.9x1.11=1.0. For a 10% drop in voltage, current increases 11%, so I^2X increases 23.4% because of 1.11^2=1.234. As a result, when the system runs close to its voltage stability limit, shipping reactive power will be quite inefficient.

1.4 Flexible AC Transmission Systems (FACTS)

The deregulation has pushed the industry to promote advanced technologies for the transmission congestion because of shortage of transmission line capacity. Besides the impact from the Blackout, the continuous technical advances in power electronics, such as Static Var Compensators (SVC), Static Synchronous Compensators (STATCOM), D-VAR, SuperVAR, etc, make the application of large amount of VAR compensation more efficient, affordable, and attractive.

Power electronics based equipment, or FACTS, provide proven technical solutions to voltage stability problems. Especially, due to the increasing need for fast response for power quality and voltage stability, the shunt dynamic Var compensators such as SVC and STATCOM have become feasible alternatives to a fixed reactive source.

More than 50 SVCs have been installed in the United States, ranging from 30 MVar to 650 MVar each [7]. STATCOMs are installed at several sites in the United States, ranging between 30 MVar and 100 MVar each [8]-[11], as shown in Table 1.1. However,

Table 1.1. STATCOM installations sample (in the U.S.)

Number	Year	Customer	Location	Voltage	Control range	Supplier
1	1995	Tennessee Valley Authority (TVA)	Sullivan Substation (Johnson City, Tennessee)	161kV	±100MVar	Westinghouse Electric Corporation
2	2000	(AEP)	Eagle Pass Station (Texas)	138 kV	±36 MVar	ABB
3	2001	Vermont Electric Power	Essex station (Burlington, Vermonnt)	115kV	-41 to +133MVar	Mitsubishi
4	-	Central & South West Services (CSWS)	Laredo and Brownsville stations (Texas)	-	±150MVar	W-Siemens
5	2003	San Diego Gas & Electric (SDG&E)	Talega station (Southern California)	138 kV	±100MVar	Mitsubishi
6	2003	Northeast Utilities (NU)	Glenbrook station (Hartford, Connecticut)	115 kV	±150MVar	Areva (Alstom)
7	2004	Austin Energy	Holly (Texas)	138 kV	–80 to +110 MVar	ABB

there are new questions raised from the shunt FACTS device application. Can the models, methods, and tools used for static Var planning be applied in dynamic Var planning? The answers to these questions are needed for the utilities to make better utilization of these new Var sources with power electronic.

1.5 Optimal Power Flow (OPF) and Security Constrained OPF

ower Flow (OPF)

Basically, Var planning is an optimization problem, which is called Optimal Power Flow (OPF) in a power system. There are six variables for each bus: generator active and reactive power output, active and reactive load, and bus voltage magnitude and angle. At the same time, there are two equations related to each bus, active power balance and reactive power balance equations. In the "conventional" power flow, four of the six variables are known or specified, the other two are unknown. For a system with n buses, power flow solves the $2n$ unknowns from the $2n$ equations. Using some suitable mathematical algorithm, a feasible solution can be obtained.

However, conventional power flow algorithms do not automatically minimize any objective functions such as fuel cost or real power transmission losses. They only obtain a single feasible solution. Hence, the need for an OPF arose in the early 1960's to achieve a desired objective, rather than just a feasible solution. Some controllable power system elements of the $4n$ known variables in power flow are relaxed into a bounded range; as a result, an infinite number of feasible solutions are obtained by solving the $2n$ equations for more than $2n$ unknown variables.

All these feasible solutions construct a feasible region. An optimal solution can be selected from the feasible region to obtain a desired objective by adjusting the optimal setting for the controllable variables with respect to various constraints. The OPF is a static constrained nonlinear optimization problem, whose development has closely followed advances in numerical optimization techniques and computer technology.

OPF is formulated mathematically as a general constrained optimization problem as:

$$\text{Minimize} \qquad f(u,x) \tag{1.1}$$

$$\text{Subject to} \qquad g(u,x) = 0 \tag{1.2}$$

$$\text{and} \qquad h(u,x) \geq 0 \tag{1.3}$$

where u is the set of controllable variables in the system, and x is the set of dependent variables called state variables. Objective function (1.1) is scalar. Equalities (1.2) are the conventional power flow equations, and occasionally include a few special equality constraints. Inequalities (1.3) represent the physical limits on the control variables u, and the operating limits on the power system.

The control variables u may be defined as follows:

- Generator active power output
- Regulated bus voltage magnitude
- Variable transformer tap setting
- Phase shifters
- Switched shunt reactive devices
- Load to shed in special conditions

The state variables x may be defined as follows:

- Voltage magnitudes at load buses
- Voltage phase angle at every bus
- Line flows

onstrained OPF (SCOPF)

A conventional Optimal Power Flow program minimizes an objective function such as production costs or losses, while maintaining the nonlinear power flow balance and the system variables, such as voltages, tap ratios, active and reactive generations, and line flows within the specified limits. However, the optimal solution is only valid for the particular system conditions and constraints presented to the OPF.

If some "credible" contingency cases (single or multiple equipment outages) occurred, that would create steady-state emergencies. Usually contingency analysis is performed in order to respond to each insecure contingency case. People had hoped to integrate the contingency/ security constraints into OPF formulation, then SCOPF debuts in the history as an important step forward in OPF technology [12][13].

The SCOPF program extends the OPF problem solving capacity to include the effect of a limited number of potential contingencies, such as outages of transmission branches, generation units, or system buses. The contingencies contribute additional constraints to the base case OPF problem in that: 1) The nonlinear power flow equations must be observed, and 2) All control variables must be within prescribed emergency limits. The SCOPF program minimizes the base case/ pre-contingency objective function while observing both the pre- and post-contingency constraints. In other words, SCOPF determines an optimal operating point, such that in the event of any contingency of a

given list, the post-contingency states will remain secure (within operating limits).

SCOPF formulation is as follows: the engine of SCOPF is the basic OPF problem. The original OPF formulation in (1.1) (1.2) (1.3) can be expanded to include contingency constraints, thus

$$\text{Minimize} \qquad f(u^0, x^0) \tag{1.4}$$

$$\text{Subject to} \qquad g^k(u^k, x^k) = 0, \ \text{for } k = 0,1,\cdots, N_c \tag{1.5}$$

$$\text{and} \qquad h^k(u^k, x^k) \geq 0, \ \text{for } k = 0,1,\cdots, N_c \tag{1.6}$$

where superscript "0" represents the pre-contingency (base-case) state being optimized, and superscript "k" (k>0) represents the post-contingency states for the N_c contingency cases.

Note that the solution of the SCOPF includes both the pre- and post-contingency power flow states, and that all constraints during those states are satisfied. As far as the power flow equations are concerned, the SCOPF models two constraints for each system bus: the active and reactive power equations.

Thus, for a 1000-bus system, there are 2000 nonlinear constraints for each system condition. The post-contingency constraints are of the same dimensional order as those of the pre-contingency case. If there are m total constraints in a given base case optimal power flow, there will be (k+l)•m constraints in a security constrained OPF problem with k contingencies. As a result, a 1000-bus system with nine contingencies would be equivalent to solving a 10,000-bus optimal power flow. It is obvious that the complexity of SCOPF increases greatly compared with the OPF problem.

1.6 Organization of the dissertation

This dissertation consists of nine chapters. In Chapter II, a literature survey is made on static reactive power planning. In Chapter III, a literature survey is made on dynamic reactive power planning. In Chapter IV, a generalized assessment of the economic benefits from reactive power compensation is proposed. In Chapter V, the sensitivity analysis of the economic benefit of reactive power compensation is presented and modeled. In Chapter VI, an enumerative method based on Var economic benefits is proposed to incorporate voltage stability margin in the reactive power planning. In Chapter VII, the voltage stability constrained OPF with two sets of variables is implemented with a new objective. In Chapter VIII, the voltage stability constrained OPF with two sets of variables is simplified using approximation method such as interpolation, least square. In Chapter IX, STATCOM model is incorporated into the simplified voltage stability constrained OPF model.

2 . A LITERATURE REVIEW OF STATIC VAR PLANNING: MODELS AND ALGORITHMS

Reactive power or Var is critical to support voltage and regulate power factor in electric power systems. Consequently, there is a growing interest in the optimal location and size of reactive power compensators. This is also popularly known as reactive power planning (RPP) or Var planning. Many different models as well as different optimization techniques have been presented by power engineering researchers.

This chapter will first review various Var planning models such as Optimal Power Flow (OPF) model, Security Constrained OPF (SCOPF) model, OPF with Voltage-Stability consideration (OPF-VS), and SCOPF with Voltage-Stability consideration (SCOPF-VS), the current state of the art in Var planning.

The relationship between the four models is shown in Figure 2.1. Then, the literature will be categorized by different solution techniques including Linear Programming (LP), Nonlinear Programming (NLP), Mixed Integer Programming (MIP), Mixed Integer Non-Linear Programming (MINLP), etc. Meanwhile, some tools without optimization technique such as modal and eigenvalue analysis will also be demonstrated to handle the voltage stability in line with the optimal allocation. Finally, the chapter will conclude the discussion with a summary matrix for different objectives, models, and algorithms.

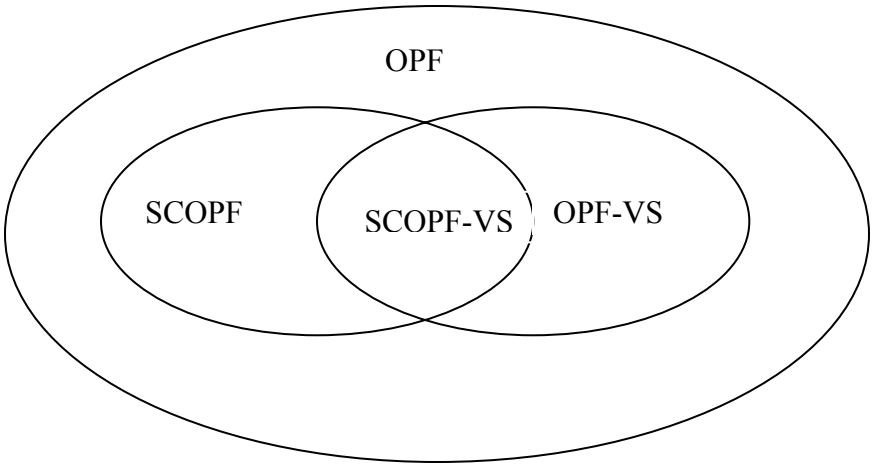

Figure 2.1. RPP models' relationship.

2.1 Present solution technique for RPP

Essentially, RPP is a large-scale nonlinear optimization problem with a large number of variables and uncertain parameters. There are no known ways to solve such Nonlinear Programming Problems (NLP) exactly in a reasonable time. The solution techniques of OPF have evolved over many years, and dozens of approaches have been developed, each with its particular mathematical and computational characteristics [14]. The majority of the techniques discussed in the literature of the last 20 years use at least one of the following 3 categories of methods, which also include some subcategories.

- Conventional methods (Local optimum): A group of methods such as Generalized Reduced Gradient (GRG), Newton's Approach, and Successive Quadratic Programming (SQP) for NLP problem are often trapped by a local optimal solution.
- Heuristic methods (Near-global optimum): In recent years, the intelligent optimization techniques such as Simulated Annealing (SA), Genetic Algorithms

(GA), and Tabu Search (TS) have received widespread attention as possible techniques to find the global optimum for the RPP problem, but these methods need more computing time.

- Sensitivity based methods: index, modal/ eigenvalue analysis

2.2 OPF model

of OPF constraints

The compact format of mathematical formulation of OPF is introduced in section 1.5. The detailed OPF constraints are categorized in this section as follows. Equalities (2.1) are the conventional power flow equations. Inequalities (2.2) represent the physical limits on the control variables u, and (2.3) represent the physical limits on the state variables x.

1) Power flow constraints

- $P_{gi} - P_{li} - P(V,\theta) = 0$ (active power balance equations)
- $Q_{gi} + Q_{ci} - Q_{li} - Q(V,\theta) = 0$ (reactive power balance equations) (2.1)

2) Control variables limits

- $P_{gi}^{\min} \le P_{gi} \le P_{gi}^{\max}$ (active power generation limits)
- $V_{gi}^{\min} \le V_{gi} \le V_{gi}^{\max}$ (PV bus voltage limits)
- $T_l^{\min} \le T_l \le T_l^{\max}$ (transformer tap change limits)
- $Q_{ci}^{\min} \le Q_{ci} \le Q_{ci}^{\max}$ (Var source size limits) (2.2)

3) State variables limits

- $Q_{gi}^{\min} \le Q_{gi} \le Q_{gi}^{\max}$ (reactive power generation limits)

- $V_i^{\min} \le V_i \le V_i^{\max}$ (PQ bus voltage limits)
- $\left|LF_l\right| \le LF_l^{\max}$ (line flow limit) (2.3)

4) Other limits

- Power factor constraints

where Q_{ci} — Var source installed at bus i ; P_{gi} — generator active power output;

P_{Li} — load active power; Q_{gi} — generator reactive power output;

Q_{Li} — load reactive power; LF_l — transmission line flow;

V_i — bus voltage; V_{gi} — PV bus voltage;

T_l — *transformer tap change*; i — *the set of buse;*

l — *the set of lines;*

ion of the OPF model based on the objective functions

The majority of the VAR planning objective was to provide the least cost of new reactive power supplies with feasible voltage magnitudes as constraints. Many variants of this objective from economic and technical benefits point of view were also presented by many researchers. The five objectives are discussed as follows.

1) Minimize Var source cost

Generally, there are two Var source cost models. In the majority of the literature, Var source costs with the format $C_{1i} \cdot Q_{ci}$ are treated as linear functions with no offset, only considering the variable cost relevant to the rating of the newly installed Var source Q_{ci}; the common unit for C_{1i} is \$/MVar·hour. This means the costs of two 200 MVar reactive

power sources are exactly the same as one 400 MVar source. This formulation would always bias a solution toward placement of several smaller sizes sources instead of a small number of larger ones.

A better formulation with the format $(C_{0i} + C_{1i} \cdot Q_{ci}) \cdot x_i$ is to approximate the cost as a fixed charge per source along with an incremental/variable cost per MVar, the unit for C_{0i} is $. This is a much more realistic model of cost, but this would complicate the problem from a NLP to a mixed integer NLP (MINLP), because there will be a binary variable x_i to show installing or not in the cost model. The slight difference in the cost model leads to dramatic difference in the OPF model type and the corresponding mathematics technique to solve it.

As a result, the OPF with the first cost function as an objective is a traditional LP or NLP problem [15]; however, the second one is a Mixed Integer Nonlinear Programming (MINLP) problem [16-18], and some special techniques are needed for it. The recursive mixed integer programming technique is employed in [16] to solve the linearized load flow equations, which constructs a Mixed Integer Linear Programming (MILP).

Successive Linear Programming (SLP) can change the problem into a MILP in the initial phase, thereafter Branch and Bound is used to solve the MILP [17]. In [18], MILP is constructed by successive linearization of the original nonlinear model, and it is solved by applying a hybrid procedure in which the genetic algorithm substitutes branch and bound method when numerical problems occur. The objective function is the overall cost of Var compensation.

2) Minimize weighted sum of Var cost and real power losses

This is the most common objective in the Var planning problems. Based on the Var cost model, this group of OPF is divided into NLP and MINLP models.

1. NLP model objective: min $F = C_1(Q_c) + C_2(P_{loss})$

MINOS, a NLP solver, is used in [19] for optimal capacitor planning. Bender's decomposition is applied in [20] where a Genetic Algorithm (GA) is used to select the location and the rating of the Var source and Successive LP is used to solve operational optimization sub-problems assuming the investment cost to be linear with respect to the amount of newly added Var source. Tabu Search (TS), which is a heuristic optimal technique characterized by avoiding local optimal solutions in high probability, is proposed in [21] for the optimal Var planning problem considering 3 different load operation conditions, called heavy, normal, and light load conditions. SLP in [22] linearizes the NLP problem. Modal analysis is used to site and the successive multiobjective fuzzy LP technique (SMFLP) is used to size the capacitors in [23].

2. MINLP models objective: min $F = (C_0 + C_1Q_c)\cdot x + C_2(P_{loss})$

The reactive power planning problem has been stated as a mixed nonlinear-integer constrained optimization problem – to minimize the fixed as well as variable cost of Var source installation and the cost of the active power transmission losses.

Evolutionary Programming (EP) in [24], an artificial intelligent optimization method based on the mechanics of natural selection, is applied to minimize operation cost by reducing real power loss and the cost of Var source including fixed and variable cost.

Hybrid Evolutionary Programming (HEP) in [25] is proposed to speed up the computation for obtaining an exact global optimum, while keeping the same model in [24].

In the 1990's, combinatorial algorithms were introduced as a means of solving the capacitor placement problem: a hybrid method is based on GA and SLP in [26]. The hybrid partial gradient descent/simulated annealing (HPGDSA) in [27] is an innovative fast global optimization technique, which can reduce the CPU time of SA while retaining the main characteristics of SA.

A hybrid GA and SA algorithm [28] is to start with GA for a fairly good feasible solution instead of starting completely at random, then SA is applied to search from this solution to find the optimal one, the efficiency is expected to increase. Another hybrid algorithm based on Tabu Search (TS) and sensitivity analysis is proposed in [29]; the sensitivity is used to reduce the number of candidate buses, which measures the impact of a change in the reactive injection in a given bus on the active power losses in the system.

3) Minimize weighted sum of Var cost and generator fuel cost:

Rather than the usual real power loss, the fuel cost is adopted as a direct measure of the operation cost, because the minimization of real power loss can not guarantee the minimization of the total fuel cost unless all units have the same efficiency. Instead, minimization of the total fuel cost already includes the cost reduction due to the minimization of real power loss.

This objective consists of the sum of the costs of the individual generating units:

$$C_T = \sum_{i=1}^{n} f_i(P_{gi}) \tag{2.4}$$

where $f_i(P_{gi}) = a_{0i} + a_{1i}P_{gi} + a_{2i}P_{gi}^2$ is the generator cost-versus-MW curves modeled as a quadratic function approximately, and a_{0i}, a_{1i}, a_{2i} are cost coefficients.

In the 1970's, the Generalized Reduced Gradient (GRG) method was used to solve the NLP model with the combined Var cost and fuel cost as the objective $F = C_I(Q_c) + C_T$, by providing a movement direction through reduced gradient and a step length through line search [30]. A modified OPF with the same objective in [30] is solved by MINOS in the 1990's [31]. A MINLP OPF model with objective $F = (C_0 + C_1Q_c)\cdot x + C_T$ is designed in [32]; three different Evolutionary Algorithms (EAs): Evolutionary Programming (EP), Evolutionary Strategy (ES), and Genetic Algorithm (GA) are compared for the same model.

4) Minimum Deviation from a Specified Point

This objective is usually defined as the weighted sum of the deviations of the control variables from their given target values. The target values correspond to the initial or some other specified operating point. Minimizing voltage deviation such as min $F = \sum_i (V_{imax} - V_i)$ is the objective in [33], before Nonlinear Optimization Neural Network approach (NLONN) is used to optimize the Var variables to improve the voltage profiles, Analytic Hierarchical Process (AHP) uses parallel analytical criteria for accommodating the ranks based on different indices such as sensitivity index and stability margin index.

5) Multi-objective (MO)

Several single objectives have been discussed above, even though there are weighted sum of different objectives such as active power losses and Var cost, usually the weights

are easily decided by transferring the objective to $. However, the goal of Var planning problem is to provide the system with efficient Var compensation to enable the system to be operated under a correct balance between security and economic concerns. If both security and cost are all included in the objective function, then the weights can not be decided directly and easily. The objective in [34] includes Var investment cost minimization, power loss reduction, and voltage deviation reduction as equ. (2.5):

$$\text{Min} \qquad F = (C_0 + C_1 Q_c)\cdot x + C_2(P_{loss}) + \text{maximum} \mid V_{imax} - V_i \mid \qquad (2.5)$$

A Two-Layer Simulated Annealing (TLSA) [34] technique has been proposed to efficiently find a desirable, global optimal solution in the MO problem, involving a decision level concerned with the decision strategy and an analysis level which generates efficient solutions to meet the decision maker's (DM) goal. The same objective exists in [35], and the "fuzzy satisfying method" for a MO problem is employed to transform the complicated multi-objective optimization problem into a single-objective optimization problem by virtue of assigning each objective function with a fuzzy goal by the decision maker (DM). Then, hybrid Expert System Simulated Annealing (ESSA) is proposed to improve the computing time of traditional SA for the global optimum.

GA is used in [36] to handle the Multi-objective function as equ. (2.6):

Min F= 10 $\sum$(voltage violation)^2 + 5 $\sum$(generator Var violation)^2 + power losses in p.u. (2.6)

2.3 SCOPF model

Security constrained optimization was introduced in the 1960's and early 1970's. The original formulations ignored the non-linearity of the network power flow equations and

simply used the DC power flow equations for equality constraints. Alsac and Stott [37] in 1974 introduced the security constrained OPF with exact AC power flow equations. More work has been done on the topic since then. With the development of SCOPF scheme, the objective of Var planning is extended to determine a minimum cost allocation plan of new reactive resources in terms of size and location so as to guarantee feasible operation both under normal conditions and after contingencies.

evel and Operation Modes

The SCOPF is aimed at scheduling the power system controls to achieve operation at a desired security level, while optimizing an objective function such as cost of operation. SCOPF usually treats security level 1— "secure" and level 2— "correctively secure", which are in secure state. Level 1 security is the ideal operating requirement but is more expensive than operating with a level 2 security.

A system with security level 1 corresponding to the preventive mode is one where all load is supplied, no operating limits are violated and no limit violations occur in the event of a contingency; in other words, level 1 has the ideal security, the power system survives any of the relevant contingencies without relying on any post-contingency corrective action.

A system with security level 2 corresponding to the corrective mode is one where all load is supplied, no operating limits are violated and any violations caused by a contingency can be corrected by appropriate control action without loss of load, within a specified period of time [38]. Note that the solution of the SCOPF is not assured to be transiently stable.

ion of the SCOPF model based on the objective functions

The classification of SCOPF has been developed for the benefit of the reactive power operation and planning problem. The three objectives are discussed as follows.

1) Minimize Var cost

NLP cost model is built and linearized through SLP process [39]. The new Var sources are required to satisfy voltage constraints for not only normal but also contingent states of operation of the system. The algorithm processes the cases sequentially, instead of optimizing them simultaneously.

2) Minimize weighted sum of Var cost and real power losses

1. NLP model objective: min $F = C_1(Q_c) + C_2(P_{loss})$

The optimum placement of shunt capacitance is studied by running the contingency constrained Optimal Power Flow in preventive mode [40], which minimizes an objective function such as real power losses and new capacitor bank cost.

The real power losses consumed in the base case and all contingency cases are taken into account in [41], so the objective is as equ. (2.7):

$$\min F = C_1(Q_c) + \sum_{K=0}^{N_C} C_2(P_{loss})_k \tag{2.7}$$

where $k = 1, \cdots N_c$ is the k-th operating case, and includes (1) base case ($k = 0$), (2) contingencies under preventive mode ($k = 1, \cdots L$), and (3) contingencies under corrective mode ($k = L, \cdots N_c$). Both preventive mode and corrective mode are considered.

A preventive contingency constrained OPF is explicitly introduced in the Var

planning problem [42], whose objective is to maximize the benefit from the viewpoint of real power losses reduction due to new Var source installation. It can be expressed as equ. (2.8):

$$\max \quad -C_1(Q_c) + C_2(P^0_L - P_{loss}) \quad \text{or} \quad \min \; C_1(Q_c) + C_2(P_{loss} - P^0_L) \tag{2.8}$$

where P^0_L is the minimum value of the losses obtained from the base case without Var compensation situation.

2. MINLP models objective: min $F = (C_0 + C_1 Q_c) \cdot x + C_2(P_{loss})$

The traditional two-level methodology including investment and operation levels is extended to take into consideration the load change in operation sub-problem [43]. The ability to represent multiple load levels is particularly important in reactive planning studies, because the reactive requirements for low and high-load levels may be significantly different.

The preventive mode methodology in [44] can also be extended to accommodate a variable load level situation. Since the objective function is non-differentiable, General Bender Decomposition (GBD) is used to decompose the problem into a continuous problem and an integer problem; thereafter SA is adopted to handle the integer variables.

The corrective control strategy is more economical and is more easily solvable (through decomposition strategies) than the preventive approach [45]. The post-contingency corrective actions are carried out and limited not only by the capacity decisions but also by the deviation from the “base case” operating point. Bender Decomposition Method (BDM) is used to decouple the problem into an investment subproblem and operation subproblem.

3) Multi-objective (MO)

A multi-objective Var planning model is proposed in [46], the objective is designed as a minimize weighted sum of Var cost + real power losses + deviation of voltage + deviation of line flow. The contingency constrained multi-objective optimization problem is transformed into a single objective optimization problem by employing ε constraint method, and SA technique is applied to the single objective optimization problem.

In the ε-Constraint method, one must choose a main objective function, while the other components of the original multi-objective function are treated as constraints, where ε *is* a threshold value chosen by the user for the "secondary" objective function. Choosing a value for ε is usually easier than selecting appropriate values for weights of the multi-objectives, as ε defines a minimum stability margin, which has a more "physical" meaning.

2.4 Static voltage stability analysis (VSA) techniques

Voltage collapse studies, an integral part of VSA of power systems, are of growing importance for the design and operation of power systems. The main function of shunt reactive power compensation is for voltage support to avoid voltage collapse. Then, voltage stability is a very important consideration when the location and size of new Var sources need to be determined during Var planning.

Many analytical methodologies have been proposed and are currently used for the study of this problem, such as P-V and V-Q curve analysis, Continuation Power Flow (CPF), optimization methods, modal analysis, and saddle-node bifurcation analysis.

Static voltage stability analysis is concerned with two main aspects:

- Determination of how far the system is operating from the voltage collapse point using CPF based on bifurcation theory, or OPF considering a given load increase pattern and generator sharing scheme.
- Identification of buses or areas prone to voltage instability problems by using modal analysis.

ion Power Flow (CPF)

The Point of Collapse (PoC) is given by the nose point of P-V or V-Q curve, where the voltage drops rapidly with an increase in load demand as shown in Figure 2.2. PoC is also known as the equilibrium point, where the corresponding Jacobian becomes singular, power flow solution fails to converge beyond this limit, which is indicative of voltage instability, and can be associated with a saddle-node bifurcation point.

Of the different types of bifurcations, saddle-node bifurcations are of particular interest in power systems, because they are one of the primary causes for "static" voltage collapse problems [47]. These instabilities are usually local area voltage problems due to the lack of reactive power, and hence by increasing the static voltage stability margin (SM) defined as the distance between the saddle-node-bifurcation point and the base case operating point as shown in Figure 2.2, one could expect an improvement in the stability of the system for that operating point. Hence, determining the location of this point is of practical importance in power systems.

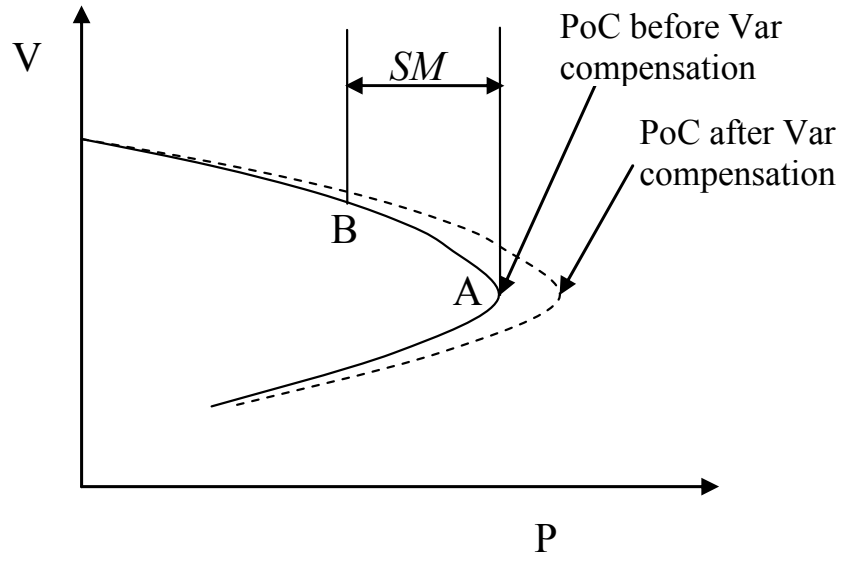

Figure 2.2. P-V curve.

CPF was originally developed to determine bifurcation points of Ordinary Differential Equations (ODE) systems, and have been successfully applied to the computation of collapse points in power systems [48][49][50]. CPF was first developed to overcome the ill-conditioning near the critical point, where the Jacobian matrix of the Newton-Raphson method becomes singular.

ower Flow (OPF)

Most of the numerical tools such as continuation methods used in voltage collapse studies are based on concepts and/or techniques developed from bifurcation analysis of power systems. More recently, however, new optimization-based tools have been developed to study voltage collapse problems in power systems. It is demonstrated in [51] that bifurcation theory, is basically equivalent to some typical optimization methodologies. A voltage collapse point computation problem can be formulated as an

optimization problem, known as Total Transfer Capability (TTC).

It is obvious that there are similarities and strong ties between tools developed for the computation of collapse points from bifurcation theory and those based on optimization techniques. Several computational methods based on bifurcation theory have been shown to be efficient tools for VSA; however, it is difficult to introduce operational limits and computationally expensive to use continuation method, especially for large systems with multiple limits. Using optimization techniques for these types of studies present several advantages, especially due to their limit handling capabilities. Further extension has been made to include the security (contingency) constraints in the OPF model, which is known as SCOPF model.

alysis

Modal or eigenvalue analysis of the system Jacobian (J) matrix of the system load flow equation, near the point of voltage collapse, which is obtained at the point of maximum power transfer capability of the system, can be used to identify buses vulnerable to voltage collapse and locations where injections of reactive power benefit the system most.

The participation of each load in the critical mode (near PoC) determines the importance of the load in the collapse. The use of both left and right eigenvector information of the critical mode (PoC) leads to the notion of participation factors. The participation factors indicate which generators should be motivated to inject more active or reactive power into the system, and where the load shedding would be more effective to increase the stability margin.

2.5 Var planning OPF considering static voltage stability (OPF-VS)

Traditionally in Var planning, the feasible operation has been translated as observing voltage profile criteria ensuring that the system voltage profile is acceptable for system normal and post contingency conditions. Voltage itself is a poor indicator of proximity to system collapse conditions. Thus, the incorporation of voltage stability margin in the operation of power systems has become essential.

se of voltage stability margin

In this section, the voltage stability margin is converted into several voltage stability indices, which can be used to select weak nodes as new Var source locations or as candidate locations for OPF process. It also can be applied as the OPF objective, which results in the index relevant to voltage stability instead of direct voltage stability margin, is considered as the optimization objective.

Venkataramana et al. introduces a method of determining the minimum amount of shunt reactive power support which indirectly maximizes the real power transfer before voltage collapse happens [52]. A *voltage stability index* is available from continuation power flow (CPF) method served as an *indirect* measure to indicate the closeness to voltage collapse point from present system load level, which is defined as the ratio of variation of load parameter from CPF and the voltage variation. The weak buses are chosen by the voltage stability index, which are the sites of the shunt Var source injection; thereafter a nonlinear constrained optimization routine will be employed to minimize the Var injection at the selected weak bus for deciding the size of the Var source.

Sensitivity method and voltage stability margin index are used to rank the locations of

the new Var source in [33], but the result may be different, and then analytic hierarchical process (AHP) uses parallel analytical criteria for accommodating the ranks. Based on the Var sites decided by the AHP, nonlinear optimization neural network (NLONN) is used to optimize the Var variables to improve the voltage profiles as min $F = \sum_i (V_{imax} - V_i)$.

In [53], the algorithm uses three indices based on power flow Jacobian matrix to identify weak buses and selects those buses as candidate buses for installing new reactive power sources to enhance system security. At last, simulated annealing (SA) is applied to solve a constrained, non-differentiable optimal reactive power planning problem. The objective is to maximize the minimum singular value of the power flow Jacobian matrix, which is used as a static voltage collapse index. Thus, the static voltage stability indices are used both in the predefined candidate buses selecting process and the Var planning OPF objective.

of voltage stability margin

Traditionally, the system security margin has not been taken into consideration. The following papers all directly use voltage stability margin as an objective function.

1) Voltage stability margin as single objective

The Var planning problem is formulated as maximization of the active power supply margin (P-margin) in order to improve the static voltage stability [54]; PoC calculation is incorporated in the Var planning model only from the viewpoint of static voltage stability. However, the obtained solutions are sometimes too expensive since they satisfy all of the specified feasibility and stability constraints. This implies that the formulations do not evaluate the cost reduction effect in operation by the devices to be invested. Therefore, it

is preferable to take into consideration both the economical cost and system security.

2) Voltage stability margin as one of the multi-objectives

Y. L. Chen and C. C. Liu [55]-[58] incorporate the voltage stability margins (S-margin) directly into the objective function and create a comprehensive multi-objective model as equ. (2.9):

$$\begin{aligned} \min F1 &= (C_0 + C_1 Q_c)\cdot x + C_2(P_{loss}) \\ \min F2 &= 1\text{- SM} \\ \min F3 &= \sum_i \frac{\Phi\left(\left|V_i - V_i^{ideal}\right| - dv_i\right)}{V_i} \end{aligned} \tag{2.9}$$

where *F1* is to minimize operation cost caused by real power losses and Var source investment cost; *F2* attempts to maximize the voltage stability margin (SM), which is defined by equ. (2.10)

$$SM = \frac{\sum_i S_i^{critical} - \sum_i S_i^{normal}}{\sum_i S_i^{critical}} \tag{2.10}$$

where S_i^{normal} and $S_i^{critical}$ are the MVA loads of load bus *i* at normal operating state B and the voltage collapse critical state (PoC) A as shown in Figure 2.2, respectively; *F3* attempts to minimize the voltage magnitude deviation, where $\Phi(x)=0$ if $x<0$; and $\Phi(x)=x$ otherwise, V_i^{ideal} is the ideal specific voltage at load bus *i* and is usually set to be 1 p.u., and dv_i is the tolerance of maximum deviation in the voltage.

The four papers [55]-[58] all use the same MINLP model, but different methods to deal with MO problems such as the goal-attainment based simulated annealing (SA) [55],

a weighted- norm approach based on SA [56], fuzzy goals [57], and ε-constraint method [58]. This model considers the economical cost and system security trade-off.

In addition to the above four papers, [59] is another example to treat the voltage stability as one objective in the MO problem with objectives as min $F1 = C_1 Q_c$, min $F2 = C_2(P_{loss})$, and max $F3$ = the maximum loadability associated with the critical state, which is calculated using the continuation method, assuming a proportional load increment through all buses of the network. A new approach based on a Strength Pareto Evolutionary Algorithm (SPEA) is applied to handle the Multi-objective Optimization.

2.6 Var planning OPF considering static voltage stability (SCOPF-

Recently, due to a necessity to include the voltage-stability constraint, a few papers in 2.5 incorporate the static voltage stability margin in the Var planning OPF objective in normal state, which provides more realistic solutions for the Var planning problem, but it can not guarantee the voltage stability margin still exists when contingencies happen. Thus, it is preferable to count on the voltage stability constraints in the contingency states. Several papers that can cover the two key points, contingency analyses and voltage stability margin, will be introduced in this section.

The voltage stability margin is treated as an objective in 2.5 section, and the continuation, or optimization methods are used as the tools to obtain the PoC for the voltage stability margin in every iteration. However, the SM is incorporated as the constraints instead of objective in [60], the Var planning takes into account voltage stability margin and contingencies analysis, whose purpose is not only to guarantee the

voltage at all buses lies within a pre-defined range at normal condition, but also to ensure the operating point should be away from the point of collapse or critical point (PoC) at least by a pre-defined "distance" measured in MVA, which is also called S-margin/MVA-margin as shown in Figure 2.3.

It is not necessary to use a separate tool to calculate PoC like before, but two sets of constraints, one for normal operating state, and the other for critical state are required in this model.

The objective in [60] is to minimize a linear combination of fixed and variable Var costs, which is a typical MINLP problem. The same model is adopted in [61], which is solved by MINLP solver (DICOPT++) in GAMS — an optimization modeling language combined with different solvers.

The model in [62] is the same with [60], [61]. The sensitivity information derived from the optimization model is discussed in this paper, including sensitivity of load

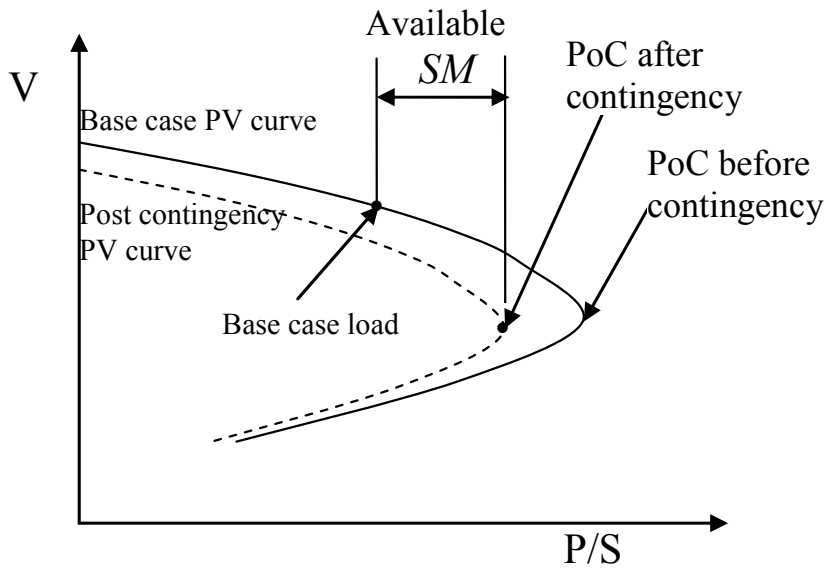

Figure 2.3. PV curve for base case and contingency.

distribution pattern, power factor, stability margin (SM), load growth. These sensitivities are the good economic indicator of the Var cost associated with marginal increasing of some control variables.

The complexity of the voltage stability constrained model lies in the requirement of having two sets of network variables and power flow constraints corresponding to the "normal operation point" and "point of collapse (PoC)". The paper [63] explores the use of statistical linear/quadratic approximation function of the path of PoC as shown in Figure 2.4 as an alternative of the variables and constraints for PoC state.

In general, the PoC increases with Var compensation at different buses. The locus of PoC can be expressed as a function of the bus reactive compensation as equ. (2.11) or (2.12):

$$PoC = a + b_i * Q_{ci} \tag{2.11}$$

$$\text{or} \quad PoC = a + b_i * Q_{ci} + c_i * Q_{ci}^2 \tag{2.12}$$

where PoC is the maximum MVA loadability for the system with reactive compensation, a, b_i, c_i, are parameters of the locus which may be estimated using the multivariate ordinary least square (OLS) regression method, and Q_{ci} is the reactive compensation from new sources at bus i. However, if we increase the number of candidate buses, the procedure will involve evaluating a high number of Var support configurations to capture the interaction of Var compensation at different locations with specified accuracy.

Voltage stability constrained optimal Var planning in [64] is used to determine a minimum cost Var support scheme, which satisfies voltage profile criteria and ensures a minimum voltage stability Q-margin under normal and contingency conditions. A

combined solution satisfying both criteria (voltage profile and voltage stability Var

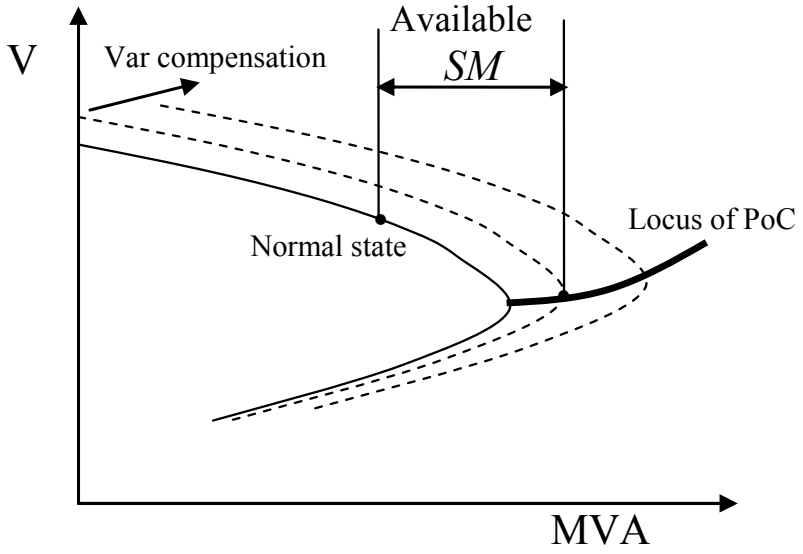

Figure 2.4. Locus of PoC with reactive compensation.

margin) is derived to ensure the Var requirement will be the greater of the two solutions at any candidate bus. However, manual examination is used to guarantee that the final solution is feasible, which will lose the robustness of the program.

2.7 Conclusion

In the end, the technologies in the literature of static reactive power planning are summarized in Table 2.1. This chapter introduces the reactive power planning general purpose, objective category, constraints development with time, and methods or tools used for corresponding models, taking into account the Var source as static Var source, therefore, the new Var source is modeled as a control variable Q_{ci} at bus i.

With the rapid development of Flexible AC Transmission System (FACTS) device, the shunt dynamic Var source such as SVC and STATCOM have become feasible

alternatives to a fixed reactive source. How to model these dynamic Var source? Can the

Table 2.1. Static Var source planning model category table

Objective category		OPF(22)	SCOPF(7)	OPF-VS(7)	SCOPF-VS(4)
Obj.1 ***Min*** Var source cost	NLP	[15] interior point algorithm	[39]SLP		
	MINLP	[16] recursive MIP [17]SLP & B&B [18]SLP & GA			[60]NAG&APEXIV(SM) [61]GAMS/DICOPT++(SM) [62]GAMS/DICOPT++(SM)
Obj.2 ***Min*** Total Var	NLP				[64]EPRI's VSTAB program
Obj.3 ***Min*** weighted sum of cost of Var and real power losses	NLP	[19]MINOS [20]SLP & GA [21]TS [22]SLP & Modal [23]SMFLP	[40]PM [41]BDM, PM & CM [42]recursive LP, PM		
	MINLP	[24]EP [25]HEP [26]SLP & GA [27] HPGDSA [28]GA & SA [29]TS	[43] BDM, CM [44]GBD& SA, PM		
Obj.4 ***Min*** weighted sum of cost of Var and generator fuel cost	NLP	[30]GRG [31]MINOS			
	MINLP	[32]EP & ES &GA			
Obj.5 ***Min*** voltage deviation	NLP	[33]NLONN & AHP			
Obj.6 ***Min*** Var cost + real power loss + voltage deviation	MINLP	[34]TLSA [35]ESSA			
Obj.7 ***Min*** voltage deviation + generator Var deviation + real power losses	MINLP	[36]GA			
Obj.8 ***Min*** Var cost + real power losses + voltage deviation + line flow deviation	MINLP		[46]ε-constraint method & SA		

Table 2.1, continued

Objective category		OPF(22)	SCOPF(7)	OPF-VS(7)	SCOPF-VS(4)
Obj.9 ***Max*** the minimum singular value of Jacobian matrix	NLP			[53]SA	
Obj.10 Max P-margin	NLP			[54] Newton approach	
Obj. 11 ***Min*** real power losses+ Var source cost + voltage deviation & ***Max*** voltage stability margin (S-margin)	MINLP			[55] goal-attainment &SA [56] weighted-norm approach & SA [57] fuzzy logic & SA [58] ε-constraint method & SA	
Obj. 12 ***Min*** real power losses + Var source cost & ***Max*** PoC	NLP			[59]SPEA	

models, methods, and tools used for static Var planning be applied in dynamic Var planning? The answers to these questions are needed for the utilities to make better use of these new power electronic controlled Var sources. These questions will be answered in next chapter.

Note:
MIP- mixed integer programming
SLP- Successive Linear Programming
B&B- Branch and Bound
GA- Genetic Algorithm
MINOS- a NLP solver
TS-Tabu Search
SMFLP-successive multiobjective fuzzy LP technique
EP- Evolutionary Programming
HEP- Hybrid Evolutionary Programming
SA- Simulated Annealing
HPGDSA-hybrid partial gradient descent/SA
GRG -Generalized Reduced Gradient
EP- Evolutionary Programming
ES-Evolutionary Strategy
Analytic Hierarchical Process (AHP)
NLONN - Nonlinear Optimization Neural Network approach
TLSA -Two-Layer Simulated Annealing
ESSA- hybrid Expert System Simulated Annealing
SM - Security Margin
PM- preventive mode
CM- corrective mode
BDM- Bender Decomposition method
GBD- General Bender Decomposition
SPEA- Strength Pareto Evolutionary Algorithm
NAG – Numerical Algorithm Group software package
APEXIV- software package
GAMS - General Algebraic Modeling System
DICOPT++ - MINLP solver in GAMS

3 . A LITERATURE REVIEW OF DYNAMIC VAR PLANNING: SVC AND STATCOM

The previous chapter focuses on static Var planning tools and models. This chapter categorizes the literature relevant to optimal allocation of shunt dynamic Var source SVC and STATCOM, based on the voltage stability analysis tools used. Those tools include static voltage stability analysis ones such as P-V and V-Q curve analysis, continuation power flow (CPF), optimization methods (OPF), modal analysis, saddle-node bifurcation analysis, and dynamic voltage stability analysis ones such as Hopf bifurcation analysis and time-domain simulation. Static voltage stability analysis techniques are also used in dynamic Var planning. At the end of the paper, the advantages of static and dynamic voltage stability analysis tools are summarized.

3.1 Dynamic voltage stability analysis (VSA) techniques

rcation Point

Not all events of voltage collapse in power systems can be associated to saddle-node bifurcations, as other bifurcations have also been shown to induce collapse, such as Hopf bifurcations which corresponds to dynamic voltage stability [65]. Therefore, voltage instabilities directly related to Hopf bifurcations have been categorized as dynamic voltage collapse problems. The Hopf bifurcation occurs when the pair of complex eigenvalues of Jacobian lies exactly on the imaginary axis when the parameter is slowly varied.

ain Simulation

The conventional transient stability time domain simulation programs have been greatly enhanced over recent years to make them suitable for assessment of long-term and voltage stability problems. However, time domain simulation is usually combined with static voltage stability analysis tools such as modal analysis in dynamic Var planning.

3.2 SVC planning

ased Algorithm

1) CPF and Modal Analysis

Traditional voltage stability analysis tools such as continuation power flow (CPF) for PoC or modal analysis at PoC to determine weak areas or buses are used in [66] for SVC location. The SVC size is determined based on the need to continuously meet the voltage stability margin requirement. The speed with which the shunt device should operate is a separate issue. The dynamic aspects of the voltage collapse phenomenon cannot be properly analyzed by modal analysis based on power flow static models.

CPF and modal analysis are also used to indicate the candidate buses for voltage support in [67]. However, the modal analysis is helpless regarding the minimum amount of reactive support to solve the voltage collapse problem. As a result, OPF is used to determine the MVar rating of the reactive compensator, SVC is still described as voltage independent Var source Q_c like in static Var planning, but in fact it is voltage dependent Var source.

The location of a SVC device is determined by the participation factors from modal analysis and the use of controllability indices of the most critical stability state in the modal analysis in [68]. It evaluates the extended steady-state voltage stability margins in electric power system due to FACTS controller such as SVC and UPFC.

In [69], the dynamic voltage stability margin has been considered as the distance between the Hopf bifurcation point and the base case operating point, the static voltage stability margin as equ. (2.10). SVC should be placed at a bus, which produces maximum enhancement in both margins. The saddle-node bifurcation points have been obtained by a continuation power flow software package UWPFLOW. A method has been proposed to combine the two margins in [69], which computes static and dynamic participation factors and thereafter, combined hybrid participation factors at different buses. The bus with maximum value of the hybrid participation factor for the intact system and critical contingency cases has been selected as the candidate bus for the SVC placement. This paper is one of the few papers which consider not only static margin but dynamic margin.

2) Loss Sensitivity Index

The SVC has been considered from a static point of view to reduce the total system real power transmission loss (P_L) in [70]. *Loss sensitivity index* is proposed as the sensitivity of total transmission loss with respect to the control parameters of SVC for their optimal placement. The bus with the most negative loss sensitivity value is preferred to be the SVC location. SVC has been considered as a reactive power source with the following reactive power limits as equ. (3.1):

$$Q_{SVC} = V_t(V_t - V_{ref})/X_{sl}$$

$$Q_{ind} = B_{ind} V^2_{ref}$$

$$Q_{cap} = B_{cap} V^2_{ref} \quad (3.1)$$

where X_{sl} is the equivalent slope reactance in p.u. equal to the slope of voltage control characteristics, and V_t and V_{ref} are the node and the reference voltage magnitudes, respectively. Q_{SVC} is valid as long as it is within inductive limits Q_{ind} and capacitive limits Q_{cap} set by available inductive and capacitive susceptances *(*B_{ind} and $B_{cap,}$ respectively).

After deciding the optimal location of SVC, the formulation of OPF to minimize real power losses as the objective has been developed to determine the size. The same methodology is used in [71], but the OPF objective minimizes fuel cost. The method based on *Loss Sensitivity Index* ignores the voltage stability limits, and only considers the economical aspect.

ion Based Algorithm

1) Maximize voltage stability margin

From the viewpoint of optimal reactive reinforcement for voltage stability, optimal SVC planning is evaluated in [72] such that the reactive margin (Q-margin) of the study configuration including critical modes is maximized by using a hybrid method based on the simulated annealing (SA) and Lagrange multiplier techniques. The system reactive margin is defined as the maximum amount of extra reactive demand that the system can supply, before it reaches a critical point and encounters a voltage instability problem.

The optimal SVC planning is treated as a multi-objective optimization in [73] for maximizing the system reactive power margin, minimizing system real power losses and voltage depressions at critical points. Fuzzy logic techniques are applied to transform the

multi-objective optimization problem into a constrained problem with a single objective function known as the fuzzy performance index. SVC is still modeled as voltage independent Var source Q_c.

2) Minimize Voltage Deviation

A two-stage Tabu Search (TS) is proposed in [74] for determining the location and the output of SVC devices to reduce the voltage deviation in a distribution system with DG. The location is expressed as a discrete variable, and the rating of SVC is a continuous one. SVC is treated as voltage independent Var source Q_c in the model. However, post-contingency state security and voltage stability margin are ignored in this paper.

3) Minimize Cost

The objective of the optimal allocation of SVC in [75] is to minimize the overall cost function, which includes the investment costs of FACTS and the bid offers of the market participants. The cost function of SVC is as equ. (3.2) in [76]:

$$C(s)= 0.0003\ s^2 - 0.3051s + 127.38 \text{ (US\$/kVar)} \quad (3.2)$$

where C(s) is in US$/kVar and s is the operating range of the FACTS devices in MVar. The proposed approach converts the objective into minimizing the overall cost function consisting of FACTS like SVC devices investment cost and fuel cost in [77]. Genetic Algorithm (GA) is used in both papers [75] [77]; however, post-contingency state security and voltage stability margin are still ignored.

The location of SVC for reactive compensation is chosen according to *reactive*

marginal cost criterion in [78], whose value can be obtained from the OPF solution corresponding to the Lagrange multiplier of the reactive power constraint. The objective is the $ improvement due to the reduction of the fuel cost in this paper. Thus, for each bus in the system, there will be a corresponding reactive marginal cost. The bus with the highest reactive marginal cost will be chosen as the SVC location.

In most of the work, the placement of FACTS controllers has been considered for the intact system normal operating state. Very limited efforts have been made to study the impact of these controllers and their placement under contingencies. Therefore, if contingency and voltage stability are considered, it may be a considerable improvement in this field.

In [79], the objective is to minimize the sum of the new FACTS investment costs such as $F = (C_0 + C_1 Q_c) \cdot x$, corrective control cost such as fast load shedding cost, and preventive control cost to improve the voltage stability margin in all predefined contingencies. Meanwhile, the bus voltage profile and voltage stability margin are kept within specified limits in normal and the corresponding contingency states. Two sets of constraints including normal condition constraints and critical mode constraints are formulated in the OPF. The problem is formulated as a large-scale Mixed Integer Nonlinear Programming (MINLP), which is solved by a two level hybrid GA/SLP method. However, the shunt FACTS model is still a voltage independent Var source Q_c in the OPF.

3.3 STATCOM planning

Modal analysis

The main goal of the voltage stability study in [80] is to keep the static voltage Stability Margin (*SM*) based on active power (P-margin) greater than at least 5% at N-1 contingency states, usually such a margin is treated as a safe one, which is defined as equ. (3.3):

$$SM = \frac{\sum_i P_i^{critical} - \sum_i P_i^{normal}}{\sum_i P_i^{normal}} \tag{3.3}$$

where P_i^{normal} and $P_i^{critical}$ are the MW loads of load bus *i* at normal operating state and the voltage collapse critical state (PoC), respectively. This means that after a single branch outage, the power system can afford 5% active load increment without voltage collapse occurring.

For this purpose, the software package Interactive Power Flow Program (IPFLOW) is the main tool for steady state calculation, and then the Voltage Stability Analysis Program (VSTAB) by EPRI for PoC calculation and modal analysis is used to determine the best location for installing STATCOM as remedial measures against voltage collapse. VSTAB is also for contingency assessment to ensure the rating of STATCOM is enough to keep the 5% stability margin.

The optimal location of some FACTS devices including STATCOM in [81] is determined from the viewpoint of increasing the loadability margin of a power system by applying continuation power flow tool. Power System Analysis Toolbox (PSAT) software with power flow and continuation power flow functions is applied to calculate

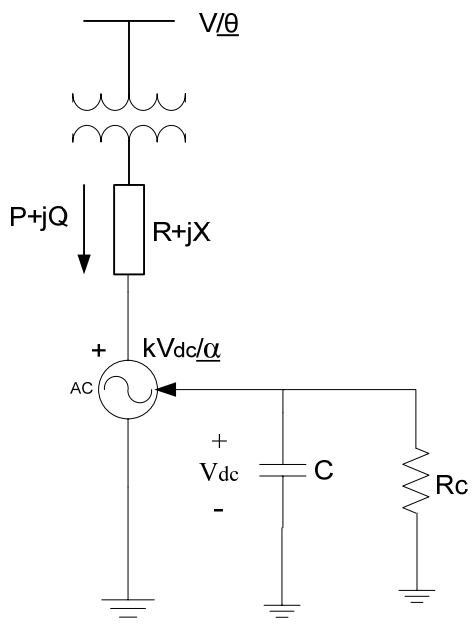

Figure 3.1. STATCOM power injection model.

and compare the P-V curves with and without FACTS device. A detailed STATCOM power injection model is proposed to use in the continuation power flow as shown in Figure 3.1. In the several buses with the same minimum loadability margin, the one with the weakest voltage profile is chosen as the STATCOM location. However, no contingency cases are involved in the analysis.

So far no work has been reported in open literature for the optimal location of STATCOM considering the effects on economical cost and voltage stability margin under both normal and contingency circumstances.

ain Simulation vs. Static Voltage Stability MW Margin

Reference [82] focuses on a STATCOM as a dynamic Var source providing voltage support in a power system. Both static voltage stability margins based on P-V curve and

time-domain dynamic simulation are carried out and compared to verify the agreement between the two study methods. Even though one method is static analysis and the other is dynamic analysis, the two different methods lead to the same result. For example, voltage collapse in time-domain simulation reflects on P-V curve as the operating point out of the range of maximum load capability.

ain Simulation vs. Modal Analysis

Modal analysis and time-domain simulation are used to determine the best location for the STATCOM controllers in [83]. Three violations for voltage stability criteria are defined in this paper, which are recovery voltage less than 90% of its initial value; transient voltage less than 80% of its initial value; and oscillations remaining for more than 20 cycles.

First, critical contingencies that result in voltage unstable condition are identified by the sign of the eigenvalues computed in modal analysis. Secondly, time-domain simulation is performed to test all critical contingencies and identify the types of criteria violations for each critical contingency. By comparing the results from both modal analysis and dynamic analysis, a good correlation between the two techniques is found: buses with high participation factors in modal analysis are the same that have violations to the voltage stability criteria in dynamic analysis.

Thirdly, the candidate locations of FACTS controllers are selected by combining the bus participation factor from modal analysis and the number of violations from the dynamic analysis. However, this testing method to decide the final size and location ignores the economic analysis. As a result, it is not accurately based on the maximum benefit.

In [84], the results for voltage stability analysis from the dynamic analysis using time domain simulations and the static analysis using modal analysis are compared, which are shown to be consistent in indicating system voltage stability.

3.4 Conclusions

Voltage stability is indeed a dynamic phenomenon and may be studied using a set of differential and algebraic equations. However the static approach is shown to have a number of practical advantages over the dynamic approach, which make the static approach more attractive.

- It requires only small modifications of a standard load flow program, so it is computationally less intensive.
- The P-V curves can cover a wide range of system operating conditions, whereas the time-domain simulations are for only one operating point. As a result, time-domain simulation usually requires a large number of study cases at different system operating conditions and contingencies.
- The P-V curves can provide much more information on the relationship between system and control parameters and voltage stability. An index value "voltage stability margin" is effectively used to illustrate the impact on the voltage stability for changing system parameters and Var source size parameters. Time-domain simulation gives us the voltage profile of every bus, but can not demonstrate how far away to the voltage collapse point from the present operating point.
- Modal analysis can clearly indicate whether the system is stable or not at the given operating mode. In addition, the participation factors clearly define areas

prone to voltage instability and indicate elements which are important to improve the system voltage stability most effectively.

Advantage of dynamic analysis is as follows:

- Time-domain simulation can clearly show the transient process and how long it will take to transfer to another stable operating point, which would not be illustrated in the P-V curve. The static voltage stability margin in the P-V curve can not guarantee transient stability.
- It is necessary to use dynamic analysis when to decide how fast the Var source needs to respond to the contingencies, thereafter, to decide the type of Var source such as dynamic Var source or static Var source.

The response of system voltage to a disturbance and system behavior during a voltage collapse situation can be considered as dynamic power system phenomena. However as far as reactive long term planning is concerned, a steady-state analysis has been shown to be generally adequate for providing an indicator of the margin from current operating point to voltage collapse point and for determining the location and MVar rating of any necessary reactive power source.

Although dynamic analysis is separately used to design the controls for system reactive support, the advantages of the above static analysis make it suitable for the Var planning under a large number of conditions. In the end, the technologies in the literature of SVC and STATCOM planning are summarized in Table 3.1. Some methods that are originally designed for one compensator may be applied to the other with slight modification due to the similarity of SVC and STATCOM. If detailed models of SVC or

STATCOM are desired, the specific features of the compensators need to be incorporated in the Var planning method, as shown in some previous works.

After the literature review on static and dynamic reactive power planning, a method based on maximizing reactive power economic benefits will be introduced to select Var size and location in the following chapters. How to evaluate the reactive power economic benefits will be immediately proposed in the next chapter.

Table 3.1. Dynamic Var source planning technology.

Technology	SVC(12)	STATCOM(4)
CPF+ Modal analysis (no CA)	[66][67][68]	[80] IPFLOW, VSTAB
CPF+ P-V curve (no CA)		[81] PSAT
P-V curve + time-domain dynamic simulation (CA)		[82]
Modal analysis+ time-domain dynamic simulation (CA)		[83]
Saddle-node &Hopf bifurcation (CA)	[69]	
Loss sensitivity index (no CA)	[70][71]	
Max Q-margin (NLP)(SA)(no CA)	[72][73]	
Min voltage deviation (NLP)(TA)(no CA)	[74]	
Min Var cost and bid offers (SA)(no CA)	[75]	
Min Var cost and fuel cost (SA)(no CA)	[77] [78]	
Min Var cost+ load shedding cost+ preventive control cost (MINLP)(GA/SLP)(CA)(P-margin)	[79]	

Note: CA- contingency analysis
IPFLOW, VSTAB- software package for voltage stability analysis
PSAT - Power System Analysis Toolbox software
NLP – Nonlinear Programming
MINLP – Mixed Integer Nonlinear Programming

4 . ASSESSMENT OF THE ECONOMIC BENEFITS FROM REACTIVE POWER COMPENSATION

Before reactive power planning is studied, it is necessary to make clear the benefits obtained from reactive power compensation and their quantitative evaluation. The optimal location chosen is based on maximizing the quantitative benefits evaluation. However, the cost of local dynamic Var sources is high and no a standard method to evaluate the economic benefits exists. Although it is generally known that there are technical benefits for utilities and industrial customers to provide local reactive power support, a thorough quantitative investigation of the economic benefit is greatly needed.

This chapter demonstrates a possible quantitative approach to assess the "hidden" benefits from Var sources at the demand side. This chapter investigates the benefits including reduced losses, shifting reactive power flow to real power flow, and increased transfer capability. These benefits are illustrated with a simple two-bus model and then presented with a more complicated model using Optimal Power Flow. Tests are conducted on a system with seven buses in two areas. It should be noted that the discussion in this paper is from the viewpoint of the load-serving utility.

4.1 Benefits from Var source in a two-bus system

To help readers understand these benefits, a two-bus system shown in Figure 4.1 is used to illustrate the systematic methodology for capturing the hidden benefits. In Figure

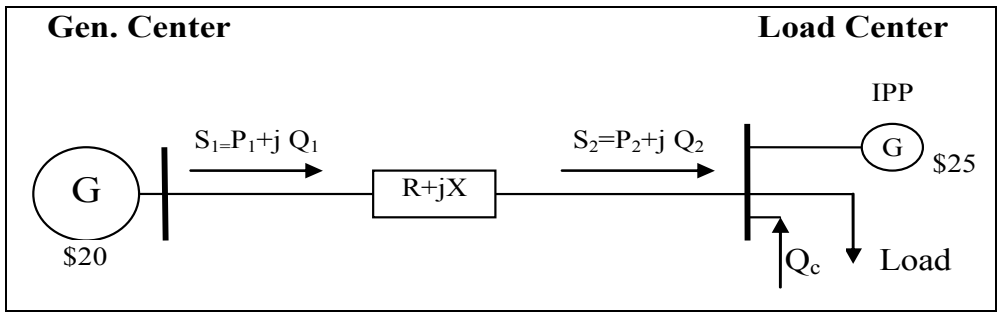

Figure 4.1. A two-bus system.

4.1, there is a generation center with a cheap unit of $20/MWh cost, a load center with a large amount of load, and an expensive unit of $25/MWh cost, and a tie line connecting the two areas. The net load of the load center (i.e., the total load minus the total local generation) is 100 MVA with 0.9 lagging power factor. This implies an import of 90 MW and 43.59 MVar (P_2 and Q_2, respectively) from the generation center through the tie line.

The other parameters are as follows: the power base is 100 MVA; the voltage at the generation center bus is fixed at $1.0\angle 0^o$ per unit; and the line impedance is 0.02 + j0.2 per unit. It is assumed that the load center is stressed and the tie-line is congested at its maximum transfer capability of 100 MVA at the receiving end, constrained by voltage stability. Also, the assumption is that the local compensation device will constantly inject Q_c = 14.01 MVar to lift the load power factor to 0.95, i.e., $P'_2 = P_2 = 90$ MW and $Q'_2 = Q_2 - Q_c = 43.59 - 14.01 = 29.58$ MVar. The economic benefits from local Var compensation are classified into three categories. Each of these is discussed below. Also, hard-to-quantify benefits are mentioned.

m reduced losses (*B1*)

Injection of reactive power at the receiving end reduces the reactive power through the tie line and therefore reduces the line current. Since the real power loss is I^2R, the loss will be reduced if the current is reduced. With the consideration of the load-side voltage magnitude remains unchanged and very close to 1.0, the original line loss and the power at the delivery end before the Q_c compensation are given as follows.

$$P_{loss} = I^2 R = \frac{P_2^2 + Q_2^2}{V^2} R = \frac{0.9^2 + 0.4359^2}{1.0^2} \cdot 0.02 = 0.02\ p.u. = 2\ MW$$

$$P_1 = P_2 + P_{loss} = 90 + 2 = 92\ MW$$

After Q_c is connected, the power losses and delivery end power are as follows.

$$P'_{loss} = I^2 R = \frac{(P'_2)^2 + (Q'_2)^2}{V^2} R = \frac{0.9^2 + 0.2958^2}{1.0^2} \cdot 0.02 = 0.018\ p.u. = 1.80\ MW$$

$$P'_1 = P'_2 + P'_{loss} = 90 + 1.80 = 91.80\ MW$$

Therefore, the total loss savings at the delivery end is 0.2 MW (92-91.8) or 10% reduction of the original 2 MW losses for every 14.01 MVar compensation at the load center. This loss reduction represents reduced total generation. The annual saving will be \$35,040/year (\$20/MWh x 0.2 MW x 8760hr) if the same amount of load is assumed for every hour. Therefore, the savings in dollars per MVar-year is \$2,501/MVar-year [(\$35,040/year) /14.01 MVar].

m shifting reactive power flow to real power flow (*B2*)

As previously assumed, the tie line is congested due to the maximum transfer capability of 100 MVA at the receiving end. If this is the case, it is still assumed that the

limit of S_2 remains at 100 MVA after the local Var compensation. The reason is that the possibly increased amount of transfer capability affects the tie-line tariff collected by the transmission owner, as discussed in the next sub-section.

Since the reactive power flow, Q_2, has been reduced due to local compensation, this makes it possible to have more real power delivered from the lower-cost generator while the 100 MVA limit is still respected because of $P_2 = \sqrt{S_2^2 - Q_2^2}$. This benefit of transferring more cheap real power while keeping the same transfer capability is classified as the benefit of shifting reactive power flow to real power flow, as in the title of this subsection. With the same case in Figure 4.1, after the compensation, Q_2 has been reduced to 29.58 MVar to give a 0.95 lagging power factor for the net load at load center. The new real power transferred over the tie-line is given as

$$P_2 = \sqrt{100^2 - (Q_2 - Q_C)^2} = \sqrt{100^2 - 29.58^2} = 95.52\,MW$$

Hence, the additional deliverable real power is 5.52 MW. Ignoring the additional loss due to the 5.52 MW, this is the amount of additional lower-cost real power from the generation center to the load center. Therefore, if a re-dispatch is performed, the local higher-cost generation will be reduced by 5.52 MW. The economic benefit to the load-serving utility will be the reduced production cost equal to the 5.52 MW times the price difference between the two generators.

When a full year is considered, an hour-by-hour accumulation is needed for hours when the maximum transfer capability is reached and limits additional power transfer. Assuming the tie line is congested during 2 peak months, the total savings due to the shifting of reactive power flow to real power flow is equal to \$39744/year [(\$25/MWh -

$20/MWh) x 5.52MW x 60day x 24hr]. Hence, the savings per MVar-year for the load center is $2,837/MVar-year [($39744/year) / 14.01MVar].

Under this category, the load will pay less due to the shift of reactive power flow to real power flow. Meanwhile, the unit at generation center will receive increased revenue due to increased MW dispatch. Similarly, the IPP unit at load center will receive reduced revenue due to reduced dispatch.

m increased maximum transfer capability (*B3*)

In the previous analysis, the maximum transfer capability is assumed to be unchanged. However, it is very possible that the local Var compensation in the stressed area may increase the maximum transfer capability constrained by voltage stability. This is shown in Figure 1.1. There are various ways to calculate the change of transfer capability with respect to a change of system conditions including local Var injection. Here the equation of the maximum real power transfer in a two-bus model [85] is employed as (4.1):

$$P_{\max} = \frac{E^2(-k+\sqrt{1+k^2})}{2X},\ where\, k = \frac{Q}{P} \tag{4.1}$$

Again, assume the compensation lifts the power factor from 0.9 to 0.95, i.e., from 90 MW + j43.59 MVar to 90 MW + j29.58 MVar. Also assume the generation center voltage remains at $1.0\angle 0^o$. It can be easily verified that the maximum transfer capacity has been improved by 15.5%. Therefore, the load center may receive 103.95 MW (90 x 1.155), which means it may receive another 8.43 MW (103.95-95.52) of lower-cost power from the generation center due to the increase of the transfer capability.

Ignoring the line loss caused by this transfer capability increase, the lower-cost

generation dispatch is increased by 8.43 MW while the higher-cost local generator dispatch is decreased by 8.43 MW. With the previously assumed 2 months of peak load, the saved production cost due to the increased transfer capability is equal to $61,416/year [($25/MWh -$20/MWh) x 8.43MW x 60day x 24hr]. Hence, the benefit in $/MVar-year is $4384 /MVar-year [($61416/year) / 14.01MVar].

Similar to the second category, the load will pay less under this consideration due to the increased transfer through the tie-line. Also, the unit at the generation center will receive increased revenue and the IPP unit at the load center will receive reduced revenue. In addition, the transmission company may receive more transmission tariff due to more MVA flow through the tie-line. This is also an important reason to distinguish this benefit from the previous one.

Given the sample system above, it is straightforward to conclude the following equations:

$$Bt = B1 + B2 + B3 \tag{4.2}$$

$$B1 = \sum_{all\_hours} C_L \cdot \Delta P_{loss} \tag{4.3}$$

$$B2 = \sum_{congested\ hours} (C_L - C_G) \cdot \Delta P_{shift} \tag{4.4}$$

$$B3 = \sum_{congested\ hours} \left(C_L \cdot \Delta P_{inc\_trans\_L} - C_G \cdot \Delta P_{inc\_trans\_G} \right) \tag{4.5}$$

where

Bt = the total benefit from local Var compensation;

B1 = the benefit from reduced loss;

B2 = the benefit from shifting reactive power flow to real power flow without considering change of transfer capability;

B3 = the benefit from the increased transfer capability;

C_G *= the average cost of the generators at the generation center;*

C_L *= the average cost of the generators at the load center;*

ΔP_{loss} *= the reduced loss;*

ΔP_{shift} *= the shift of reactive power flow to real power flow;*

$\Delta P_{inc\_trans\_L}$ *= the transfer change at the receiving end;*

$\Delta P_{inc\_trans\_G}$ *= the transfer change at the delivery end.*

In (4.5), the change of transfer at the delivery end and the receiving end are considered different due to the additional loss caused by the additional transfer in the tie-line. If the additional loss is ignored as in the previous subsection, $\Delta P_{inc\_trans\_L}$ should be the same as $\Delta P_{inc\_trans\_G}$.

It should be noted that while *B1* applies to all hours, *B2* and *B3* apply only to the hours when congestion due to transfer capability occurs. In the hours when maximum transfer capability is not reached, it is not likely to get more real power imported through the tie line after compensation. Otherwise, the base case should have more real power import capability. Other constraints such as generation output limits or other transmission limits may restrict more real power transfer.

There are many other benefits which are difficult to quantify such as improvements in voltage regulation and voltage quality due to local Var compensation. More detailed

investigation is needed to address all these benefits more fully.

4.2 Quantitative evaluation of reactive power benefit

valuation of reactive power benefit

This section presents a generic formulation to assess the economic benefits of Var compensation via comparisons of five different cases of optimal generation dispatch. The dispatch is performed for the three cases using Optimal Power Flow (OPF) with respect to transmission limits and inter-tie transfer capability limits [86]. The three cases are as follows:

Base Case*: Base system without Var compensation (Q_c=0);*

Case1: *Compensation is available at a given bus in a given amount, and the original interface transfer limit is maintained;*

Case2: *Compensation is available as in Case 1, and a new interface transfer limit is applied;*

The objective of the OPF for the above three cases is to minimize the fuel cost. The constraints include the limits of the transmission networks. The dispatch formulation in the OPF model can be written as (4.6):

$$Min: \sum f(P_{Gi}) \tag{4.6}$$

Subject to:

$P_{Gi} - P_{Li} - P(V,\theta) = 0$ *(Real power balance)*

$Q_{Gi} + Q_{ci} - Q_{Li} - Q(V,\theta) = 0$ *(Reactive power balance)*

$P_{Gi}^{\min} \le P_{Gi} \le P_{Gi}^{\max}$ *(Generation real power limits)*

$Q_{Gi}^{\min} \le Q_{Gi} \le Q_{Gi}^{\max}$ *(Generation reactive power limits)*

$V_i^{\min} \le V_i \le V_i^{\max}$ *(Voltage limits)*

$Q_{ci}^{\min} \le Q_{ci} \le Q_{ci}^{\max}$ *(Compensation limits)*

$\left|LF_l\right| \le LF_l^{\max}$ *(Line flow thermal limits)*

$\sum_{l \in Lt} S_l \le \sum_{l \in Lt} S_l^{\max}$ *(Tie line MVA transfer capability limits considering security margin)*

where *Lt— the set of tie lines*.

After the optimal dispatches are performed for the three cases, the benefits *B1+ B2*, *B3*, and *Bt* may be calculated by simply a comparison of the total fuel cost for each of three cases as (4.7-4.9). Assuming *z*, *z1*, *z2* are the fuel cost for the Base Case, Case1, Case2 respectively. However the simple comparison of the fuel cost can not facilitate the separation of *B1* and *B2*.

$$B1+ B2 = z - z1 \quad (4.7)$$

$$B3 = z1 - z2 \quad (4.8)$$

$$Bt = z - z2 \quad (4.9)$$

The *B1*, *B2* and *B3* also can be identified using the following approach by adopting equations (4.2-4.5). In this approach, but the result may not be accurate as that from (4.7-4.9) due to the adoption of average cost of the generators in (4.3-4.5).

1. Perform OPF for Base Case and Case1.
2. Calculate the total reduced MW generation from Base Case to Case1. This MW

amount

is $\Delta P_{loss} + \Delta P_{shift}$.

3. Find the reduced system losses, ΔP_{loss}. Then, ΔP_{shift} can be easily obtained.

4. Perform OPF for Case2.

5. Calculate the changes of MW dispatch in the generation center and the load center from

Case1 to Case2. These changes are $\Delta P_{inc\_trans\_G}$ and $\Delta P_{inc\_trans\_L}$.

6. Obtain the average marginal costs in generation center and load center from Base Case.

These values are C_G and C_L, respectively.

7. Apply Eqs. (4.3-4.5) to calculate the three economic benefits, *B1*, *B2*, and *B3*.

8. Obtain the fuel cost difference between Base Case and Case2. This is the total accurate economic benefit, *Bt*.

9. Because *Bt* is not usually equal to *B1+B2+B3* due to non-linearity of the system, *B1*, *B2*,

and *B3* may be adjusted proportionally such that *B1+B2+B3 = Bt*.

10. Steps 1-9 need to be repeated if many different hours or scenarios are considered.

alculation of total transfer capability (TTC)

In the two-bus system, the P_{max} equation is used to obtain the change of tie line transfer capability with respect to the local Var injection. However, the P_{max} equation is not suitable for the multi-bus system. Then how to calculate TTC becomes a key point in the evaluation of reactive power benefits, which is also a discussion topic in the literature.

In chapter 2, various ways to calculate Point of Collapse (PoC) of a P-V curve are introduced such as continuous power flow (CPF) and OPF. In this section, OPF is applied to obtain the TTC because it is easy to incorporate various limits into the OPF model such as generator real power and reactive power limits, bus voltage limits, which is difficult to realize for CPF. The TTC formulation in the OPF model can be written as (4.10-4.14):

$$\textit{Max: } f(P_{Gi}(i \in Source), P_{Li}(i \in Sink), Q_{Li}(i \in Sink)) = \sum_{i \in Sink} P_{Li} - \sum_{i \in Sink} P_{Li}^{0} \tag{4.10}$$

Subject to:

$P_{Gi} - P_{Li} - P(V, \theta) = 0$ *(Real power balance)*

$Q_{Gi} + Q_{Ci} - Q_{Li} - Q(V, \theta) = 0$ *(Reactive power balance)*

$\left|LF_k\right| \le LF_k^{\max}$ *(Line flow limits)*

$P_{Gi}^{\min} \le P_{Gi} \le P_{Gi}^{\max}$ *(Generation real power limits)*

$Q_{Gi}^{\min} \le Q_{Gi} \le Q_{Gi}^{\max}$ *(Generation reactive power limits)*

$V_i^{\min} \le V_i \le V_i^{\max}$ *(Voltage limits)*

$Q_{ci}^{\min} \le Q_{ci} \le Q_{ci}^{\max}$ *(Compensation limits)*

$$P_{Li} \ge P_{Li}^{0} \quad (i \in Sink)$$

$$Q_{Li} \ge Q_{Li}^{0} \quad (i \in Sink)$$

$$P_{Gi} \ge P_{Gi}^{0} \quad (i \in Source) \tag{4.11}$$

$$P_{Gi} = P_{Gi}^0 + \frac{(\sum_{i \in Source} P_{Gi} - \sum_{i \in Source} P_{Gi}^0) \times (P_{Gi}^{\max} - P_{Gi}^0)}{\sum_{i \in Source} (P_{Gi}^{\max} - P_{Gi}^0)} \qquad (i \in Source) \quad (4.12)$$

$$P_{Li} = P_{Li}^0 + \frac{(\sum_{i \in Sink} P_{Li} - \sum_{i \in Sink} P_{Li}^0) \times P_{Li}^0}{\sum_{i \in Sink} P_{Li}^0} \qquad (i \in Sink) \quad (4.13)$$

$$P_{Li} / P_{Li}^0 = Q_{Li} / Q_{Li}^0 \qquad (i \in Sink) \quad (4.14)$$

where

P_{Li}^0, Q_{Li}^0, P_{Gi}^0= initial operation point;

Generation center is named as *Source* area, and load center is named as *Sink* area. The objective is to maximize the load demand increase from the initial operation point in *Sink* area. The real power outputs of generators in *Source* area increase following a specified pattern, which is the ratio of reserved real power of generator *i* to the total reserved real power of the generators in *Source* area.

The reserved real power is the power available for use to balance the load demand increase, which can be expressed as $P_{Gi}^{\max} - P_{Gi}^0$. The real power loads in *Sink* area raise by the ratio $P_{Li}^0 / \sum_{i \in Sink} P_{Li}^0$. And the complex load is adjusted with constant power factor. The real power outputs of generators in *Source* area and the real/ reactive load in *Sink* area can be adjusted in order to get the maximum transfer capability.

Assuming the Q_{ci} is zero, the tie line transfer capability limit for Base Case can be

achieved by running the TTC OPF model. Then assigning the Q_{ci} a specified value, an increased tie line transfer capability limit may be obtained for Case2. Both limits can be put into the three OPF models in section 4.2.1.

4.3 Case study with results

In this section the 7 bus test system from PowerWorld [87] is used to demonstrate the economic benefits from Var compensation. The diagram of the test system is shown in Figure 4.2. The data for the loads, generation, transmission thermal limits and voltage limits are shown in Table 4.1. In order to study the increased maximum transfer capability for the tie lines, the test system is divided into two areas, the Top Area and the

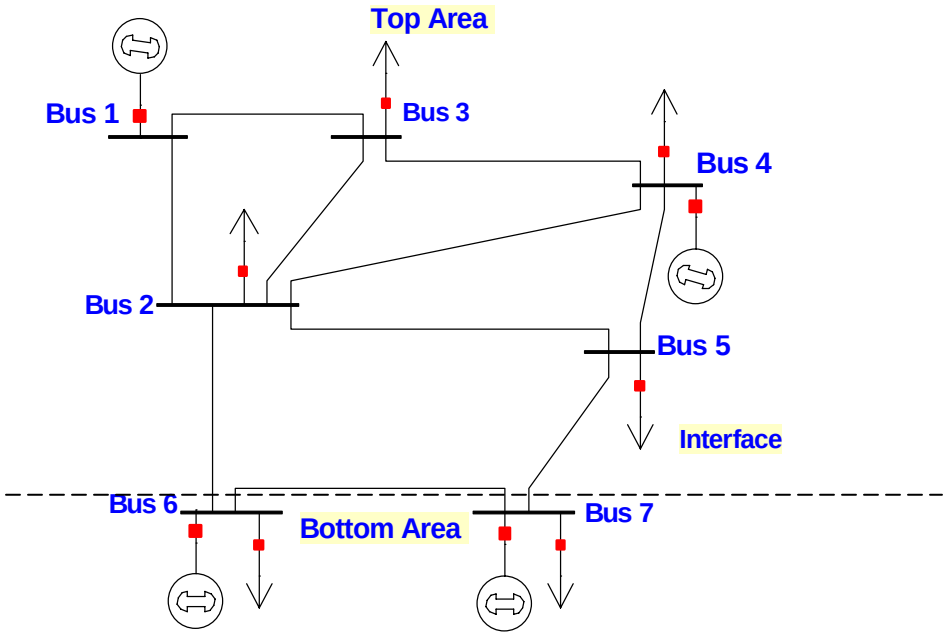

Figure 4.2. Diagram of a seven-bus test system.

Table 4.1. Parameters of the test system

Power base: 100MVA										
Voltage base: 138kV										
Load										
Bus	1	2	3	4	5	6	7			
P_L (MW)	0	100	190	150	200	50	80			
Q_L (MVar)	0	40	75	50	60	20	40			
Generator fuel consumption coefficient										
Bus	1	4	6	7						
a ($/h)	798.92	814.03	515.34	400.41						
b ($/MWh)	20	19	14	15						
Marginal cost ($/MWh)	20	19	14	15						
Active power generation limits (MW)										
Bus	1	4	6	7						
P_G^{max}	150	200	300	300						
P_G^{min}	70	50	60	0						
Reactive power generation limits (MW)										
Bus	1	4	6	7						
Q_G^{max}	100	100	100	100						
Q_G^{min}	-100	-100	-100	-100						
Transmission line thermal limits (MVA)										
Line	1-2	1-3	2-3	2-4	2-5	4-3	5-4	6-2	6-7	7-5
Limit	120	100	100	100	100	120	80	250	100	250
Voltage limits (p.u.)										
V_{max} =1.05 and V_{min}=0.95 for every bus.										

Table 4.2. Load and Generations in Two Areas

Area	Bus	Gen. Cap. (MW)	Load (MW)	Margin (MW)
Load Center	1, 2, 3, 4, 5	350	640	-290
Gen. Center	6, 7	600	130	470

Bottom Area, as shown in Figure 4.2 and Table 4.2. The Top Area is a load center, and the Bottom Area is a generation center. The generators in the load center are owned by IPPs and more expensive than those in the generation center.

The interface tie lines between the two areas are line 6-2 and line 7-5. The initial operation condition without tie line limit is as shown in Figure 4.3. The inter-tie line voltage stability limit from the TTC OPF (the nose point of the P(S)-V curve) is 464 MVA (233MVA+231MVA) as illustrated in Figure 4.4, which is lower than the sum of their thermal limits (500 MVA). If the voltage stability margin is assumed to be 25%, then the interface transfer limit is 464 *75%=348 MVA.

margin, the new interface limit is set as 492.25*75%=369 MVA.

The OPF models for the three cases are solved by the Nonlinear Programming (NLP) solver MINOS.

In this test, it is assumed that a 15 MVar compensator will be installed at Bus 3, where the lower voltage occurs as indicated by the power flow study of the base case. Although the location and amount of Var installation should follow a more rigorous approach considering engineering and economic tradeoff, in this case it is chosen simply for illustrative purposes. The 15 MVar compensation at Bus 3 raises the voltage stability limit to 492 MVA (243MVA+249MVA) as illustrated in Figure 4.5. Considering 25%

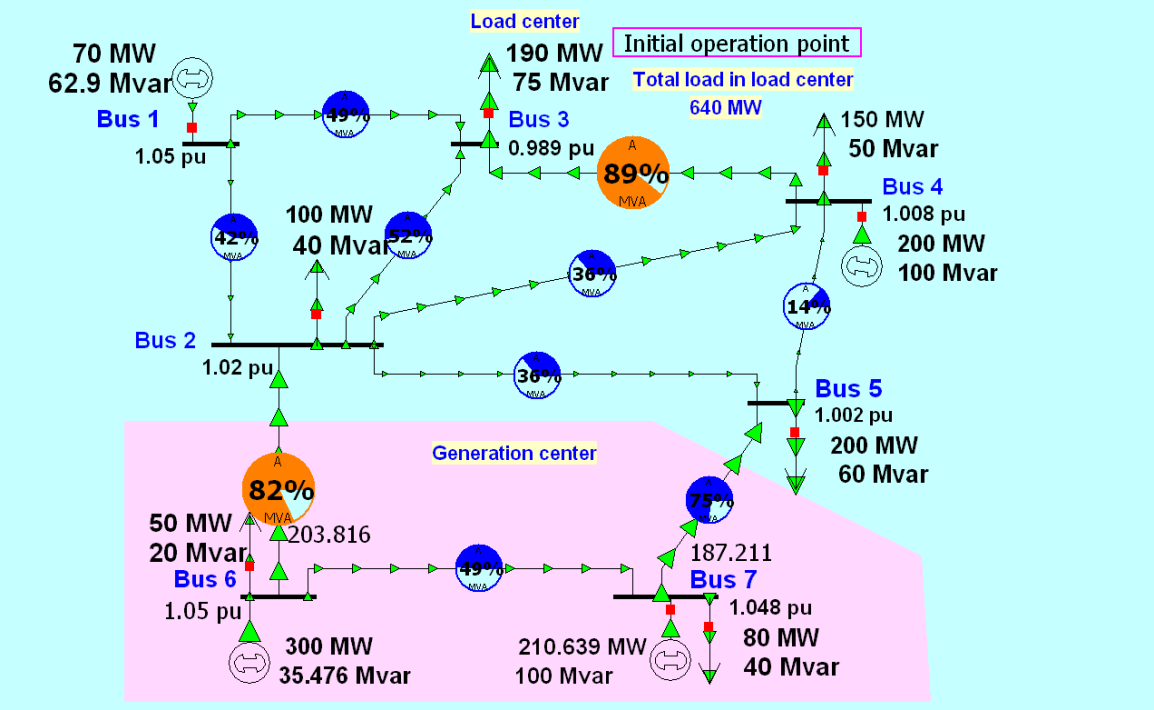

Figure 4.3. Initial operation point.

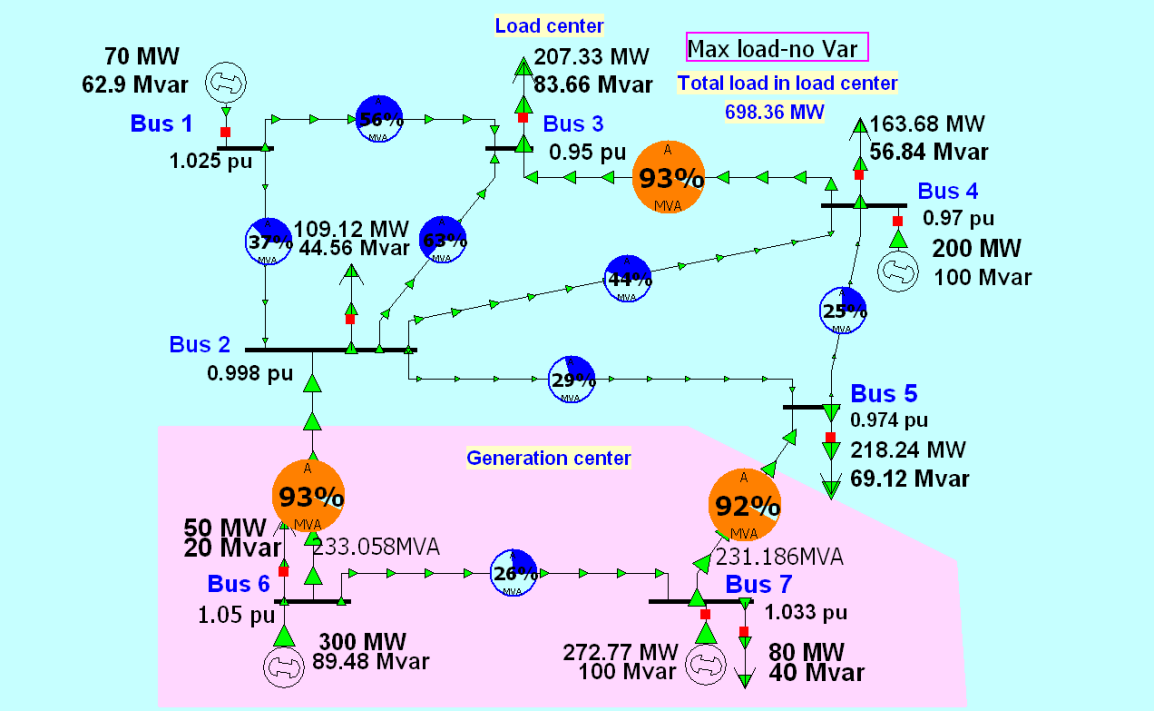

Figure 4.4. PoC (point of collapse) without Var compensation.

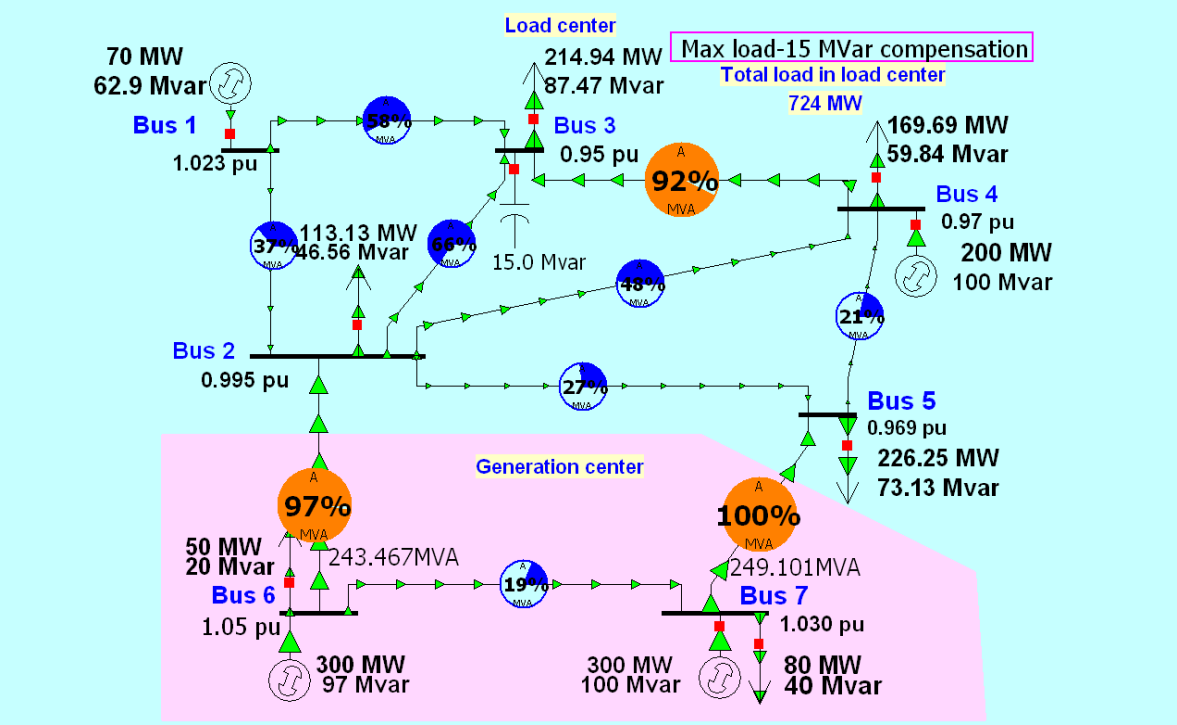

Figure 4.5. PoC (point of collapse) with 15MVar compensation.

(4.7-4.9) results

1) *B1* +*B2* calculation

Assuming the tie line transfer capacity limit stays constant after the Var compensation, the fuel cost drop owing to Var compensation can be divided into two parts, one is the loss cost reduction corresponding to *B1*, the other is more cheap power delivery to the customers corresponding to *B2* by reducing the reactive power transfer. The fuel cost difference between Base Case as shown in Figure 4.6 and Case1 as shown in Figure 4.7 is the sum of *B1* and *B2*:

$$B1 + B2 = z - z1 = \$15283.28/hr - \$15273.04/hr = \$10.24/hr$$

2) *B3* calculation

The above cases are all under the assumption of tie-line limit being constant, however, the maximum transfer capability of tie lines has been improved from 4.64 p.u. to 4.92 p.u. after Var compensation, as a result, the interface flow limit should be changed 4.92 x 75% = 3.69 p.u. considering the 25% security margin. Case2 is created by changing the tie-line limit form 3.48 p.u. to 3.69 p.u. The result is shown in Figure 4.8, the fuel cost reduction due to the tie-line maximum transfer capability improvement is as follows:

$$B3 = z1 - z2 = \$15273.04/hr - \$15169.13/hr = \$103.91/hr$$

In conclusion, the total economic benefits are $Bt = B1+B2+B3 = z - z2 = \$15283.28/hr - \$15169.13/hr = \$114.15/hr$, which is equivalent to \$7.61/MVar·hr. delivers 20.833 MW more to the load center in Case2 than in Case1, and the load center generates 20.82 MW less than in Case1. The slight difference, 0.013 MW, is due to the loss because of the additional MW transfer capability. The additional import of 20.833

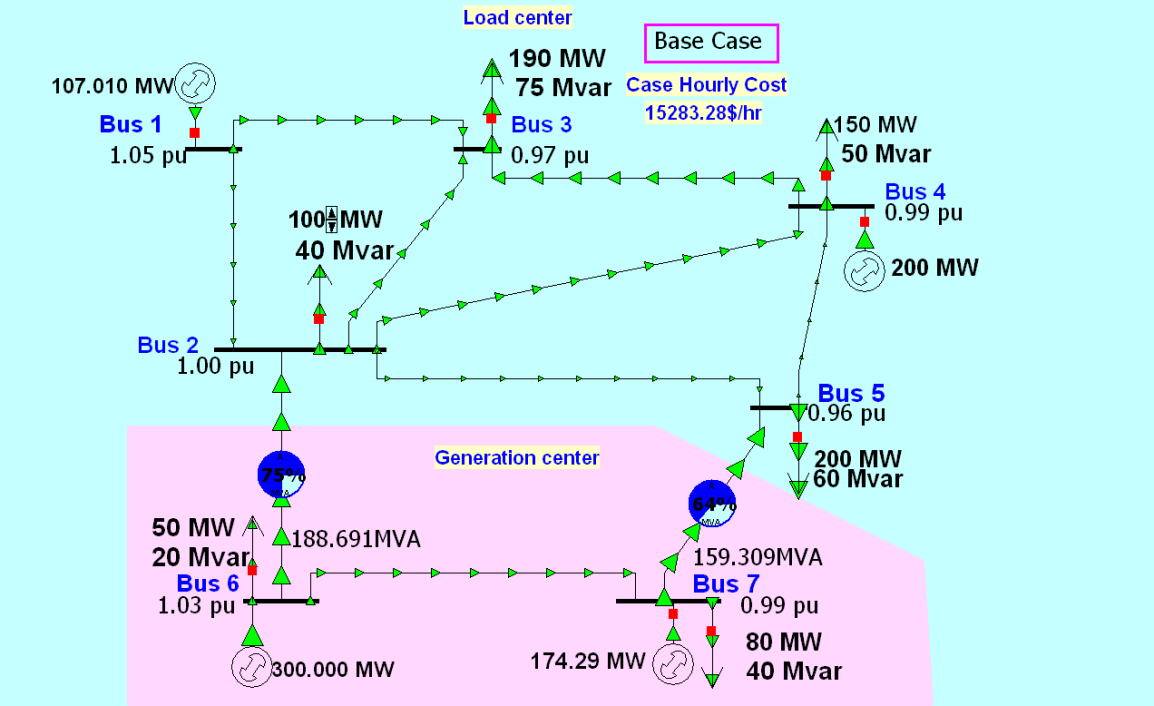

Figure 4.6. Base case.

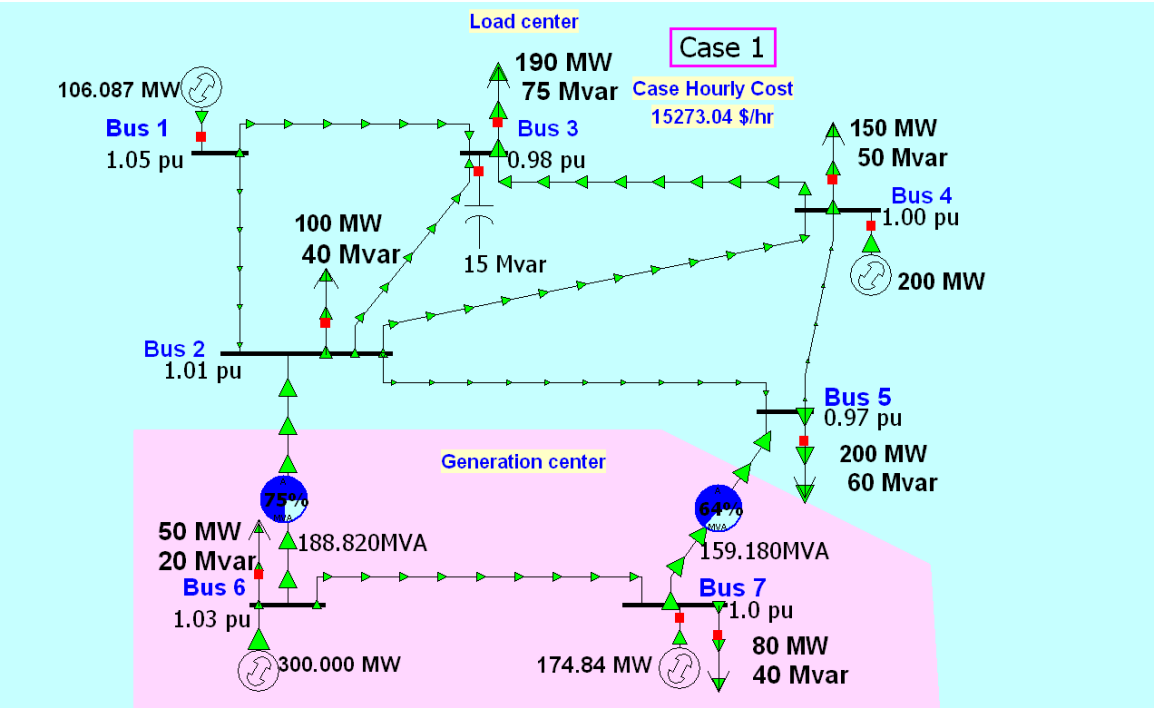

Figure 4.7. Case1.

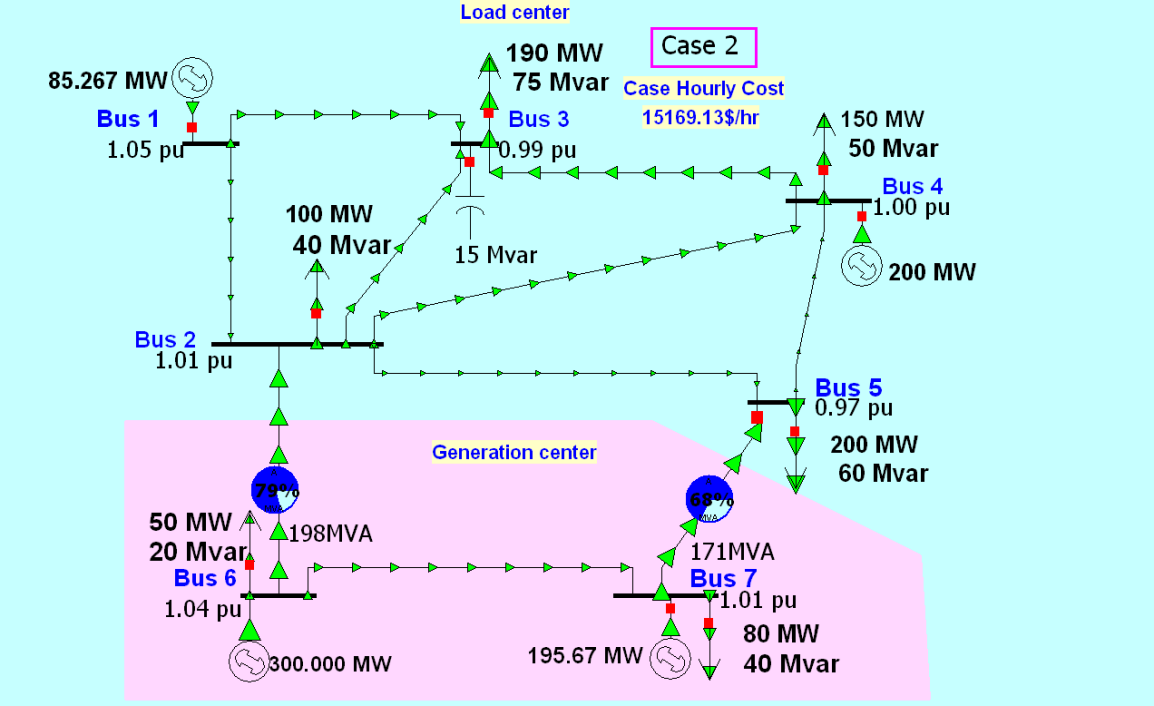

Figure 4.8. Case2.

(4.2-4.5) three cases results

Equation (4.2-4.5) also can be adopted to calculate the benefits. The detailed procedure is as follows. From Tables 4.3 and 4.4, it is shown that the total amount of dispatch has been reduced by 0.375 MW in Case1 from the Base Case. The dispatch of the generation center is increased by 0.547 MW. With the assumption that the reduced loss is due to the dispatch reduction at the load center, this implies that 0.547MW additional real power is dispatched from the generation center because of the shift of reactive power flow to real power flow. Hence, we have ΔP_{loss} = 0.375 MW and ΔP_{shift} = 0.547 MW.

Table 4.5 shows the test results from Case2, in which the transfer capability is increased from 348 MVA to 369 MVA. Table 4.5 shows that the generation center power

Table 4.3. Base Case Results.

System: **No Var source**, tie lines limit is **348** MVA				
Total fuel cost : 15283.28$/hr				
Real power loss: 11.30191MW				
Active power generation (MW)				
Bus	1	4	6	7
P_G	107.010	200.000	300.000	174.292
Interface flow (MVA)				
Tie Line	Line 6-2	Line 7-5	Total	
Flow	188.691	159.309	348	

Table 4.4. Case1 Results.

System: **15 MVar** source at Bus 3, tie lines limit is **348** MVA				
Total fuel cost : 15273.04 $/hr				
Real power loss: 10.92668MW				
Active power generation (MW)				
Bus	1	4	6	7
P_G	106.087	200.000	300.000	174.839
Interface flow (MVA)				
Tie Line	Line 6-2	Line 7-5	Total	
Flow	188.820	159.180	348	

Table 4.5. Case2 Results.

System: **15 MVar** source at Bus 3, tie lines limit is **369** MVA				
Total fuel cost : 15169.13$/hr				
Real power loss: 10.939343MW				
Active power generation (MW)				
Bus	1	4	6	7
P_G	85.267	200.000	300.000	195.672
Interface flow (MVA)				
Tie Line	Line 6-2	Line 7-5	Total	
Flow	198	171	369	

MW is very close to the increased transfer capability, 21 MVA (369 - 348). This means that almost all increased MVA capacity is used to deliver cheaper real power to the load center. This is very reasonable.

In this test, the average cost, weighted by generation changes, of the marginal units is employed to calculate the marginal cost of the whole generation (or load) center. Hence, considering fuel price and fuel consumption in $a + bP_{Gi}$, we have C_G = \$15/MWh and C_L = \$20/MWh. Please note the generator at Bus 4 and Bus6 is not considered when calculating C_G *and* C_L because they are at its maximum output and are not a marginal unit. Using (4.2-4.5), we can obtain the benefits as follows:

B1 = \$20/MWh x 0.375 MW = \$7.5/hr

B2 = (\$20/MWh - \$15/MWh) x 0.547 MW = \$2.735/hr

B3 = \$20/MWh x 20.82MW -\$15/MWh x 20.833MW = \$103.905/hr

Bt = *B1* + *B2* + *B3* = \$114.14 /hr

In this test, the two sets of equations (4.2-4.5) and (4.7-4.9) obtain very similar results. Equations (4.7-4.9) are more direct and simple as they only need one variable— fuel cost from each case. In addition, the results are accurate because no approximate assumption is made, but can not directly separate *B1* and *B2*. Equations (4.2-4.5) are very useful to separate *B1* and *B2*, however, the approximation for the fuel cost and loss lead to the error.

d payment comparison

The above simulation is a test for one hour. If multiple hours need to be simulated, we may simply employ a chronological simulation or some estimation from several typical

hours. Assuming that the *B2* and *B3* only exist during 4 peak months, and *B1* exists for the whole year, the total saving for the whole year is ($7.5/hr x 8760hr + ($2.735/hr + $103.905/hr) x 120day x 24hr) /15MVar = $26,047.2 /MVar·year.

As a reference and comparison, the capacity payment to central generators from ISOs may be used as a rough evaluation of the value of local Var compensation, because more local Var means less Var capacity from central generators. Various ISOs in the U.S. provide payment in the range of $1,000~$4,000/MVar-year to generators with reactive capability.

Another viewpoint of Var value is the penalties that may be applied to some U.S. power utilities. The penalties are set by the transmission companies or system operators to ensure the distributors meet the minimum power factor requirement. The power factor penalty costs are then passed to customers. The data among nationwide utilities shows that the typical penalty is about $0.10/kW-month [6], which may be translated to a few thousand $/MVar-year depending on the required power factor and the present low power factor. Despite the above two approaches for rough estimation of local Var value, they do not truly represent the economic benefits of the local Var support.

It can be verified that the total benefit in $/MVar-year is very comparable to the Var payment to central generators or power factor penalties, if the tie-line congestion is assumed to be a few months.

4.4 Conclusion

In this chapter, the economic benefits from Var sources are discussed through a quantitative approach. Certainly, it is not possible to include all benefits in the form of

dollars. However, the method developed in this chapter does present a systematic approach to quantify some important benefits from Var compensation in dollars. The conclusions and need for future work based on this research may be summarized as follows:

- The economic benefit to utilities from local Var compensation is significant if compared with the payment to central generators or power factor penalties.
- Other entities may have reduced or increased revenues from local Var compensation under each of the three benefit categories. Therefore, the allocation of the installation cost and operation benefit of Var compensators needs further investigations in the future.
- The major and quantifiable economic benefit may be classified into three categories: reduced losses, shifting reactive power flow to real power flow, and increased transfer capability.
- The economic benefit can be obtained by a set of OPF runs.
- Since the benefit is significant and comparable to the payment to central generators, it will be necessary to include DERs or other local Var sources into future Var markets.
- The separation of the three benefits may be helpful to design future reactive power market and pricing for different components. So, reasonable payment or revenue may be collected and distributed to different market participants.
- This paper assumes a constant Var injection and a fixed location. In the future, an in-depth analysis of different Var sources and locations is needed because they

may have different voltage-power characteristics.

The next chapter will discuss the reactive power economic benefit sensitivity to the size of Var compensation and sensitivity to the generator marginal cost. The sensitivities can be used to estimate the effect on the economic benefits variations in parameters such as size of Var compensation and generator marginal cost.

5 . SENSITIVITY ANALYSIS OF THE ECONOMIC BENEFIT OF REACTIVE POWER COMPENSATION

The previous chapter has discussed the economic benefits of local reactive power compensation. Under a competitive market environment, the economic efficiency should be considered with engineering requirements. This chapter investigates the sensitivity analysis of the economic benefit with respect to the size of the Var compensator and the generator marginal cost.

A new procedure is proposed in this chapter to estimate the economic sensitivity subject to different Var requirements. With the proposed model and procedure, system planning engineers may easily identify where the most economic upgrade can be achieved while respecting all engineering requirements among many different upgrade options, and what is the economic effect to the Var benefit if the generator marginal cost increases with the surge of the fuel price. Tests are performed in a standard system to verify the proposed approach.

5.1 Sensitivity of Var economic benefits with respect to the size of the ensator

In the case study of chapter 4, Var compensation Q_c is chosen as 15 MVar, a question maybe raised why the size of 15 MVar is selected? This question will be answered in this section. In fact, when Q_c is 15 MVar, the total economic benefits *Bt* reaches its peak. In

order to decide the optimal Var quantity, sensitivity analysis of Var economic benefits with respect to the size of the Var compensator is necessary, which has fundamental economic interpretation of the $ benefits associated with marginally increasing the Var quantity.

tal transfer capability (TTC)

This sensitivity may be obtained by increasing the variable of Var size step by step and solving the associated OPF nonlinear problems such as Base Case, Case1, Case2, and TTC. However, tie lie TTC is a parameter in Base Case and Case1 and Case2, especially it is closely associated with Q_c quantity in Case2; in other words, it changes in Case2 with the increase of Var size as shown in Figure 2.4. Minimizing fuel cost and the calculation of TTC can not be realized in just one OPF, as a result, tie line TTC vs. Q_c curve should be calculated beforehand.

Tie line transfer limit versus reactive compensation at bus 3 is shown in Figure 5.1. The tie line transfer limit equals tie line TTC x (1 - *SM*), *SM* is 25% in our cases. The tie line transfer limit rapidly increases from 3.48 p.u. and reaches its maximum value 3.69 p.u. when Q_c(bus3) increases from 0 to 15MVar, immediately followed by a slow decline to 3.5729 p.u. over the period of Q_c = 15MVar to 130MVar. After that, it gradually increases from 3.5729 p.u. to 3.6066 p.u. during the period of Q_c = 130MVar to 200MVar. The TTC OPF model becomes infeasible if the Q_c is greater than 200MVar, so the upper limit of Q_c size in this case is 200MVar.

Usually, TTC is considered to increase with more Var compensation, but it is only true in some specific Q_c range such as 0-15MVar and 130MVar-200MVar. On the

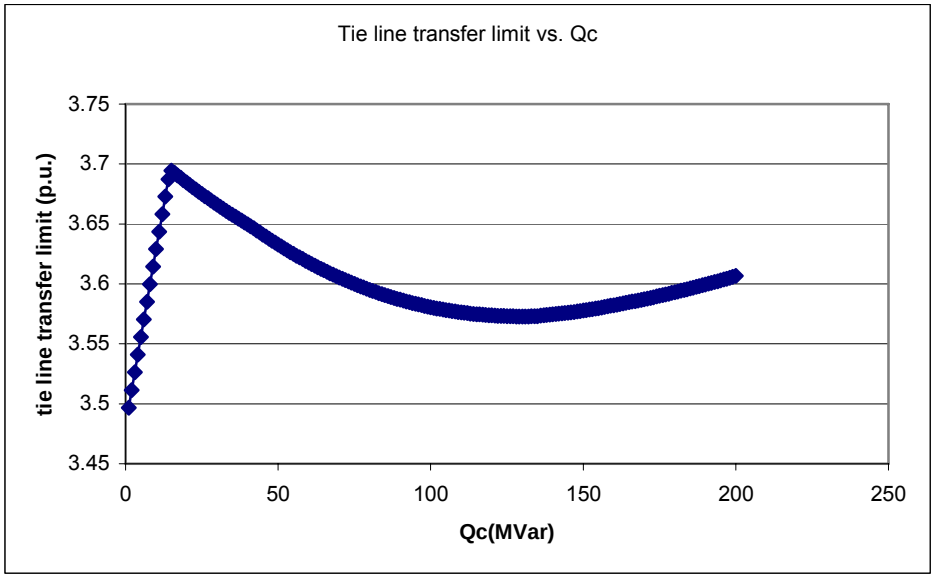

Figure 5.1. Tie line transfer limit versus reactive compensation at bus 3.

contrary, it becomes smaller with more Var compensation when Q_c = 15MVar-130MVar. This trend affects the benefit greatly.

In order to explore the shape of the tie line transfer limit vs. Q_c curve, some limits such as generator real power Pg, generator reactive power Qg, and voltage V constraints are relaxed respectively as shown in Figure 5.2. In practice, particularly when the power system is uniformly and highly stressed, there are often multiple limits encountered. Therefore, the tie line TTC may drop with Q_c going up. For example, if there is no Pg upper and lower limits, tie line TTC will be much higher than that with Pg limits after Q_c ≥15MVar. However, Pg limits do not take effect before Q_c = 15MVar since the blue line and green line overlap in that period. Thus the TTC curve shape depends on what limits it encounters.

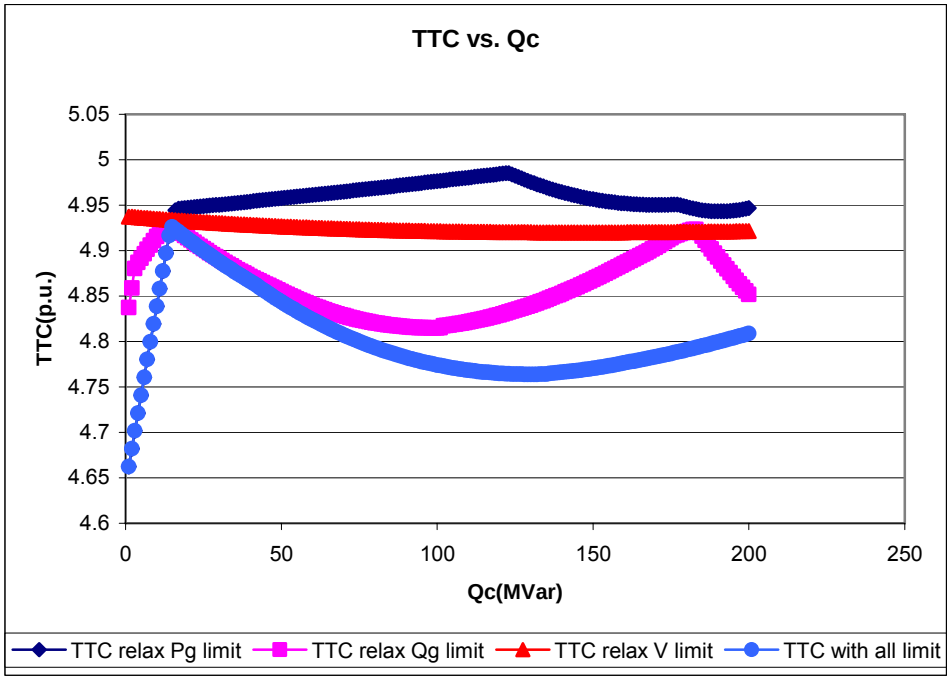

Figure 5.2. TTC with relaxed limits versus reactive compensation at bus 3.

eneral Algebraic Modeling System) procedure

The general scheme of GAMS will be summarized in this section. The basic procedure as applied to sensitivity analysis is shown in Figure 5.3. The GAMS process starts by repeating to solve the TTC model with different Q_c quantity from 1MVar-200MVar, the output is the tie line transfer limit L_1-L_{200} corresponding to Q_{c1}-Q_{c200}. The benefits calculation includes Base Case, Case1 and Case2 introduced in chapter 4.

The total fuel cost output is Z in Base Case, in which there is no Var compensation. Thus, Z will not change in the whole process. Repeating Case1 with Q_{c1}-Q_{c200} as input, the corresponding output of total fuel costs in Case1 are $Z_{1,1}$-$Z_{1,200}$. Then repeating Case2 with (Q_{c1}, L_1) - (Q_{c200}, L_{200}) as input, the corresponding output of total fuel costs in Case2 are $Z_{2,1}$-$Z_{2,200}$. Finally, $Bi_{,1}$ - $Bi_{,200}$ (i = 1,2,3) may be obtained following the procedure

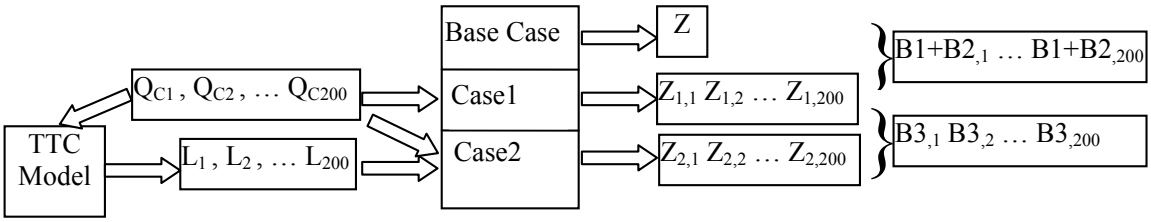

Figure 5.3. GAMS scheme for sensitivity analysis.

introduced in chapter 4. The most important feature in this process lies in the tie line transfer capability constraints changing corresponding to the quantity of Var compensation.

cost in three cases versus Var compensation at bus 3

The total fuel cost in Base Case, Case1 and Case2 versus Q_c(bus3) is shown in Figure 5.4. As introduced in section 5.1.2, Z keeps as constant during the whole process. Z_1 slips first and then climbs up at Q_c = 103 MVar. The minimum Z_1 is \$15247.12. Z_2 is closely relevant to Figure 5.2(a). It is easily noted that the shape of $Z_{2,1}$-$Z_{2,200}$ is exactly opposite to tie line transfer limit L_1-L_{200}. The reason is that the higher tie line transfer limit, the more cheap power can be delivered, then fuel cost becomes less.

mic benefits versus Q_c(bus3)

From the Figure 5.4, Var economic benefits versus Q_c(bus3) curves can be calculated directly by adopting equations (4.2-4.5) in chapter 4.

Benefit 1 from reduced losses vs. Var compensation shapes like a hill as shown in Figure5.5. The uphill part is due to the reduction of current flow from the injection of

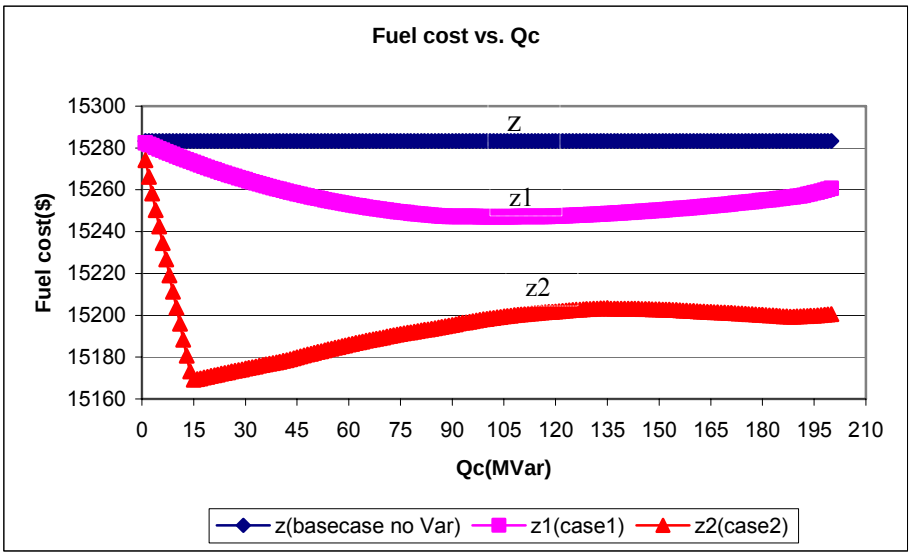

Figure 5.4. Fuel cost in five cases versus Var compensation at bus 3.

reactive power at the load center, therefore the lower losses increases benefit 1. The reason for the downhill part is the over injected reactive power that can not be consumed by the loads have to be balanced by generators. Therefore, the overprovided reactive power has to be transferred through the lines; as a result, the line current increases, then the I^2R losses increases. The top of the hill is \$23.74 at Q_c = 87MVar.

Benefit 2 from shifting reactive power flow to real power flow vs. Var compensation is shown in Figure 5.6. *B2* increases from zero to about \$14.00 until saturation at Q_c = 90MVar.

Benefit 3 from increased maximum tie line transfer capability vs. Var compensation is shown in Figure 5.7. The shape of Figure 5.7 is the same with Figure 5.2 due to the greater tie line transfer capability the more cheap power can be delivered from generation center to load center, therefore, the more benefit 3. *B3* reaches its peak \$103.91 at Q_c = 15Mvar.

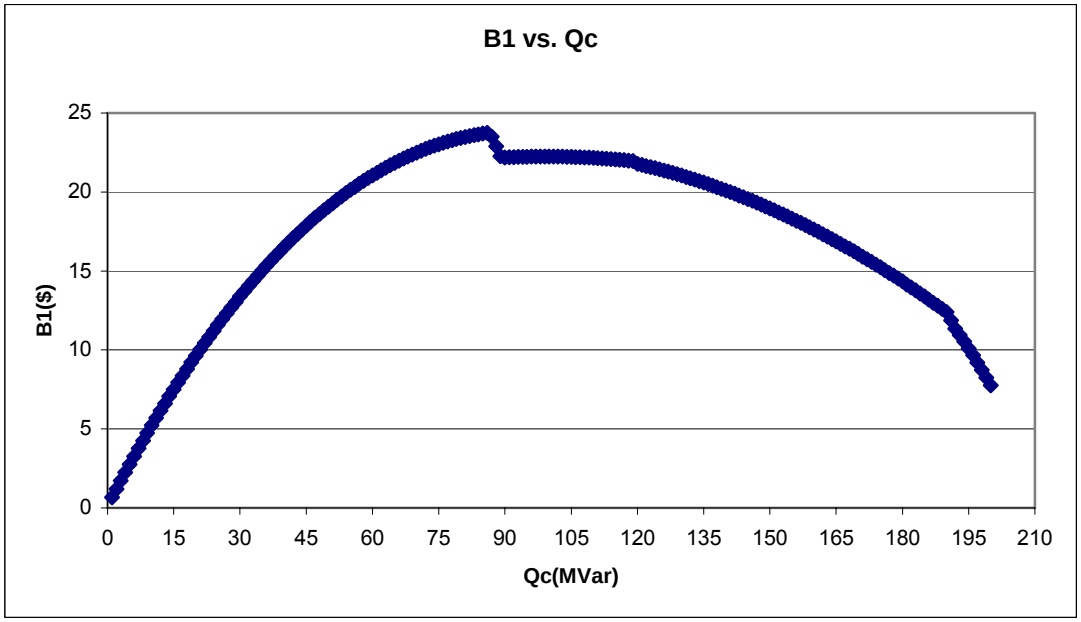

Figure 5.5. Benefit 1 versus Var compensation at bus 3.

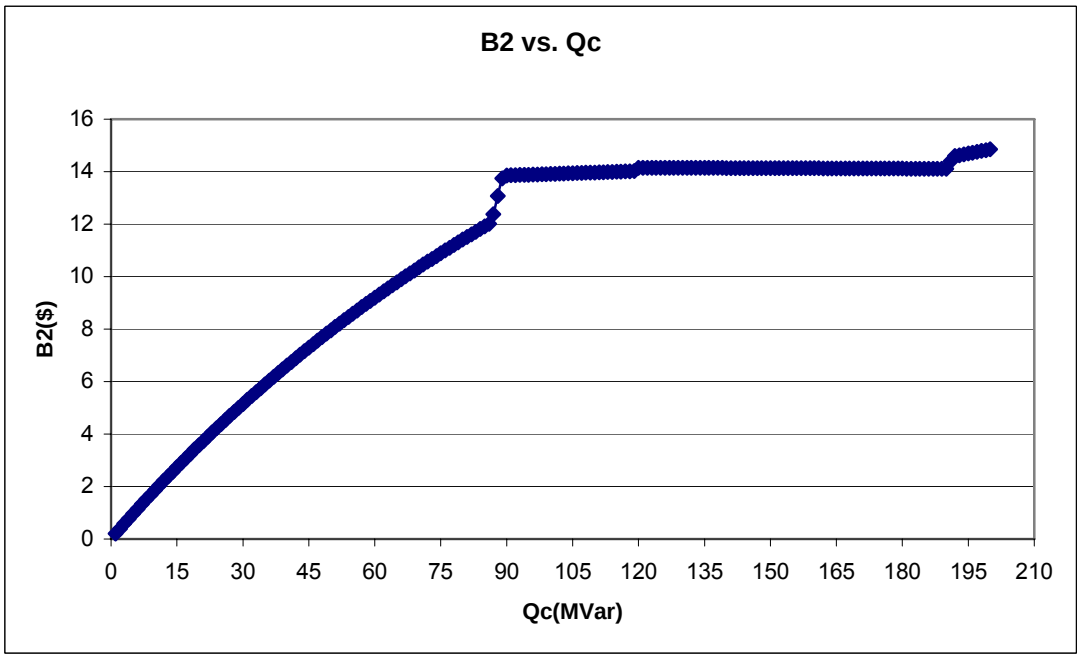

Figure 5.6. Benefit 2 versus Var compensation at bus 3.

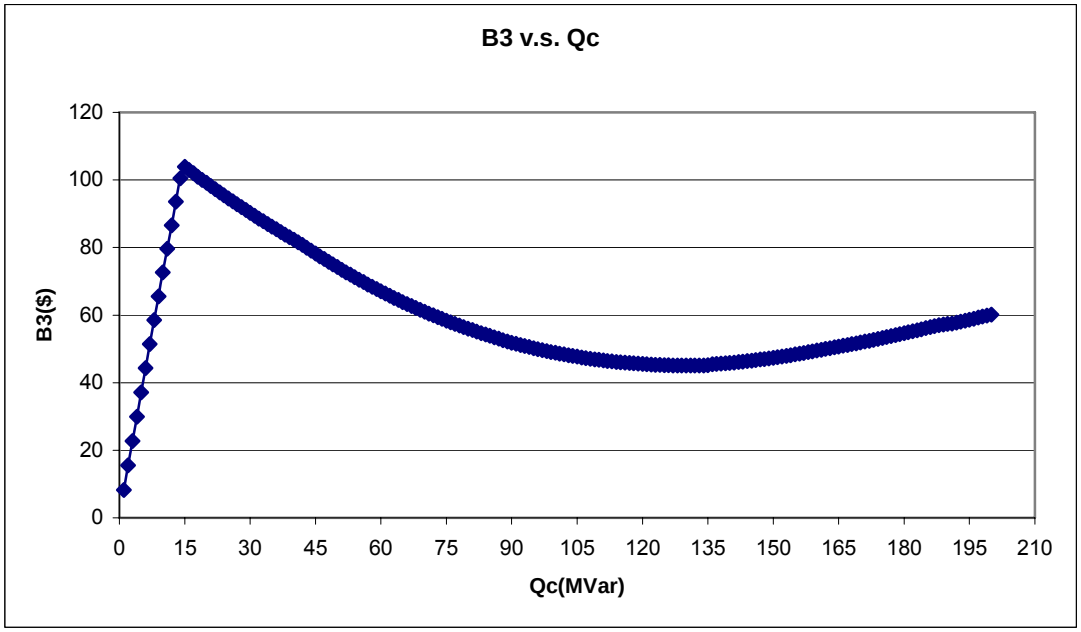

Figure 5.7. Benefit 3 versus Var compensation at bus 3.

In reactive power planning, the total benefit *Bt* is generally the most important; the criteria of location and size selection is to get maximum total benefit. The total benefit *Bt* including *B1*, *B2*, and *B3* vs. Var compensation is shown in Figure 5.8. *Bt* reaches its maximum value \$114.15 at Q_c = 15Mvar. This means if the Var is over_compensated more than 15Mvar, the potential economic benefits will decrease. In one word, continuously increasing Var is not necessarily better; the benefits may decrease at some point with the Var compensation increasing.

Figure 5.9 gives us a whole picture for the economic benefits changing tendency with Var compensation. *B1*-*B3* and *Bt* are shown in one picture for convenient comparison.

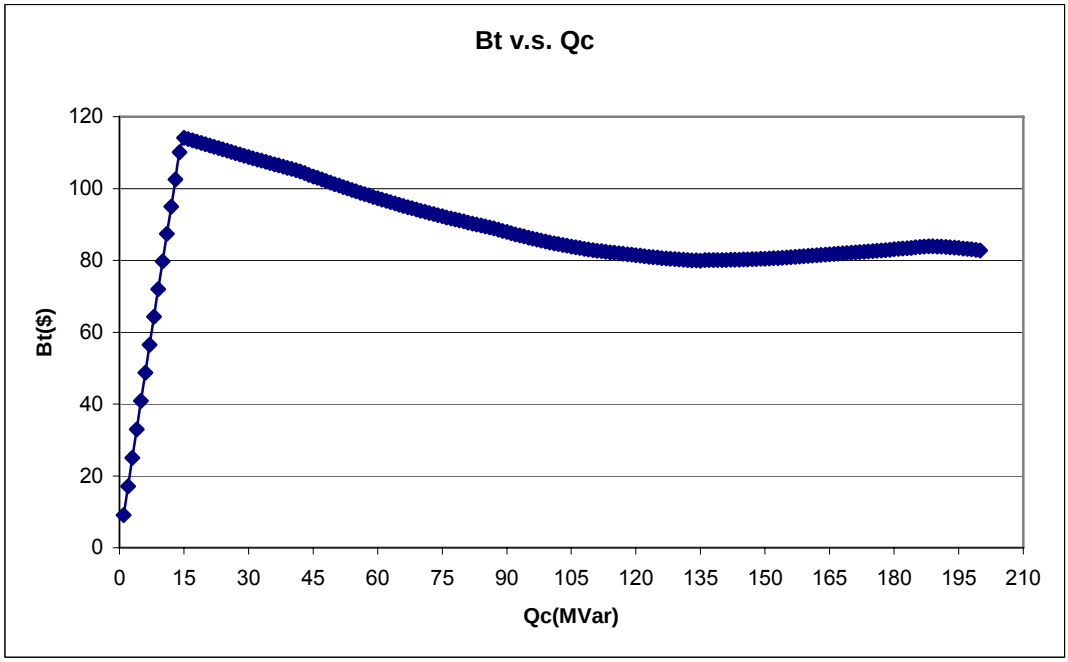

Figure 5.8. Total benefit versus Var compensation at bus 3.

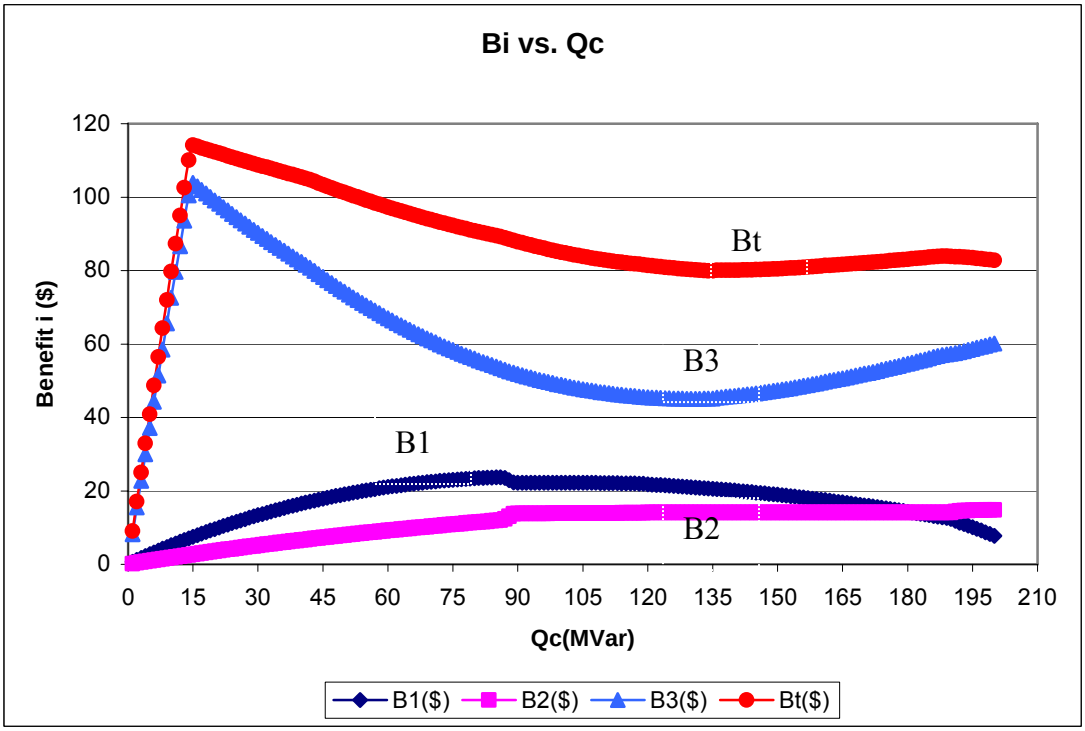

Figure 5.9. B1-B3 & Bt versus Var compensation at bus 3.

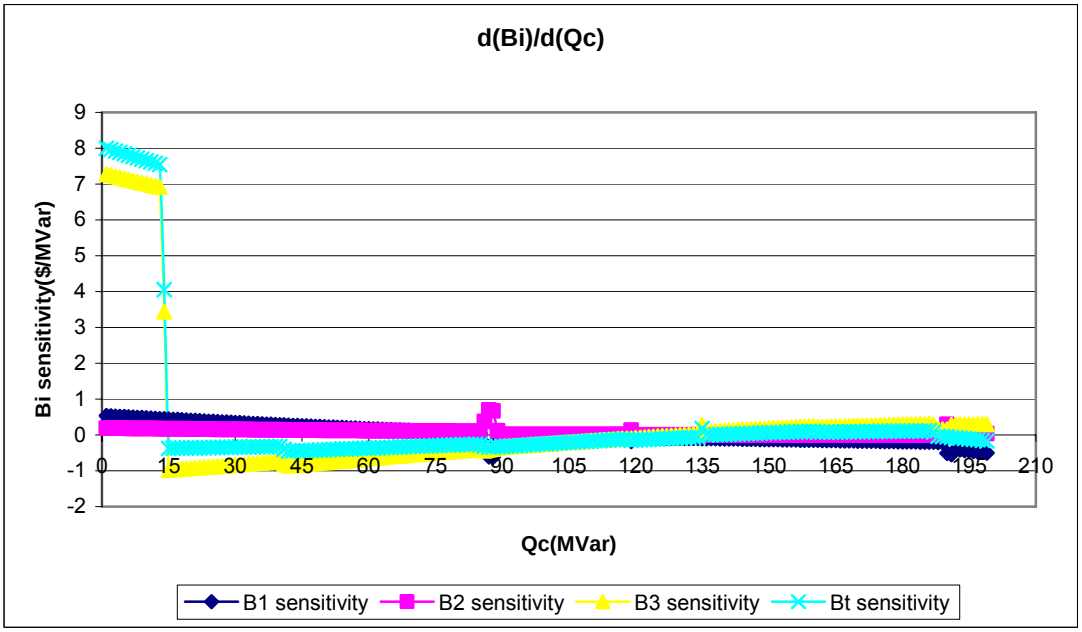

Figure 5.10. Bi sensitivity versus Var compensation at bus 3.

of Var economic benefits versus Var compensation

Sensitivity of Var economic benefits including $\frac{\partial B1}{\partial Q_C(3)}$, $\frac{\partial B2}{\partial Q_C(3)}$, $\frac{\partial B3}{\partial Q_C(3)}$, *and* $\frac{\partial Bt}{\partial Q_C(3)}$

versus $Q_c(3)$ is shown in Figure 5.10. Generally, Figure 5.9 and Figure 5.10 reflect the same principle, but it is obvious in Figure 5.10 the sensitivity becomes negative from positive at some specific point, which is the maximum point in Bi (i = 1,2,3) vs. Q_c curve. This point may be a useful indicator in deciding the Var size.

rt cost allocation

However, people may ask why Bi (i = 1,2,3) sensitivity is needed if Bt sensitivity is enough for reactive power planning analysis? The answer is Bi (i = 1,2,3) sensitivity is very useful for "Var support cost allocation". While the Var planning model determines the optimal location and size of Var support, it does not directly provide any means to

allocate the costs among the generators, transmission, and load customers in a deregulated market framework.

There is no a standard method to allocate the Var cost, which prevents people from installing some expensive Var compensator such as STATCOM because it is unclear who should pay for it. The problem of cost allocation is a hotly debated topic. We propose to allocate the Var cost based on the economic benefits percentage among the generators, transmission, and load customers, but allocation cost among different load customers will not be covered in this proposal.

Assuming 15MVar compensation is injected at bus 3, the load will pay less due to the benefits 1-3, the total amount is *Bt*. The IPP units at the load center will receive reduced revenue due to the reduced dispatch, so IPPs can not get any benefits, they will be excluded in the cost allocation, or even receive compensation at a rate acceptable to all parties.

The units at the generation center will have reduced revenue due to benefit 1, but have increased revenue due to benefit 2 and 3. The reduced dispatch of generation center in benefit 1 analysis is R1 MW, while the increased dispatch in benefit 2 and 3 analysis is R2 MW and R3 MW respectively. So, the total revenue is (R2+R3-R1) x generator marginal price. The transmission company may receive more transmission tariff due to the increased MVA flow (T1) mainly though the tie line in benefit 3 analyses.

In conclusion, the utility will get economic benefit *Bt* ($/hr), generator center will obtain benefit in dollars as (R2+R3-R1) x generator marginal cost ($/hr), the transmission company will gain T1 x transmission tariff ($/hr). Var cost allocation can follow the ratio of these benefits.

5.2 Sensitivity of Var economic benefits with respect to the generator cost

The natural gas price surged at around 2000; as a result, the marginal cost of some generators burning gas is also rising. What is the effect of generator marginal cost increase on the Var economic benefits? This section is conducted in response to the sharp increase in gas price and the corresponding generator marginal cost. The section focuses on two situations (1) load center generator marginal cost increase, (2) generator center generator marginal cost increase. These two situations have different effect on the economic benefits.

marginal cost increase in load center

The marginal costs of the generators at bus1, bus4, bus6, and bus7 in the case are \$20/MWhr, \$19/MWhr, \$14/MWhr, and \$15/MWhr respectively. One hundred steps will be executed to increase the generator marginal cost. In total, \$10/MWhr cost increase will be tested using \$0.1/MWhr for every step.

Generator dispatch in Base Case, Case1, and Case2 versus generator marginal cost increase at bus 1 is shown in Figure 5.11-5.13. The generator at bus1 is already the most expensive one in the four generators. It will keep as the most expensive one when its marginal cost increases. That is why its cost increase can not affect the dispatch as shown in the figures.

However, the average cost of the generators at the load center C_L becomes higher and higher, even the average cost of the generators at the generation center C_G, the shift of reactive power flow to real power flow ΔP_{shift}, and the increased real power transfer

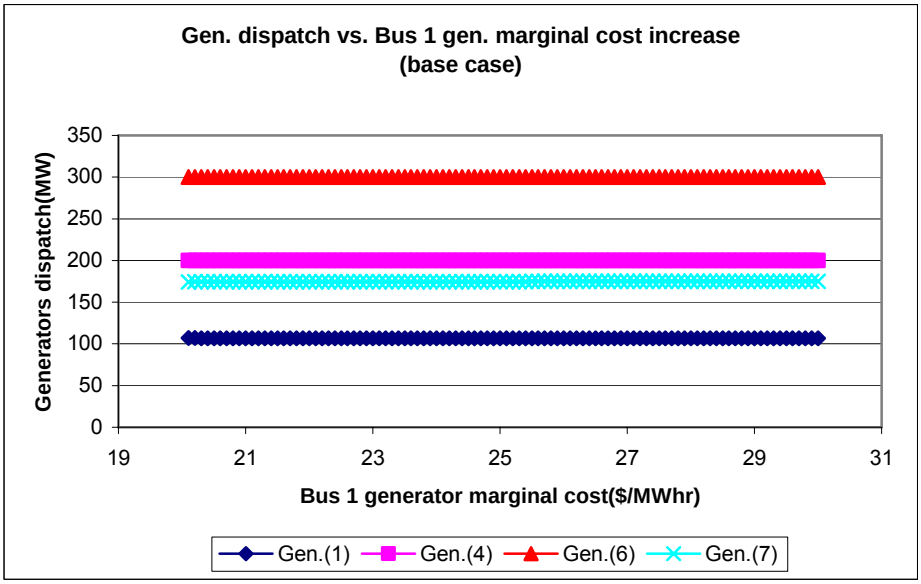

Figure 5.11. Generators dispatch in base case versus generator marginal cost increase at bus 1.

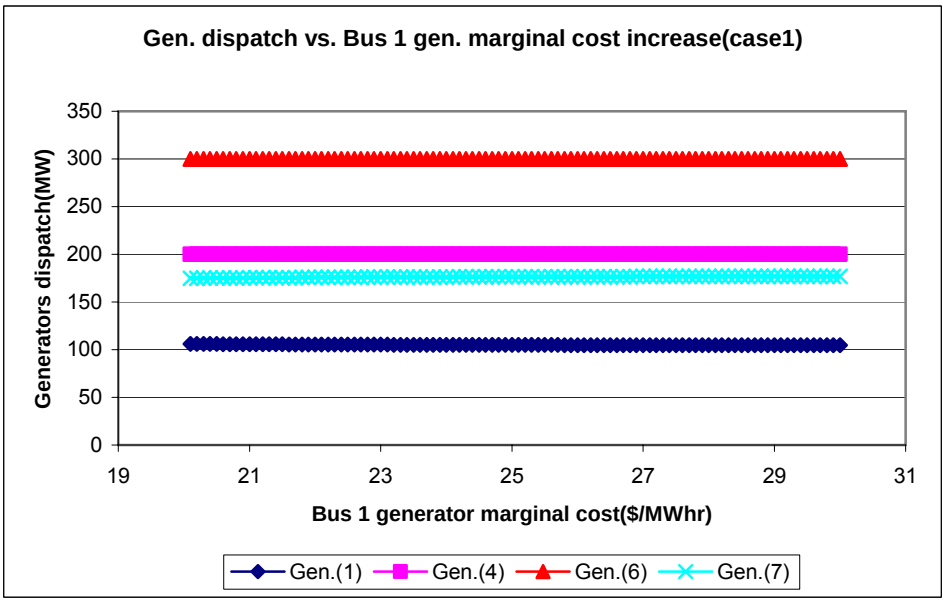

Figure 5.12. Generators dispatch in case 1 versus generator marginal cost increase at bus 1.

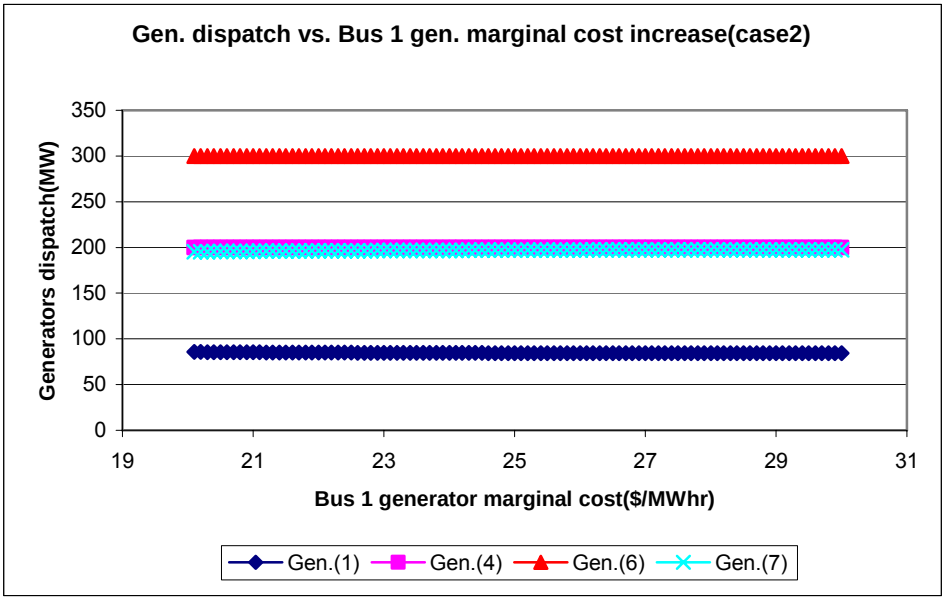

Figure 5.13. Generators dispatch in case 2 versus generator marginal cost increase at bus 1.

ΔP_{inc_trans} is kept as constant due to the unchanged dispatch. From the equations $B2 = \sum_{congested\ hours} (C_L - C_G) \cdot \Delta P_{shift}$ and $B3 = \sum_{congested\ hours} \left(C_L \cdot \Delta P_{inc\_trans\_L} - C_G \cdot \Delta P_{inc\_trans\_G} \right)$, it can be concluded that *B2*, *B3*, and *Bt* will linearly increase with the bus1 generator marginal cost increase as shown in Figure 5.14.

Generators dispatch in base case, Case1, and Case2 versus generator marginal cost increase at bus 4 are shown in Figures 5.15-5.17. The generator at bus4 is the second most expensive one in the system. Its dispatch keeps as a constant at the beginning until it drops to some lower level because it becomes the most expensive generator with the marginal cost increase. At the same time, the dispatch of generator at bus1 increases to compensate the dropped part of bus4 generator because bus1 generator is cheaper to dispatch.

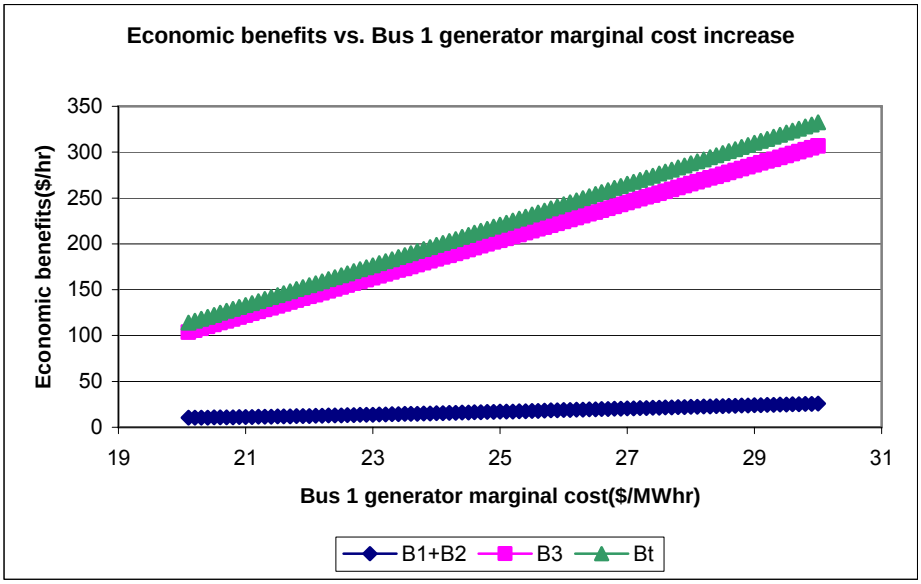

Figure 5.14. Economic benefits versus generator marginal cost increase at bus 1.

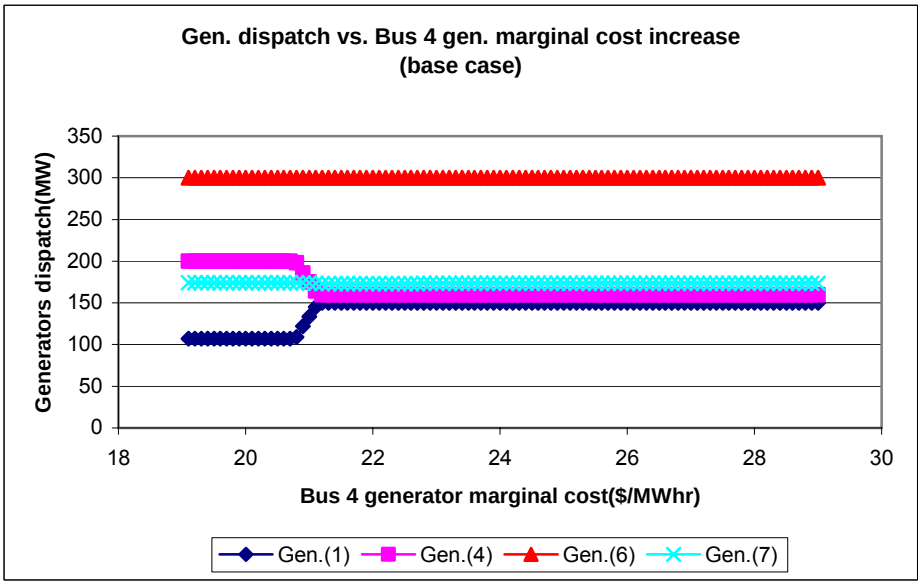

Figure 5.15. Generators dispatch in base case versus generator marginal cost increase at bus 4.

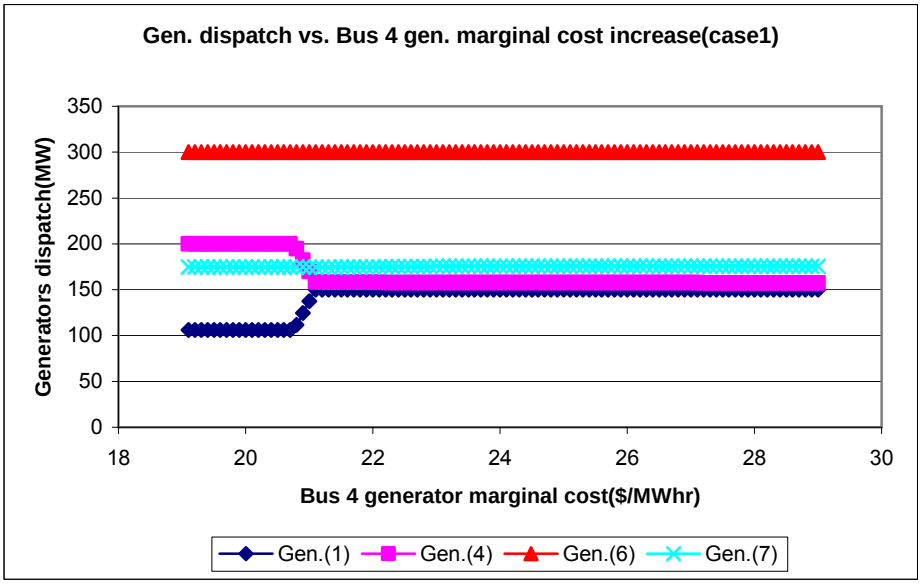

Figure 5.16. Generators dispatch in case 1 versus generator marginal cost increase at bus 4.

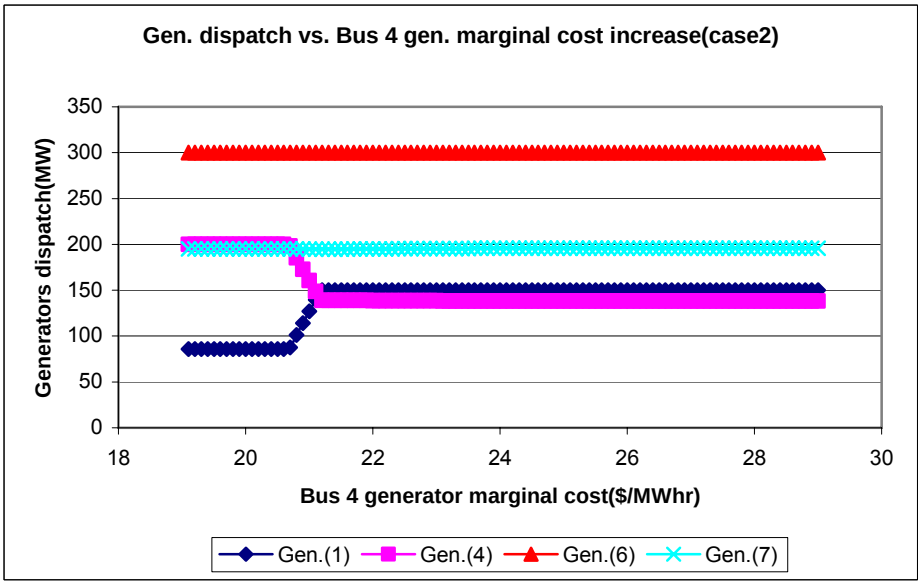

Figure 5.17. Generators dispatch in case 2 versus generator marginal cost increase at bus 4.

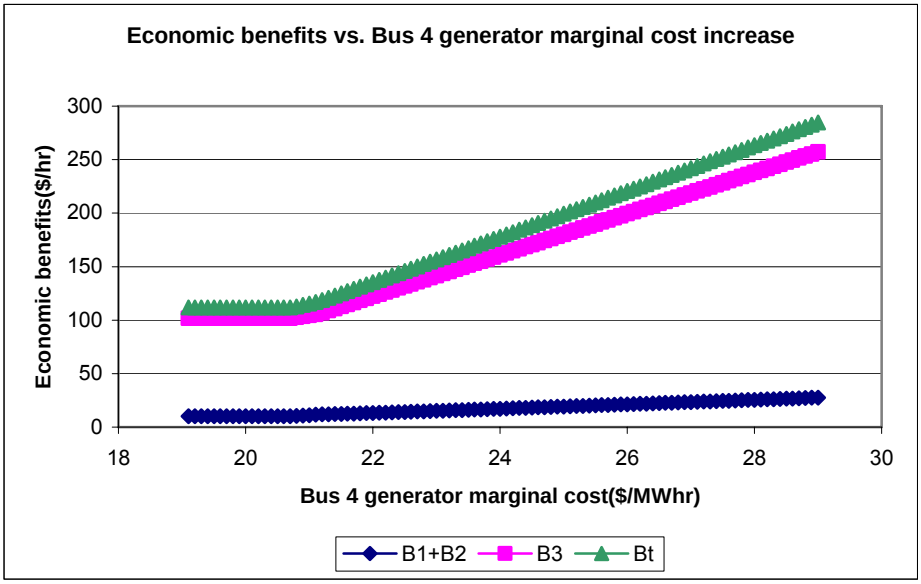

Figure 5.18. Economic benefits versus generator marginal cost increase at bus 4.

As the bus1 generator marginal cost increase, *B2*, *B3*, and *Bt* will linearly increase with the C_L becoming higher and higher when generator's dispatch keeps as constant, which is only partially true in Figure 5.18, Economic benefits versus generator marginal cost increase at bus 4.

It is easily noted that the *B1*, *B2* and *B3* are constant at the beginning of the curve when bus4 generator is fully dispatched 200MW, even C_L becomes higher and higher. That is due to the fact that the margin is zero and the marginal cost is infinity for a fully dispatched generator, alternatively, the marginal cost does not change until the dispatch of bus4 generator is less than 200MW.

The generator marginal cost in load center increase has positively contributed to the Var economic benefits since the generator marginal cost difference between load center and generation center is positive in proportion to the benefits. Thus, any time the fuel

increases in the load center the economic benefits tend to increase also. The Var compensator user will not suffer from continuous generator marginal cost increase in load center.

marginal cost increase in generator center

Generators dispatch in base case, Case1, and Case2 versus generator marginal cost increase at bus 6 are shown in Figures 5.19-5.21. The bus6 generator is the cheapest one in the four generators. The dispatch does not change until generator marginal cost at bus6 exceeds that of bus7, which leads to bus7 generator fully dispatched instead of bus6 generator, because the bus7 generator becomes the cheapest one.

There is another dispatch exchange between the generators at bus6 and bus1 when generator marginal cost at bus6 exceeds that of bus1; as a result, bus1 generator is fully

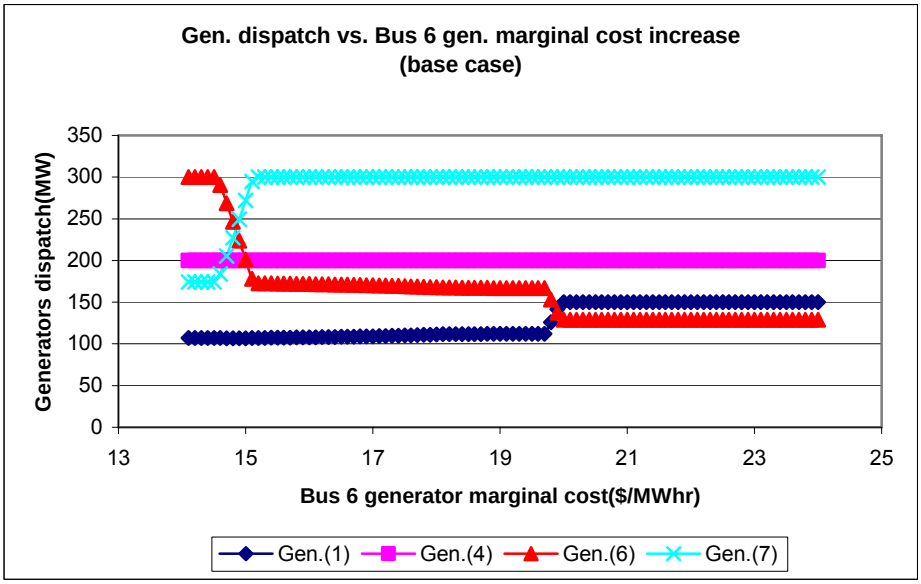

Figure 5.19. Generators dispatch in base case versus generator marginal cost increase at bus 6.

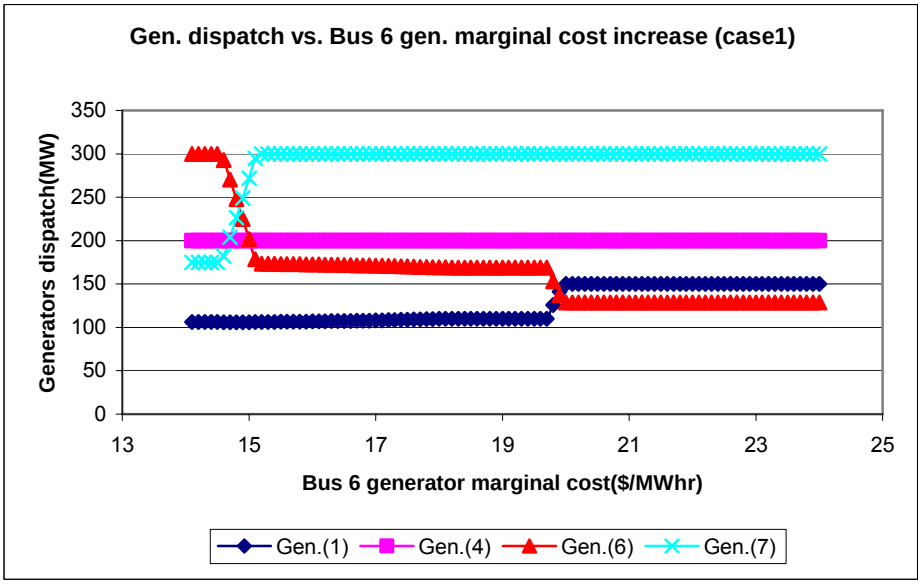

Figure 5.20. Generators dispatch in case 1 versus generator marginal cost increase at bus 6.

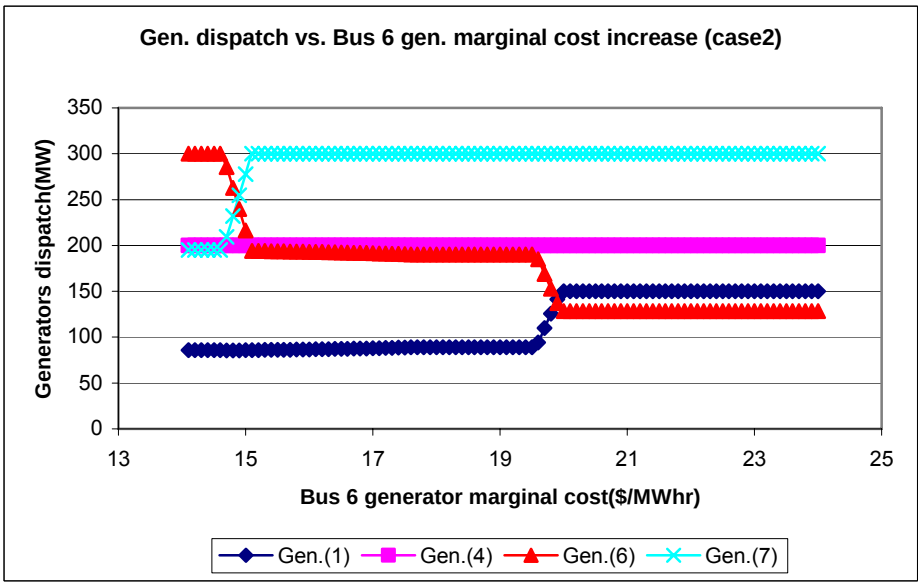

Figure 5.21. Generators dispatch in case 2 versus generator marginal cost increase at bus 6.

dispatched. In terms of bus4 generator fully dispatched, there is no dispatch exchange between the generators at bus6 and bus4; otherwise, there will be three dispatch exchanges.

Similar to the Figure 5.18, Var economic benefits remain unchanged at the beginning part concerning bus6 generator fully dispatched in Figure 5.22, Economic benefits versus generator marginal cost increase at bus 6. Afterward, it is followed by a steep decline until benefit 3 drops to zero, as a result of the average cost difference of the generators at the generation center and the load center (C_L- C_G) shrinking. The curves in Figure 5.22 end as a constant with regard to three of the four generators fully dispatched.

Generators dispatch in base case, Case1, and Case2 versus generator marginal cost increase at bus 7 are shown in Figures 5.23-5.25. One dispatch exchange happens between bus7 generator and bus1 generator when the marginal cost at bus7 goes beyond

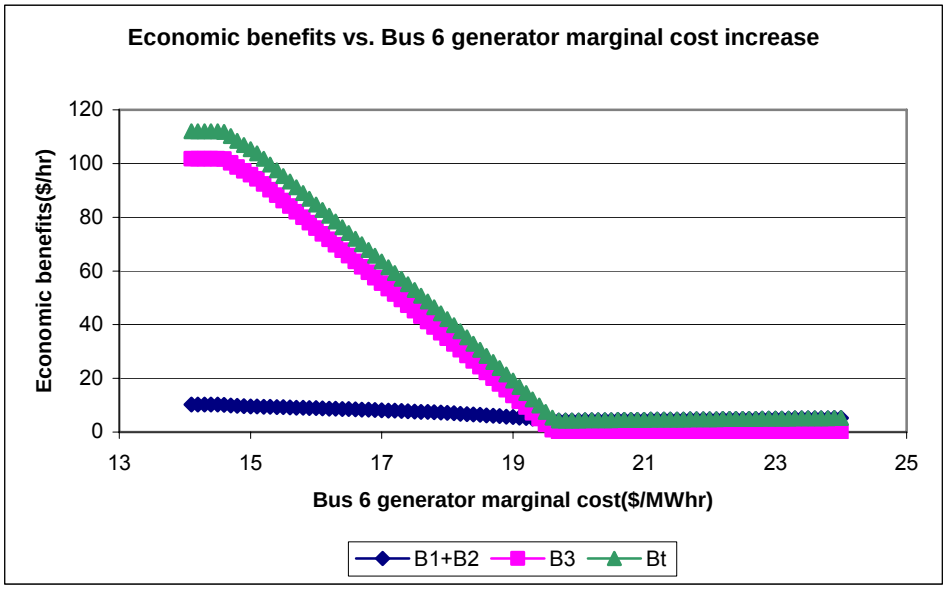

Figure 5.22. Economic benefits versus generator marginal cost increase at bus 6.

that of bus1, the dispatches before and after the exchange all remain constant.

Figure 5.26 demonstrates the economic benefits versus generator marginal cost increase at bus 7. Its trend is very similar to Figure 5.22 except the beginning constant part of the curve as bus7 generator is not fully dispatched initially, then benefits drop with the (C_L- C_G) shrinking from the start until the generators at bus 1, 4, 6 are all fully dispatched. The marginal cost increase in generator center could be attributed to the Var benefits decrease. In other words, the increased tie line transfer capability is worthless if no cheaper power is ready to be transferred.

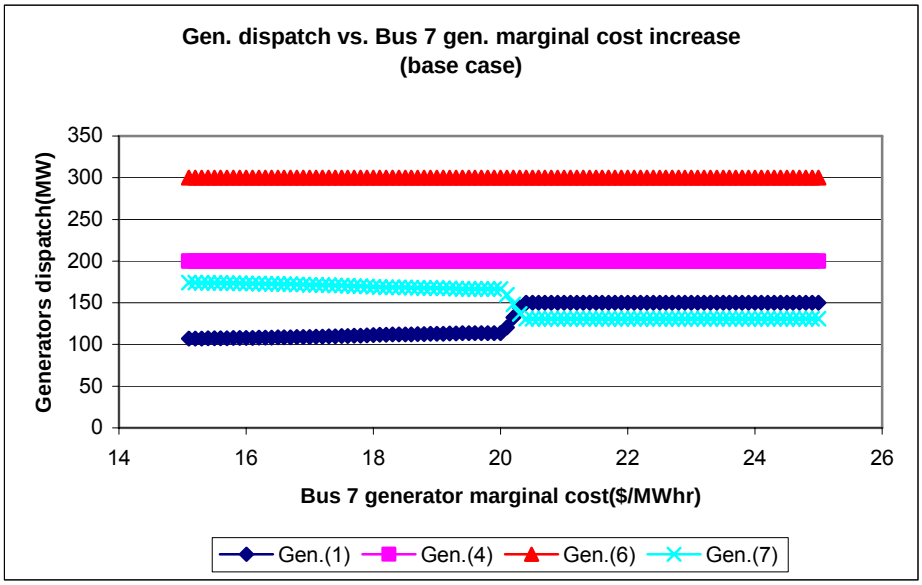

Figure 5.23. Generators dispatch in base case versus generator marginal cost increase at bus 7.

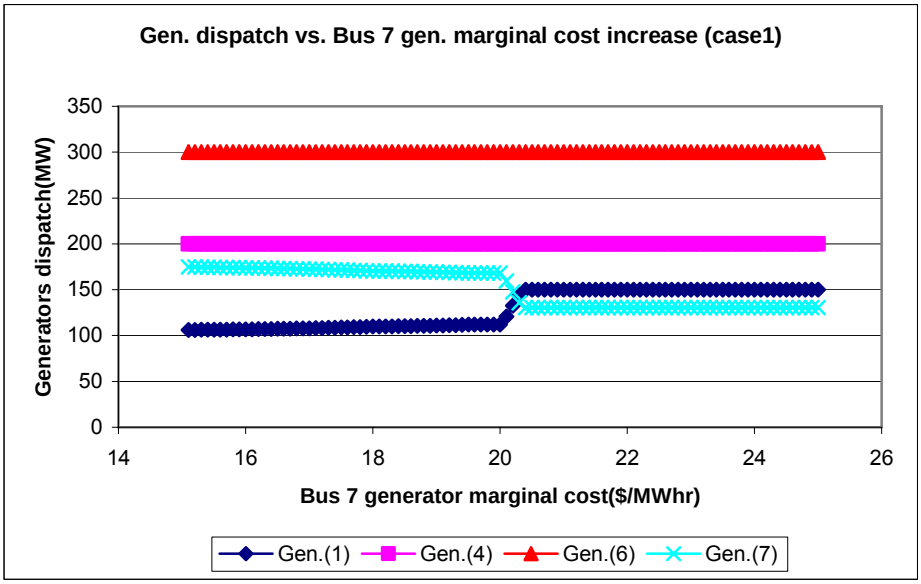

Figure 5.24. Generators dispatch in case 1 versus generator marginal cost increase at bus 7.

.

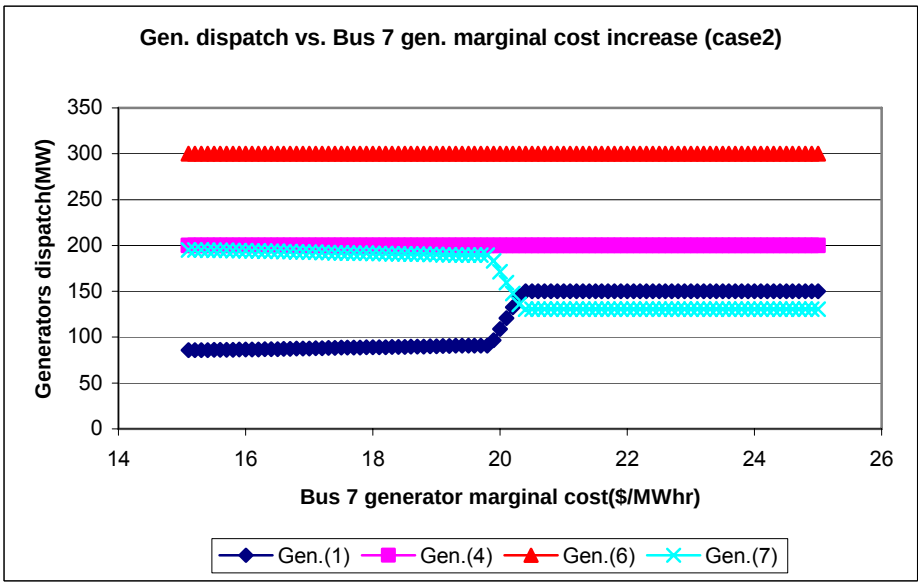

Figure 5.25. Generators dispatch in case 2 versus generator marginal cost increase at bus 7.

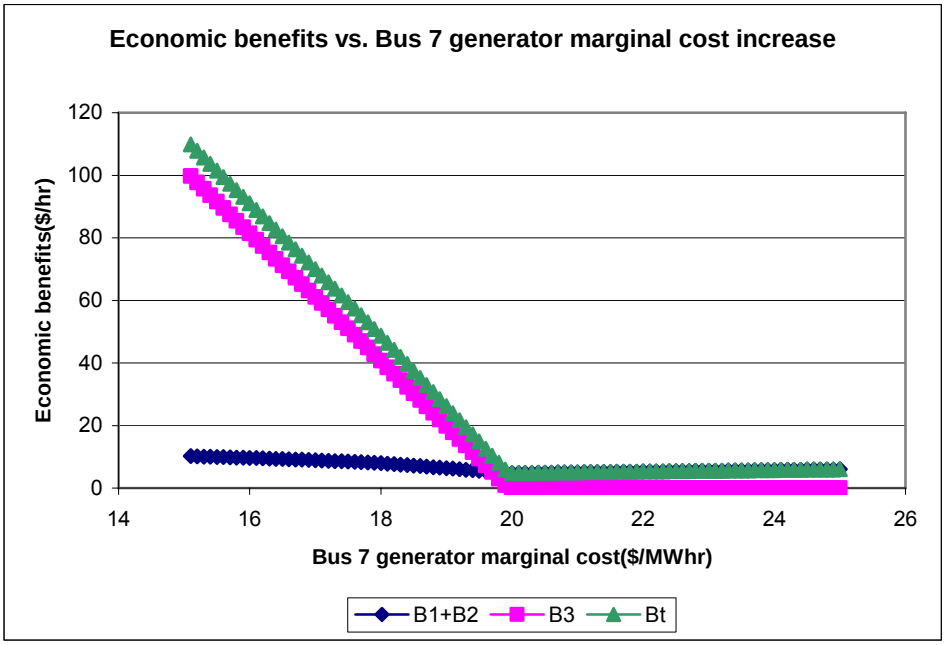

Figure 5.26. Economic benefits versus generator marginal cost increase at bus 7.

5.3 Conclusions

The conclusions based on this chapter may be summarized as follows:

- The sensitivity analysis of Var economic benefits with respect to the size of the Var compensator is adopted to decide the optimal Var quantity.
- A new procedure is proposed in this chapter to estimate the economic sensitivity subject to different Var size.
- The most important feature in this procedure lies in the change of the tie line transfer capability constraints corresponding to different amount of Var compensation.
- Continuously increasing Var is not necessarily better; the benefits may decrease at some point with the Var compensation increase.

- The shape of benefit 3 versus Q_c is the same with tie line transfer capability versus Q_c, due to the increased tie line transfer capability allows additional cheap power delivered from generation center to load center, therefore, the more benefit 3.
- *Bt* versus Q_c is used for Var planning, *Bi* (i=1,2,3) versus Q_c is helpful for "Var support cost allocation" among the generators, transmission, and distribution in a deregulated market framework.
- The sensitivity analysis of Var economic benefits with respect to the generator marginal cost is used to predict the Var benefits change if the fuel price continuously increases.
- The interesting trend revealed in the marginal cost sensitivity analysis is the positive relationship between the generator marginal cost in load center and the Var economic benefits, and negative relationship between the generator marginal cost in generation center and the Var economic benefits.
- The reason is the average generator marginal cost difference between load center and generation center is positive in proportion to the benefits.
- In general, the generators in load center are more expensive gas turbine generators whose cost is easily affected by the fuel price, so the positive relationship between the marginal cost and the benefits is common.

The main content in the next chapter is the future work including location selection based on economic benefit sensitivity analysis, a new VSCOPF (voltage stability constrained optimal power flow) model to solve location and size problem in one model, and a detailed STATCOM model incorporated in the VSCOPF.

6 . ENUMERATION METHOD FOR REACTIVE POWER PLANNING BASED ON VAR ECONOMIC BENEFITS

The assumption in Chapter 4 and Chapter 5 is that the location and size of Var compensator are assigned arbitrarily or based on engineering or financial constraints. However, this assumption may not be always true in engineering practices. The further research work will focus on optimal location and size decision strategy based on maximum economic benefits considering technical requirements such as voltage stability.

In this chapter, an enumerative method based on Var economic benefits is proposed to incorporate voltage stability margin in the reactive power planning. The study on Var planning presented in this chapter is a straightforward, two-step approach: 1) it utilizes an Optimal Power Flow (OPF) model to update the Total Transfer Capability (TTC) for different Var amounts and at different locations in order to give a more accurate evaluation of Var benefits, which is not clearly shown in the literature; 2) it then performs two OPFs for each Var location and amount combination to evaluate the Var benefits in three categories. Although this approach may be time-consuming, it does give a full spectrum and insightful information about the benefits under different categories if a Var compensator is installed at a specific location and a specific amount compared with considering only two benefits (*B1* + *B2*) in the literature. Hence, the sensitivity of economic benefits under different categories will be easily obtained. This approach may be used for benchmarking. In addition, the test results from a seven-bus system in this chapter show that it is not always economically efficient if Var compensation increases

continuously. As an example, tests are conducted on a system with seven buses in two areas and three Var installation candidate locations.

6.1 Introduction to Enumeration method

In order to decide the optimal Var quantity, sensitivity analysis of Var economic benefits with respect to the size of the Var compensator is necessary, which has fundamental economic interpretation of the $ benefits associated with marginal increase of the Var quantity.

The sensitivity to the Var quantity is a good indicator not only for size selection but also for location decision. In the economic benefits analysis, the location is fixed; if some other buses as potential candidates for Var compensator installation are tried for the benefit sensitivity analysis, a series of benefits versus Q_c curves at different buses may be obtained.

The optimal location can be achieved by a comparison of the net benefit (total benefit - Var cost) as shown in Figure 6.1 at all candidate buses, which is called *enumeration* method. If the maximum net benefit is the goal to achieve in reactive power planning, the location and amount at highest net benefit will be chosen as the optimal solution. Please note that if the cost-effectiveness is the goal, then a cost-benefit analysis can be easily employed on top of the benefit analysis in this work to identify the most cost-effective location and size of Var compensation. Nevertheless, consideration of Var cost imposes little additional mathematical complexity since it can be simply addressed by subtracting the Var cost in the objective function or other similar approaches.

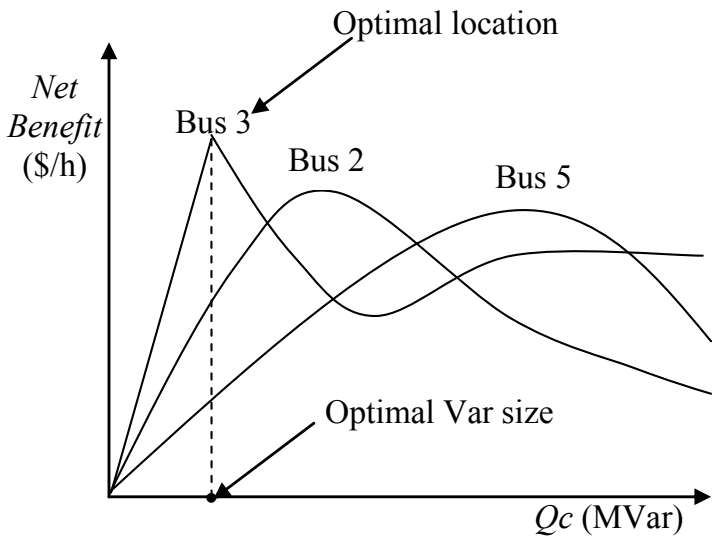

Figure 6.1. Identify the optimal Var size and location from net benefit versus Qc curve.

6.2 Implementation of Enumeration Method

The sensitivity of economic benefits with respect to the Var quantity may be obtained by increasing the Var compensation amount gradually and solving the associated OPF nonlinear problems such as Base Case, Case 1, Case 2, and TTC (total transfer capability). However, tie line TTC is a parameter in Base Case, Case 1, and Case 2. Especially, it is closely related to Q_c quantity in Case 2. In other words, the tie line TTC changes in Case 2 with the increase of Var size as shown in Figure 6.2. Minimizing fuel cost and the calculation of TTC cannot be realized in just one OPF, as a result, tie line TTC vs. Q_c curve should be calculated with the procedure introduced in section 4.2.2 (i.e., OPF model for the calculation of total transfer capability) before the reactive power planning process (i.e., another OPF model for minimizing fuel cost considering Var size and location).

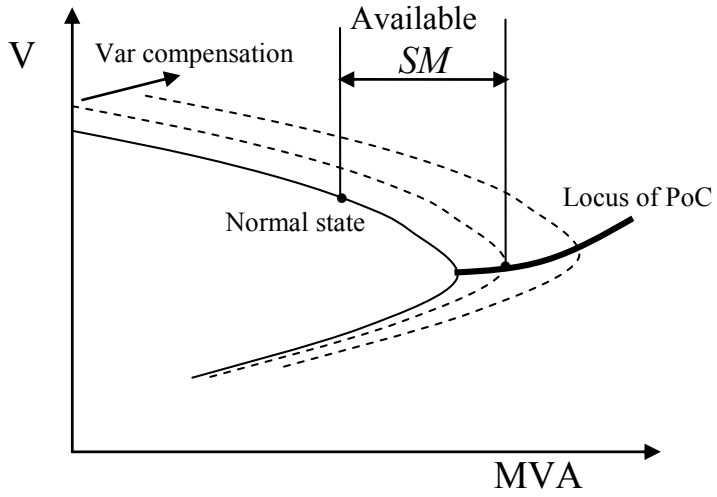

Figure 6.2. Locus of PoC with reactive compensation.

The general procedure of the enumerative method will be summarized in this section. The approach is implemented in General Algebraic Modeling System (GAMS), a programming language for optimization. The basic procedure of the enumerative method is shown in Figure 6.3. The GAMS process starts from Base Case, in which there is no Var compensation. Thus, the total fuel cost output Z_0 in Base Case will not change in the whole process. After assigning the trial location bus i and the MVar amount of Var compensation j, TTC OPF model can be run to obtain the tie line transfer limit L_{ij} corresponding to Q_{cj}. With Q_{cj} and L_{ij} as input to Case 1 and Case 2, the total benefit of Var compensation corresponding to Q_{cj} at bus i may be obtained as ΔZ_{ij}. Then, the net benefit, $\Delta Z_{ij}'$, can be easily obtained by subtracting the Var cost from the total benefit. By repeating the above process, the full spectrum of benefits under different bus locations in various amounts may be drawn in a graph shown in the next section. The most important feature in this process lies in the update of the tie line transfer limit corresponding to a

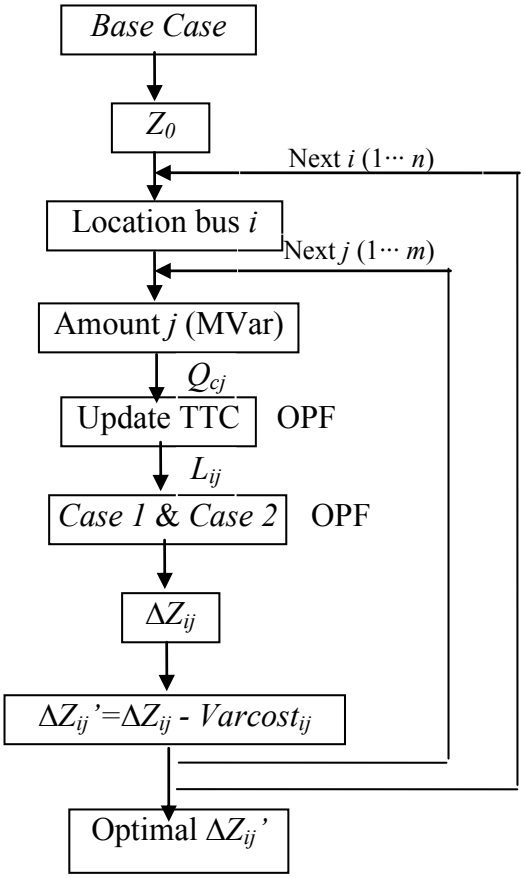

Figure 6.3. GAMS procedure for enumeration method.

different quantity and a different location of Var compensation.

Four OPF models are involved in this approach: Base Case, Case 1, TTC, and Case 2 models. If there is no need to identify *B1*, *B2* and *B3*, and only *Bt* is needed, then only three OPF models (Base Case, TTC, and Case 2) are involved. If we assume there are n candidate buses and m possible Var compensation amounts, the complexity for the selection of optimal location and size by adopting the above *enumeration* method is $(1 + 2mn)$ OPF runs.

6.3 Test system results

ts

Assume bus2, bus3, and bus5 in Figure 4.3 are three Var compensation location candidates. By applying the scheme in Section 6.2, Figures 6.4, 6.5, and 6.6 provide the whole picture for the tendency of the economic benefits versus Var compensation at Bus 2, Bus 3, and Bus 5, respectively. The TTC OPF model becomes infeasible if the Q_c is greater than 200 MVar, so the upper limit of Q_c size in this case is set to 200 MVar. If 1 MVar step change is chosen, m = 200 cases are calculated to draw each curve in Figures 6.4, 6.5, and 6.6.

In reactive power planning, the total benefit *Bt* is an important index. The criterion of location and size selection is to identify the maximum (total benefit – Var cost). Hence, *Bt_bus2, Bt_bus3* and *Bt_bus5* are shown in one picture for convenient comparison in Figure 6.7. The benefits, *Bt_bus2, Bt_bus3* and *Bt_bus5*, rapidly increase from 0 and then reach their maximum value \$102.04/hr, \$114.15/hr and \$110.99/hr, when Q_c_bus2 = 34

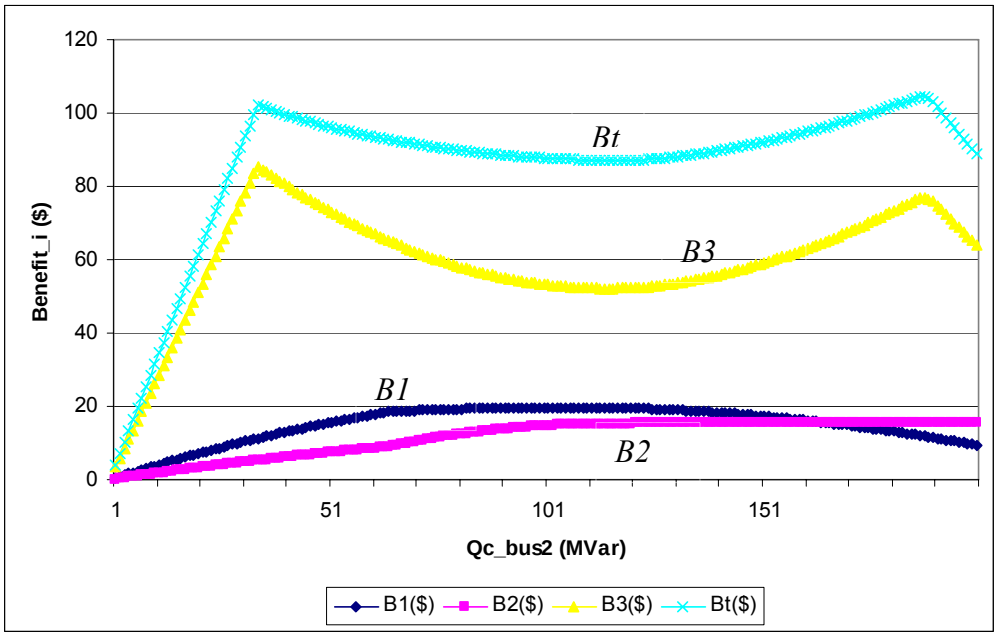

Figure 6.4. *B1*, *B2*, *B3*, and *Bt* versus Var compensation at Bus 2.

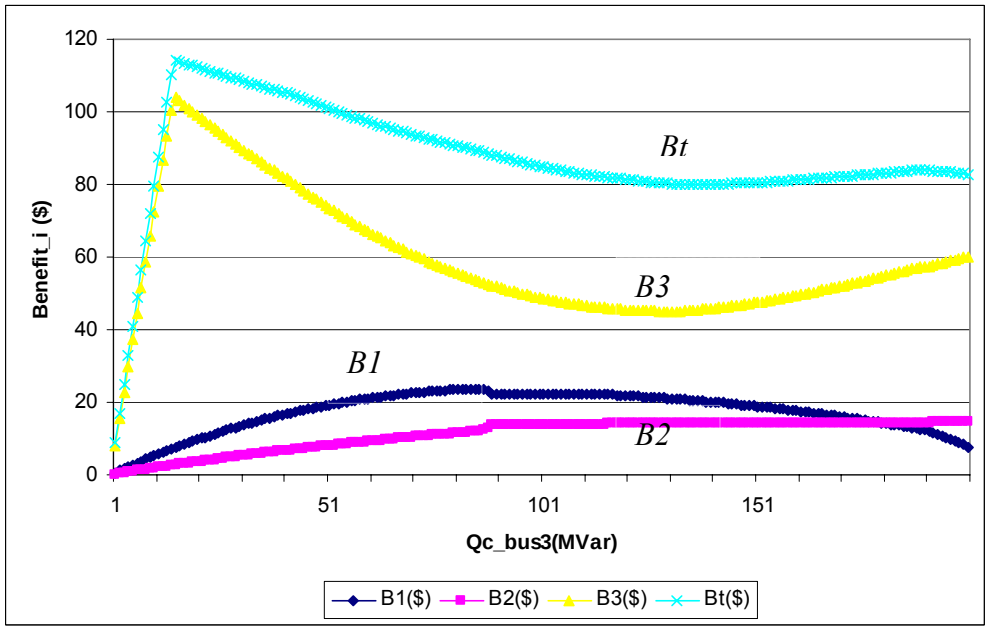

Figure 6.5. *B1*, *B2*, *B3*, and *Bt* versus Var compensation at bus 3.

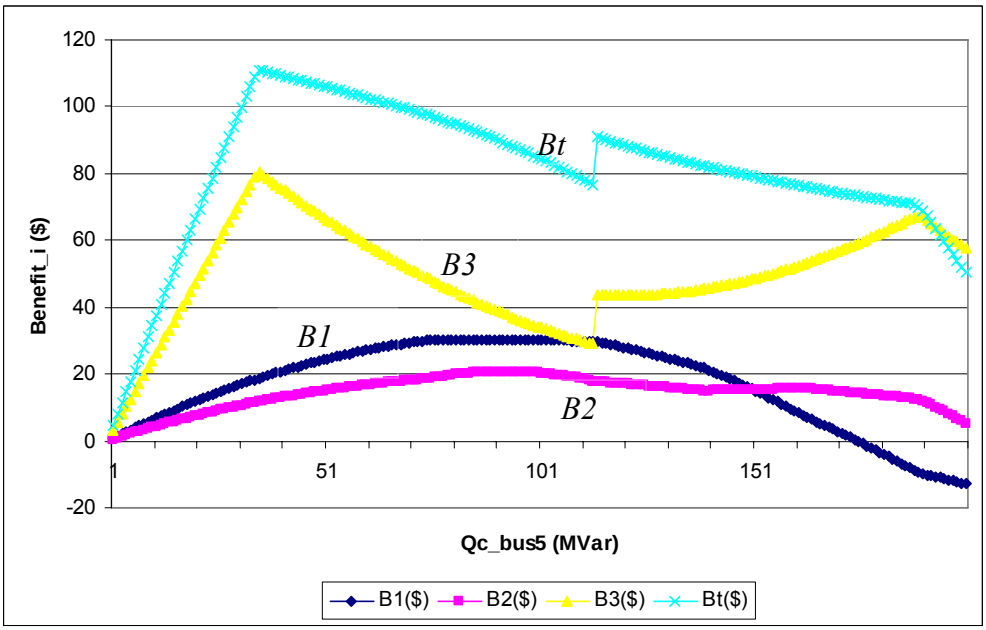

Figure 6.6. *B1*, *B2*, *B3*, and *Bt* versus Var compensation at bus 5.

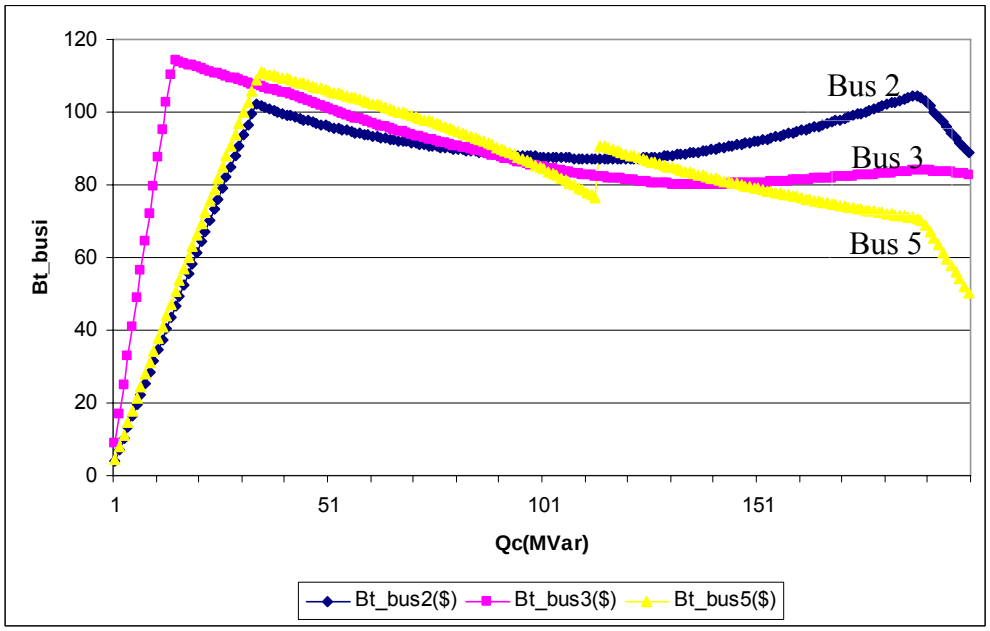

Figure 6.7. Total benefit *Bt* at candidate buses versus Var compensation.

MVar, Q_c_bus3 = 15 MVar, and Q_c_bus5 = 35 MVar, respectively, then immediately followed by a slow decline.

M cost function

Assuming the Var compensator is a STATCOM in this work, the Var cost function $f_2(Q_{ci})$ will be derived based on Figure 6.8. For typical devices' ratings, the lower limit of the cost areas shown in Figure 6.8 indicates the equipment costs, and the upper limit indicates the total investment costs including the infrastructure costs. Thirteen points from the upper limit are read as fitting points, which are given as the following (MVar, US$/kVar) pairs: (100, 130), (125, 127), (150, 123), (175, 118), (200, 116), (225, 113), (250, 110), (275, 107), (300, 105), (325, 104), (350, 103), (375, 102), and (400, 100). A least square method is employed to fit all the 13 points in order to obtain the cost function.

The quadratic polynomial cost function shown in Figure 6.8 is $y(Q_{ci}) = 0.0002466 * Q_{ci}^2 - 0.2243 * Q_{ci} + 150.527$ ($/kVar). With the assumption of 10-year lifetime, then the cost function becomes $1000 * y(Q_{ci}) /(8760 * 10)$ ($/MVar·hr). Thus, the total Var cost shown in Figure 6.9 is $f_2(Q_{ci}) = [1000 * y(Q_{ci}) /(8760 * 10)] * Q_{ci}$ ($/hr), which has consistent units with the benefits.

t for candidate buses

The net benefit at candidate buses versus Var compensation curves are shown in Figure 6.10. The maximum net benefit $88.94/hr happens at the point Q_{c3} = 15 MVar. It is obvious that installation of 15 MVar Q_c at Bus 3 is the best choice if the max benefit is the goal. Further, if the Var size goes beyond 62 MVar, Var compensation leads to

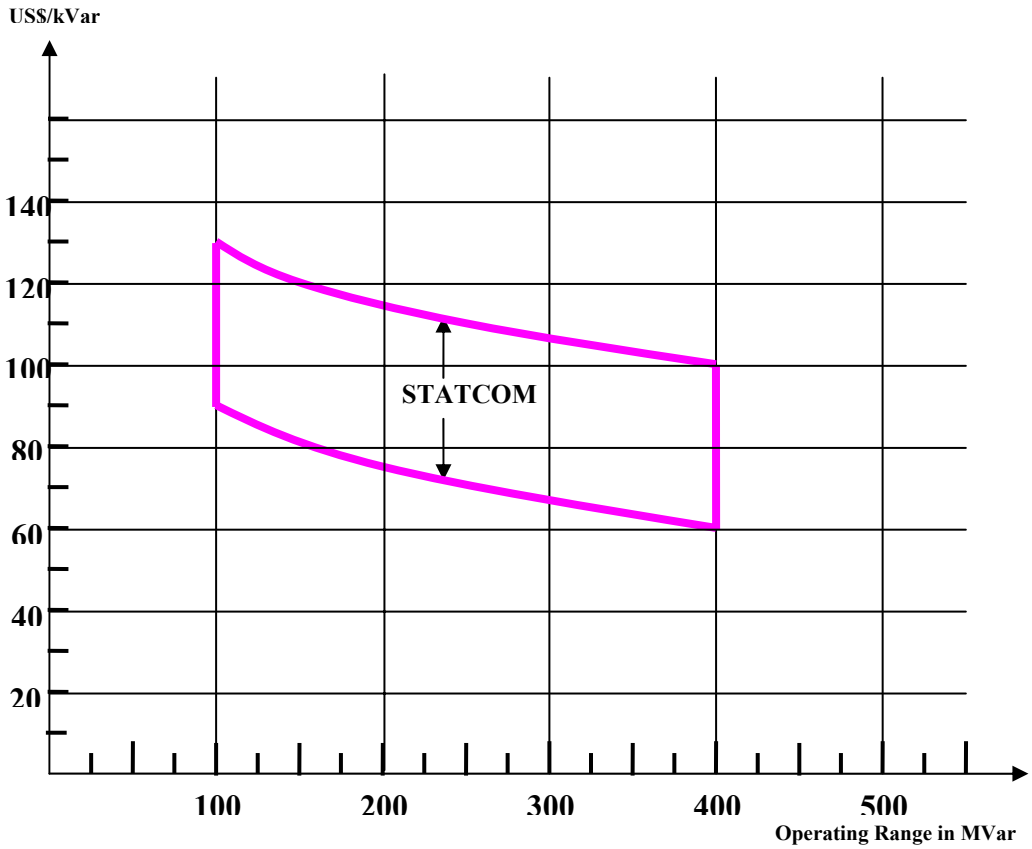

Figure 6.8. Typical investment costs for STATCOM ($/kVar).

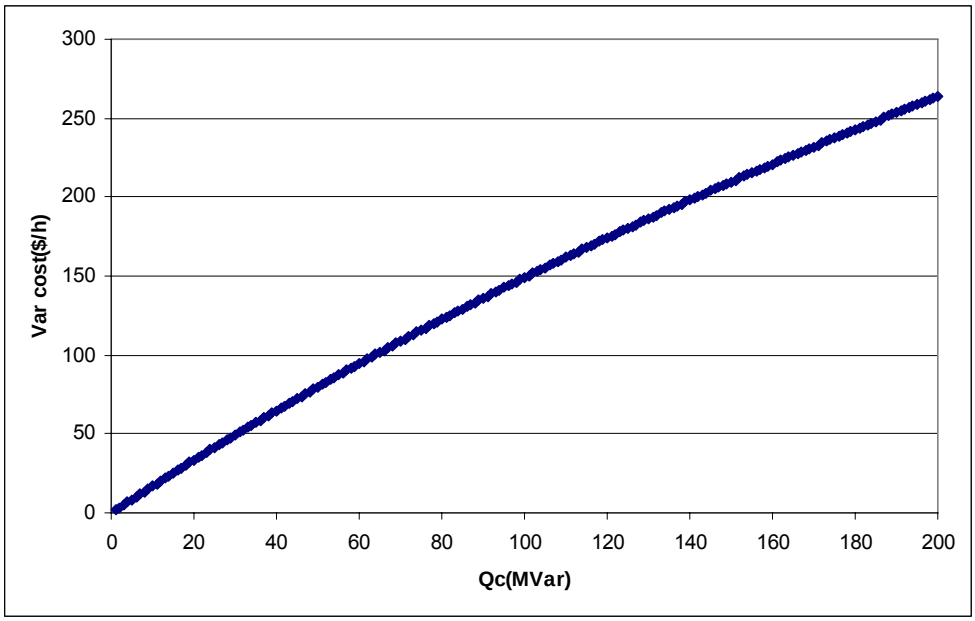

Figure 6.9. STATCOM investment costs ($/hr).

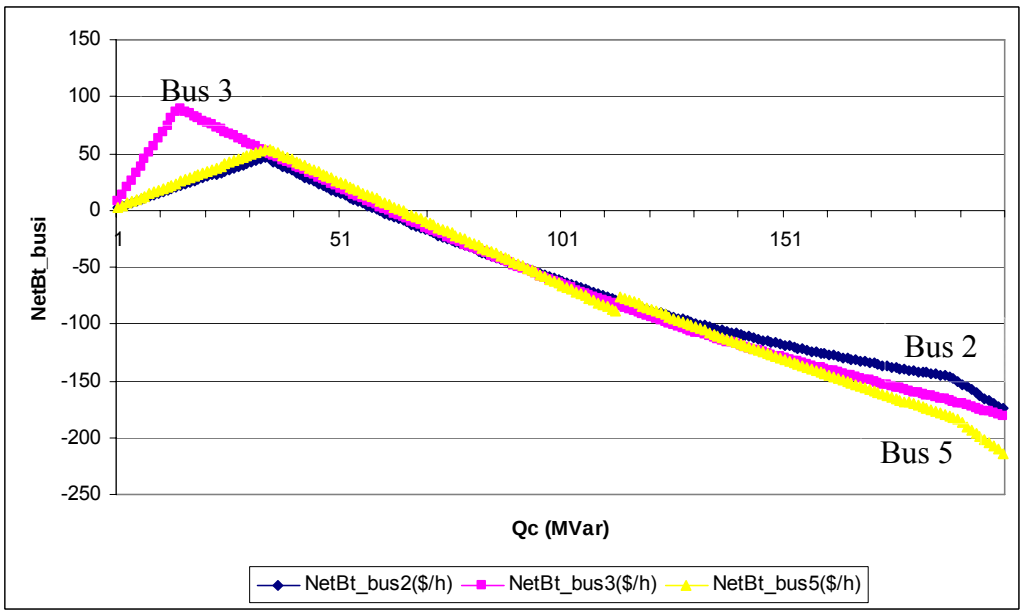

Figure 6.10. Net benefit at candidate buses versus Var compensation.

economic loss since the net benefit drop below zero. The above analysis shows that the potential economic benefits will decrease if the Var is compensated more than 15 MVar. In other words, it is not necessarily better to have more Var compensation. The benefits may decrease at some point as the Var compensation grows.

6.4 Conclusion

In this chapter, the economic benefit analysis is applied to Var planning to show the benefit under each category varies differently with respect to locations and amounts of Var compensation. The conclusions and need for future work based on this research are summarized as follows:

- An important feature in the enumerative approach lies in the impact to economic benefit from the new tie line transfer limits corresponding to different amount of Var compensation, which is not clearly shown in the literature.
- A full spectrum and insightful information about the benefits under different categories is given if a Var compensator is installed at a specific location in various amounts.
- *Net benefit* versus Q_c curves at different candidate locations may be adopted to decide the optimal location and Var quantity. Although this straightforward approach may be time-consuming, the results from this approach may be used for benchmarking purposes for future research.
- Based on the sensitivity of Var benefits, the economic efficiency may not grow as the Var compensation amount grows. The benefits may decrease at some point as the Var compensation increases.

- Three OPF models (Base Case, Case 2, and TTC models) are involved to evaluate the total benefit of Var compensation at a given location and amount. Assuming there are *n* candidate buses, *m* possible Var compensation amounts, the total OPF runs in the Enumeration Method will be (1 + 2*mn*). In the future, an efficient model to simultaneously address the change of new TTC and the new economic benefit is needed. The complexity of the efficient model is preferred to be independent of *n*. A new RPP model using two-set variables based on VSCOPF (voltage stability constrained optimal power flow) to solve location and size problem will be introduced in Chapter 7. Then, a novel algorithm using interpolation approach will be presented in Chapter 8.

7 VOLTAGE STABILITY CONSTRAINED OPTIMAL POWER FLOW (VSCOPF) WITH TWO SETS OF VARIABLES (TSV) FOR VAR PLANNING

The enumeration method for a large system is time-consuming because 3 models and 1+2*mn* OPF runs are needed. Therefore, it will be a great achievement if all the models are combined in one optimization model to maximize the net benefit (= Base Case fuel cost - Case 2 fuel cost - Case 2 Var Cost). Since Base Case fuel cost is fixed, maximizing net benefit is equivalent to minimizing the sum of fuel cost and Var cost for Case 2 (with Var compensation). A new VSCOPF (voltage stability constrained optimal power flow) model with two sets of variables (TSV) to solve the location and size simultaneously in one optimization model is introduced in this chapter, which is equivalent to a combination to the 3 models of Chapter 6.

Originally, TSV method is presented in [88] as a mathematical model to handle voltage stability issue. However, it does not address the application of TSV approach in Var planning. Other later works in [60-62] use the similar TSV constraint for Var planning with Var cost minimization as the objective function. Thus, the three Var benefits are ignored, and then the motivation to install Var compensator, especially in the de-regulated environment, is weakened. The research work in this dissertation employs a new objective goal of minimizing the sum of fuel cost and Var cost, which represents the true optimization model of Var planning. The results show that the new objective

function may lead to significant difference in the optimal Var location and size.

7.1 A general format of VSCOPF model with TSV

The objective here is to minimize both fuel cost and Var cost, and at the same time, increase system voltage security by keeping the operating point away from the PoC (point of collapse or critical point) at no less than a pre-defined distance measured by MVA. For this purpose, two sets of network variables and power flow constraints corresponding to the "normal operating point" and "critical point (PoC)" are adopted in the VSCOPF model [88] as follows:

$$\begin{aligned}
&\textit{Min: } C(x_o, \rho) \\
&\textit{Subject to:} \\
&\mathrm{F}(x_o, \rho, \lambda_o) = 0 \\
&\mathrm{F}(x_*, \rho, \lambda_*) = 0 \\
&(\lambda_* - \lambda_o)/\lambda_* = SM \\
&SM \geq SM_{spec} \\
&x_{omin} \leq x_o \leq x_{omax} \\
&x_{*min} \leq x_* \leq x_{*max} \\
&\rho_{min} \leq \rho \leq \rho_{max}
\end{aligned} \tag{7.1}$$

where "*o*" stands for the "normal operating point" and "*" for the "critical point (PoC)"; *x* represents dependent system variables such as voltage V, angle θ, generator real power and reactive power output P_G and Q_G; ρ represents power system independent parameters and control variables such as Var compensation Q_c, which are the same in both "normal operating point" and the "critical point (PoC)"; λ represents tie line load level; $C(x_o, \rho)$

represents the operating cost and the Var cost function that usually depends on some of the system variables such as P_G at the current operating point and control variables such as Q_c; F(x, ρ, λ) = 0 represents steady state power flow equations of the system; (λ_* - λ_o)/λ_* is satisfied with the definition of security margin SM = $\frac{[MVA \quad load \quad at \quad PoC - MVA \quad base \quad load]}{MVA \quad load \quad at \quad PoC}$.

By using this model, λ_* can be automatically pushed to the total transfer capability (TTC) without running another TTC OPF like what is done in Chapter 6, which is the significance of this VSCOPF model based on TSV. Because minimizing fuel cost leads to transferring cheaper power from generation center to load center as much as possible, the tie line flow at "normal operating point" λ_o will be pushed as high as possible. As a result, tie line load level for "critical point" λ_* keeping a pre-defined distance from λ_o will also be pushed as far as possible on the P-V curve until it reaches the collapse point. However if the objective function does not include minimizing fuel cost, λ_o and λ_* will not be pushed as far as possible on the P-V curve, since the motivation to increase TTC then to decrease fuel cost does not exist. The case study will show this in detailed results.

7.2 A detailed VSCOPF model with two sets of variables for Var

The above general VSCOPF format will be expanded to a detailed model especially for Var planning in this section as follows:

Min: $\sum f_1(P_{Goi}) + \sum f_2(Q_{ci}) \times y_i$

Subject to:

A. The following constraints are applicable to both normal operating point and the critical point:

$$\sum y_i = k \qquad (\textit{Number of Var compensator installations})$$

$$P_{Goi} - P_{Loi} - P(V_o, \theta_o) = 0 \qquad (\textit{Real power balance})$$

$$P_{G*i} - P_{L*i} - P(V_*, \theta_*) = 0$$

$$Q_{Goi} + Q_{ci} - Q_{Loi} - Q(V_o, \theta_o) = 0 \qquad (\textit{Reactive power balance})$$

$$Q_{G*i} + Q_{ci} - Q_{L*i} - Q(V_*, \theta_*) = 0$$

$$P_{Gi}^{\min} \le P_{Goi} \le P_{Gi}^{\max} \qquad (\textit{Generation real power limits})$$

$$P_{Gi}^{\min} \le P_{G*i} \le P_{Gi}^{\max}$$

$$Q_{Gi}^{\min} \le Q_{Goi} \le Q_{Gi}^{\max} \qquad (\textit{Generation reactive power limits})$$

$$Q_{Gi}^{\min} \le Q_{G*i} \le Q_{Gi}^{\max}$$

$$V_i^{\min} \le V_{oi} \le V_i^{\max} \qquad (\textit{Voltage limits})$$

$$V_i^{\min} \le V_{*i} \le V_i^{\max}$$

$$Q_{ci}^{\min} \le Q_{ci} \le Q_{ci}^{\max} \qquad (\textit{Compensation limits})$$

$$\left|LF_{lo}\right| \le LF^{\max} \qquad (\textit{Line flow thermal limits})$$

$$\left|LF_{l*}\right| \le LF^{\max}$$

$$SM = \frac{\sum_{l \in Lt} S_{l*} - \sum_{l \in Lt} S_{lo}}{\sum_{l \in Lt} S_{l*}} \qquad (\textit{Tie line MVA transfer capability security margin})$$

$$SM \ge SM_{spect} \qquad (\textit{Security margin limits})$$

(7.2)

B. The following constraints are only applicable to the critical point:

$$P_{L^*i} \geq P^0_{L^*i} \quad (i \in Sink) \qquad (\textit{real load in load center increases})$$

$$Q_{L^*i} \geq Q^0_{L^*i} \quad (i \in Sink) \qquad (\textit{reactive load in load center increases})$$

$$P_{G^*i} \geq P^0_{G^*i} \quad (i \in Source) \qquad (\textit{real power generation in generation center increases})$$

$$P_{G^*i} = P^0_{G^*i} + \frac{\left(\sum_{i\in Source} P_{G^*i} - \sum_{i\in Source} P^0_{G^*i}\right) \times \left(P^{\max}_{Gi} - P^0_{G^*i}\right)}{\sum_{i\in Source}\left(P^{\max}_{Gi} - P^0_{G^*i}\right)} \qquad (\textit{the pattern of generation increase})$$

$$P_{L^*i} = P^0_{L^*i} + \frac{\left(\sum_{i\in Sink} P_{L^*i} - \sum_{i\in Sink} P^0_{L^*i}\right) \times P^0_{L^*i}}{\sum_{i\in Sink} P^0_{L^*i}} \qquad (\textit{the pattern of load increase})$$

$$P_{L^*i} / P^0_{L^*i} = Q_{L^*i} / Q^0_{L^*i} \qquad (\textit{maintaining constant power factor when load increases})$$

(7.3)

where o —"normal operating point"; $*$ —"critical point (PoC)";

k — number of Var compensator installation; l — the set of lines; Lt — the set of tie lines; $f_1(P_{Goi})$ — fuel cost for generator at bus i; $f_2(Q_{ci})$ — *Var cost at bus i*;

S_l — transmission line MVA flow; y_i —binary variable, $y_i = 1$ if the bus i is selected for Var installation; $P_{L^*i}{}^0$, $Q_{L^*i}{}^0$, $P_{G^*i}{}^0$= initial operation point.

The x variable of the general VSCOPF format corresponds to $\{V, \theta, P_G, Q_G, P_{L^*}, Q_{L^*}\}$ in the detailed VSCOPF model; ρ includes independent parameters $\{P_{Lo}, Q_{Lo}, k, \mathrm{SM}_{\mathrm{spec}}, P_{L^*i}{}^0, Q_{L^*i}{}^0, P_{G^*i}{}^0$, all upper and lower bounds$\}$ and control variables $\{Q_c, y\}$; λ

corresponds to $\sum_{l \in Lt} S_l$.

7.3 Test system results

r procedure

SBB, a state-of-the-art mixed integer non-linear programming (MINLP) solver, is employed to solve the model efficiently. It is based on a combination of the standard Branch and Bound (B&B) method known from mixed integer linear programming and some standard NLP solvers supported by GAMS such as MINOS [89].

The key feature of a MINLP problem is to reduce the problem to a NLP problem once the discrete variables are fixed. During the solution process, (1) the feasible region for the discrete variables is subdivided into subsets, (2) MINLP problem is relaxed to NLP submodel by relaxing the discrete variables to continuous ones corresponding to each subset, (3) the solution from the NLP submodel is assumed to be lower bound on the objective function (assuming minimization), (4) SBB solves a number of relaxed MINLP models with tighter and tighter bounds on some of the integer variables until integer solution with acceptable termination tolerance is found. Thus the process basically breaks the big MINLP problem into manageable size subproblems.

d Bound (B&B) algorithm

This section will introduce how to improve the bounds and how to prune the nodes on a branch and bound search tree, as is shown in Figure 7.1, in order to reduce the number of nodes explored.

The branch and bound method implicitly enumerates all the feasible solutions by

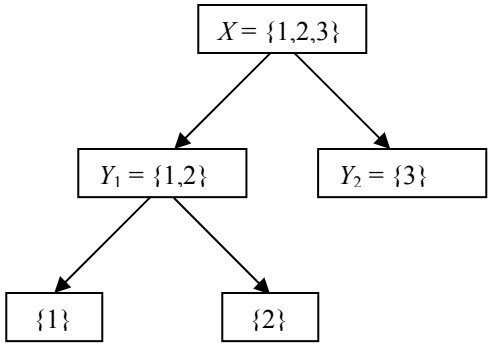

Figure 7.1. Illustration of a branch and bound tree.

using optimization problems that involve no integer constraints. The idea of the method is to partition the feasible set into smaller subsets, and then calculate certain bounds on the objective function within some subsets. At last, use these bounds to economize computation by eliminating nodes of the tree that can not contain an optimal solution [90].

The pruning criteria are explained as follows:

Given the problem of minimizing $f(x)$ over $x \in X$, and two subsets (also two nodes) $Y_1 \subset X$ and $Y_2 \subset X$, suppose that we have bounds $\underline{f}_{Y_1} \le \min_{x \in Y_1} f(x)$, $\overline{f}_{Y_1} \ge \max_{x \in Y_1} f(x)$, $\underline{f}_{Y_2} \le \min_{x \in Y_2} f(x)$, $\overline{f}_{Y_2} \ge \max_{x \in Y_2} f(x)$. Then the branch and bound tree at a node Y_i can be pruned if any one of the following conditions holds:

(1) Infeasibility: $Y_i = \phi$ (an empty set)

(2) Optimality: If upper bound equals lower bound $\underline{f}_{Y_i} = \overline{f}_{Y_i}$, an integer optimal solution is found.

(3) Value dominance: If the lower bound exceeds the best upper bound such as $\overline{f}_2 \le \underline{f}_1$, the solutions in Y_1 and its descendant nodes need not be considered

further since their objective function can not be smaller than that of the best solution in Y_2.

Branch and Bound typically uses continuous optimization problems (without integer constraints) to obtain the lower bound $\underline{f}_{Y_i}$. For example, 0-1 binary variables are treated as continuous variables, and can take any values in the interval [0, 1]. The objective function $f(\bar{x})$ of a feasible solution $\bar{x} \in Y_i$ can serve as an upper bound $\overline{f}_{Y_i}$ to the minimum cost over Y_i.

tput of the case study

1) GAMS result output for scenario I

The case in Chapter 6 will also be tested in this chapter. The Var cost function $f_2(Q_{ci})$ in model (7.3) is the same with that in Chapter 6. Still, it is assumed that Bus 2, Bus 3, and Bus 5 are Var compensation location candidates, and at most one STATCOM may be installed by setting $\sum y_i = 1$.

Variables' values at the "current operating point (o)" and the "critical point ($*$)" are shown in Table 7.1. The inter tie line MVA limit is 369.5443, which is 75% of the PoC_* (492.7257MVA). The final optimal solution for the Var planning is to install a Var compensator at bus3 with size of 14.54 MVar. The answer is very close to but more accurate than the enumeration method result – 15 MVar at bus3, since Q_c variable is treated as a continuous one instead of integer variable as in the enumeration method.

Table 7.1. Variables output from VSCOPF with two sets of variables GAMS model.

Objective							
Fuel cost ($/hr)			Var cost ($/hr)			Total cost ($/hr)	
15168.98			24.46			15193.44	
Variables output							
Bus	1	2	3	4	5	6	7
Q_c (MVar)			14.54				
y (binary)			1				
P_{Go} (MW)	85.21			200.00		300.00	195.74
Q_{Go} (MVar)	80.86			100.00		51.64	54.74
P_{Lo}(MW)		100.00	190.00	150.00	200.00	50.00	80.00
Q_{Lo}(MVar)		40.00	75.00	50.00	60.00	20.00	40.00
V_o (V)	1.05	1.01	0.99	1.00	0.97	1.04	1.01
TTC_o(MVA)	369.54						
P_{G*} (MW)	70.00			200.00		300.00	300.00
Q_{G*} (MVar)	62.90			100.00		97.56	100.00
P_{L*}(MW)		113.12	214.93	169.68	226.25	50.00	80.00
Q_{L*}(MVar)		46.56	87.47	59.84	73.12	20.00	40.00
V_* (V)	1.02	1.00	0.95	0.97	0.97	1.05	1.03
TTC_*(MVA)	492.73						

2) GAMS result output for scenario II

The same data and assumption are used in scenario II except at most two STATCOMs may be installed. Two ways are explored and compared to realize the scenario II, one is setting $\sum y_i = 2$ in model (7.3), that gives the opportunity to install two STATCOMs at the same time; the other is running model (7.3) with $\sum y_i = 1$ twice, the first case result of Var amount is treated as an assumption in the second case, that means installing one STATCOM first and then deciding whether another one is needed or not and where it is.

The same result with scenario I is obtained, only one STATCOM with size 14.543254 MVar is selected to install at bus3 in the first way, even if it is possible to install two. The result shows it does not help to decrease the total cost if an additional STATCOM is

installed. In the second way, Var compensation at bus3 is fixed as 14.543254 MVar, Bus 2 and Bus 5 are candidates, then model (7.3) with $\sum y_i = 1$ is run. The result is nothing should be installed, or every y_i is zero. In fact, the two ways obtain the same result. The additional STATCOM installation is not economic.

3) Result output for TSV model [60-62] with minimizing Var cost as objective

The objective for the above two cases is minimizing the sum of fuel cost and Var cost, but the TSV model in [60-62] treats minimizing Var cost as the only objective, which is *Min:* $\sum f_2(Q_{ci}) \times y_i$. The TSV model in this dissertation (TSV model II) considers Var benefit as well as Var cost, but the TSV model in [60-62] (TSV model I) is based on Var cost only.

Table 7.2 shows the result comparison of TSV models (TSV model I and TSV model II). The result of TSV model I does not suggest installing a Var compensator since the Var cost is minimized as zero. However the total transfer capability corresponding to the operating point (TTC_0) and the collapse point (TTC_*) are all lower than that of TSV model II. Because there is no motivation to push the "operating point" further right on the P-V curve in model I, the optimal solution stops at an "operating point" with a stability margin (*SM*) greater than required margin as shown in Figure 7.2. As is shown in Table 7.2, the total cost in model I is $322.42/hr higher than that of model II. TSV model II proposed in this dissertation is a great improvement over the TSV model I shown in literature.

Table 7.2. Result comparison of TSV model I and TSV model II.

	TSV model with minimizing Var cost (TSV model I)	TSV model with minimizing fuel cost + Var cost (TSV model II)
Fuel cost ($/hr)	15515.86	15168.98
Var cost ($/hr)	0.00	24.46
Total cost ($/hr)	15515.86	15193.44
Var location	none	Bus 3
Var size (MVar)	0.00	14.54
TTC_o(MVA)	304.39	369.54
TTC_*(MVA)	464.28	492.73
SM	34%	25%

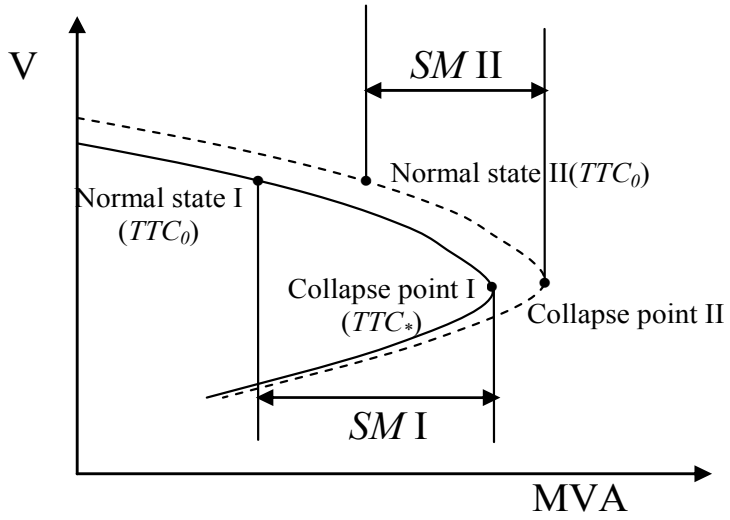

Figure 7.2. Comparison of normal state operating point TTC_0 and the collapse point TTC* of TSV model I and TSV model II.

7.4 Conclusion

The complete search tree including 6 nodes in this case is shown in Figure 7.3. By applying branch and bound method, SBB only explores 4 nodes to obtain the optimal solution. It is obvious the complexity of Var planning VSCOPF with TSV model has been significantly reduced compared with enumeration method, and is not directly related to *n*, the number of candidates. In addition, the Var planning problem is solved in only one OPF model instead of 3 OPF models (Base Case, Case 2, and TTC model) in the enumeration method. The above two important features of the VSCOPF with TSV model are the great improvement compared with the enumeration method of Chapter 6. TSV model II considers minimizing fuel cost in the objective of TSV model I [60-62], which successfully drives the "operating point" further right on the P-V curve and greatly improve the final result.

However, the VSCOPF with TSV model doubles the number of variables and constraints in the voltage stability constrained model, which extends the computation time, and in addition, increases the risk of no convergence and infeasibility. Is it necessary to apply two sets of variables in order to incorporate the voltage stability constraints related to *PoC* in Var planning? The next chapter will introduce and compare some approximation method to avoid the two sets of variables.

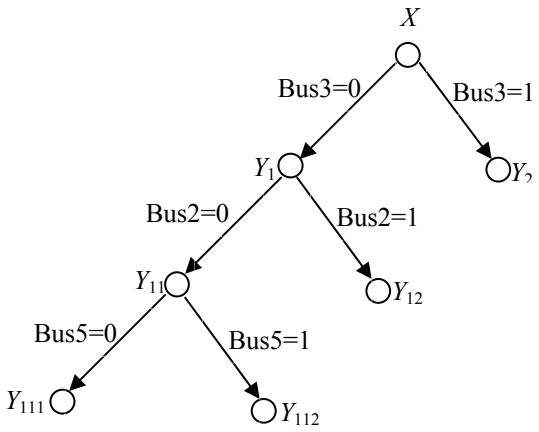

Figure 7.3. Search tree for test case.

8 .

9 VOLTAGE STABILITY CONSTRAINED VAR PLANNING OPF MODEL SIMPLIFICATION USING APPROXIMATION THEOREM

The major reason of the computational challenge of the Voltage Stability Constrained Optimal Power Flow (VSCOPF) with two sets of variables (TSV) model in the previous Chapter is the requirement of two sets of variables and constraints corresponding to the "normal operating point (o)" and "collapse point ($*$)". With no doubt, the two sets of variables become the heavy burden especially for a larger system with contingency, since n contingency constraints needs $2n$ sets of variables with the TSV model of Chapter 7. As indicated in [63], "the doubling of non-linear power flow constraints, in particular, has major impact on computation for large-scale systems. It may not only be an increase in computational time, but may have other serous implications such as non-convergence, or getting stuck at sub-optimal solutions." Hence, a model simplification may be a welcome addition in cases where the TSV model fails to provide any solution due to non-convergence, or it is prone to yield grossly sub-optimal solutions because of its size and complexity [63].

If we can use an approximation to estimate the tie line total transfer capability (TTC) path within a reasonable degree of error, this would imply a substantial simplification of the model presented in Chapter 7. First, a data set of TTC versus reactive compensation at various candidate buses is generated. Secondly, two approximation methods are

proposed and compared to represent these observation points as a function of Var compensation, which are Taylor series and interpolation. Discussions show interpolation approach is a better one. Finally, the proposed approach - interpolation is numerically tested and compared with the simplified model using least square method proposed in [63]. It is concluded that interpolation is a better simplified model and more suitable for Var planning than Taylor series and least square method.

9.1 VSCOPF model with approximated TTC path function

The analysis explores the possibility to circumvent the two sets of variables, but still incorporate voltage stability constraint such as $SM \geq SM_{spec}$ in the Var planning OPF model, by using approximation of the TTC path, as shown in Figure 8.1.

In the previous VSCOPF with TSV model, the second set of variables is used to indicate the TTC value. If the path of TTC can be approximately estimated beforehand

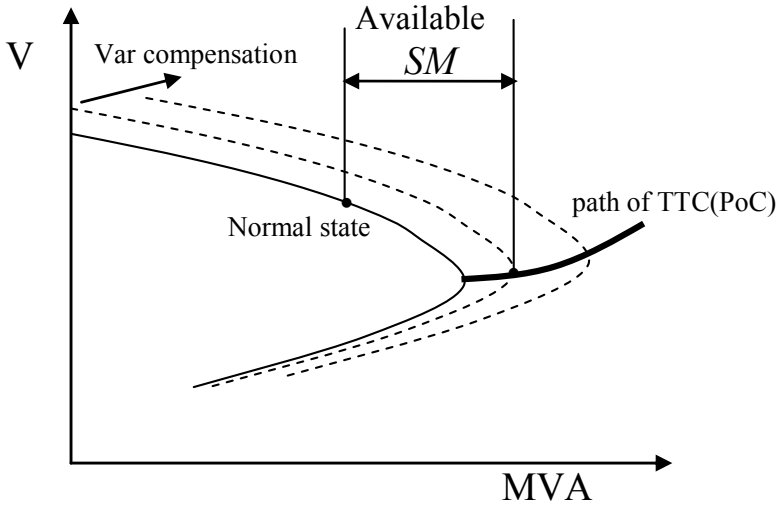

Figure 9.1. Path of TTC with reactive compensation.

for different Var compensation configurations, the second set of variables and constraints for the new TTC under compensation can be eliminated. Based on this idea, a new "VSCOPF model with approximated TTC path function" is proposed as follows. It is shown that only one set of variables related to the "normal operating point (*o*)" is needed in this model.

$$Min: \sum f_1(P_{Goi}) + \sum f_2(Q_{ci}) \times y_i$$

Subject to:

$$\sum y_i = k \qquad (\textit{Number of Var compensator installations})$$

$$P_{Goi} - P_{Loi} - P(V_o, \theta_o) = 0 \qquad (\textit{Real power balance})$$

$$Q_{Goi} + Q_{ci} - Q_{Loi} - Q(V_o, \theta_o) = 0 \qquad (\textit{Reactive power balance})$$

$$P_{Gi}^{\min} \le P_{Goi} \le P_{Gi}^{\max} \qquad (\textit{Generation real power limits})$$

$$Q_{Gi}^{\min} \le Q_{Goi} \le Q_{Gi}^{\max} \qquad (\textit{Generation reactive power limits})$$

$$V_i^{\min} \le V_{oi} \le V_i^{\max} \qquad (\textit{Voltage limits})$$

$$Q_{ci}^{\min} \le Q_{ci} \le Q_{ci}^{\max} \qquad (\textit{Compensation limits})$$

$$\left|LF_{lo}\right| \le LF^{\max} \qquad (\textit{Line flow thermal limits})$$

$$SM = \frac{\sum_{l \in Lt} S_{l*} - \sum_{l \in Lt} S_{lo}}{\sum_{l \in Lt} S_{l*}} \qquad (\textit{Tie line MVA transfer capability security margin})$$

$$SM \ge SM_{spec} \qquad (\textit{Security margin limits})$$

$$TTC = \sum_{l \in Lt} S_{l*} \qquad (\textit{Tie line total transfer capability definition})$$

$$TTC = f(Q_{ci}) \qquad (TTC \text{ is not a constant, but a function of Var } Q_{ci}) \tag{8.1}$$

where $f(Q_{ci})$ —*TTC is a function of* Q_{ci}; P_{Lo}, Q_{Lo}, SM_{spec}, and all upper and lower bounds are known parameters; the others are all variables.

9.2 Taylor series approximation for TTC function of Var planning

eorem

In the model (8.1), the key is to obtain the function $f(Q_{ci})$. The proposed approach is to statistically estimate the function $f(Q_{ci})$ based on Taylor series expansion theorem. Taylor series gives the approximation of a differentiable function near a point by a polynomial whose coefficients depend only on the derivatives of the function at that point [91]. This can be further generalized for a function with n variables. Take for example, for a function that depends on two variables, x and y, the Taylor series to second order around the point (a, b) is given as (8.2):

$$\begin{aligned} f(x,y) \approx f(a,b) + f_x(a,b)(x-a) + f_y(a,b)(y-b) + 0.5 \times [f_{xx}(a,b)(x-a)^2 + f_{yy}(a,b)(y-b)^2 \\ + f_{xy}(a,b)(x-a)(y-b) + f_{yx}(a,b)(x-a)(y-b)] \end{aligned} \tag{8.2}$$

Taylor series approximation for a function is only accurate when (x, y) is close enough to (a, b). In other words, Taylor series approximation is locally accurate, and it lacks the ability to predict the turning trend of a curve. In addition, it is difficult to calculate the convergent radius R (indicating series convergence and divergence boundary) for a function only having sample points, but no explicit expression. For

example, $\sum x_n$ is a series of nonzero terms. If we suppose $\lim_{n\to\infty}\left|\frac{x_{n+1}}{x_n}\right| = L$, then: (1) if $L < 1$, the series is absolutely convergent, and the convergent radius $R = 1/L$, which means when $|x| < R$, the series is convergent; (2) if $L > 1$, the series is divergent, and it is hard to evaluate how close it should be to keep the Taylor series approximation accurate in an acceptable error. The above two disadvantages basically limit the application of Taylor series to the TTC function approximation. The following case analysis will demonstrate how the shortcomings cause trouble to implement a Taylor series approximation.

ies implementation case study

1) Taylor series expansion equation

Suppose Bus 3 and Bus 5 are two Var compensation candidates. If the TTC path will depend on the two variables Q_{c3} and Q_{c5}, then the TTC function will be a surface. If the candidates' number is more than two, the discussion below should be applicable, although it will be difficult to visualize the multi-dimensional surface.

In order to test the Taylor series, accurate TTC results from GAMS TTC OPF model for various Q_{c3} and Q_{c5} values are needed to draw a surface, as is shown in Figure 8.2.

Assume x is Q_{c3} and y is Q_{c5}. Two points, (0, 0) from A surface and (15, 0) from B surface, are chosen to perform the Taylor series expansion. Certainly, other points in the two surfaces also can be selected. The reason that at least two points are chosen is that the Taylor series approximation is locally accurate, and can not make a turn by itself. TTC Taylor series approximation to second order about the point (0, 0) is as (8.3), and about the point (15, 0) is as (8.4):

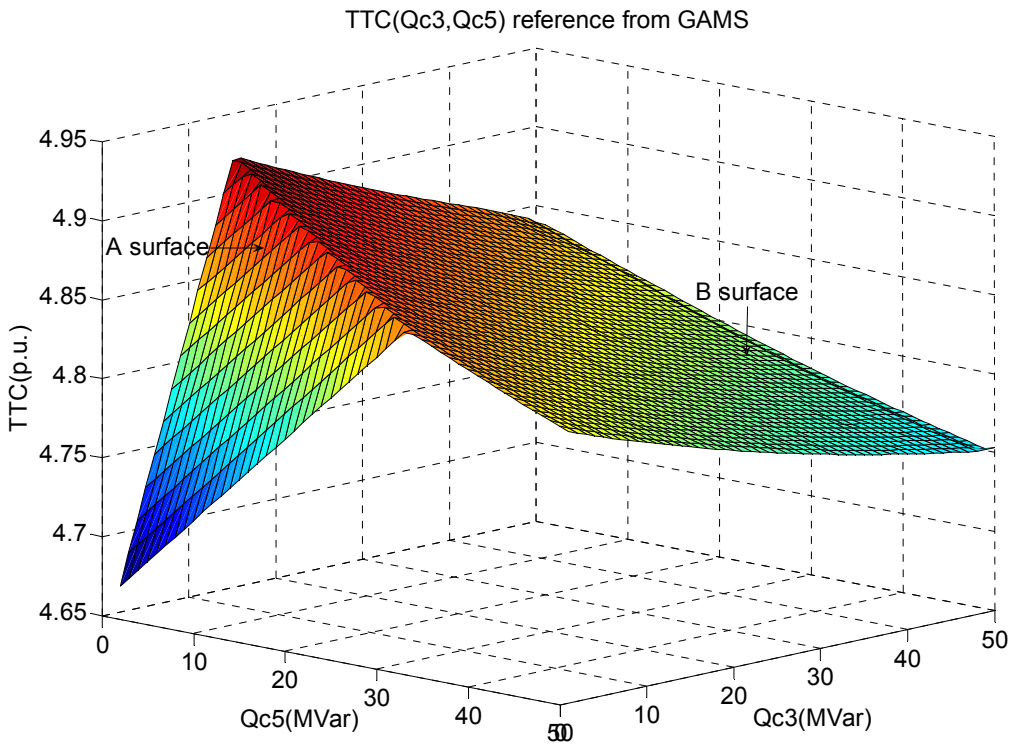

Figure 9.2. TTC with respect to Different Var amount at Bus 3 and Bus 5.

$$TTC(Q_{c3},Q_{c5}) \approx \left.\frac{\partial TTC}{\partial Q_{c3}}\right|_{\substack{Q_{c3}=0\\Q_{c5}=0}} \cdot Q_{c3} + \left.\frac{\partial TTC}{\partial Q_{c5}}\right|_{\substack{Q_{c3}=0\\Q_{c5}=0}} \cdot Q_{c5} + \frac{1}{2}\left(\left.\frac{\partial^2 TTC}{\partial Q_{c3}^2}\right|_{\substack{Q_{c3}=0\\Q_{c5}=0}} \cdot Q_{c3}^2 + \left.\frac{\partial^2 TTC}{\partial Q_{c5}^2}\right|_{\substack{Q_{c3}=0\\Q_{c5}=0}} \cdot Q_{c5}^2 \right)$$
$$+ \frac{1}{2}\left(\left.\frac{\partial^2 TTC}{\partial Q_{c3}\partial Q_{c5}}\right|_{\substack{Q_{c3}=0\\Q_{c5}=0}} \cdot Q_{c3}Q_{c5} + \left.\frac{\partial^2 TTC}{\partial Q_{c5}\partial Q_{c3}}\right|_{\substack{Q_{c3}=0\\Q_{c5}=0}} \cdot Q_{c3}Q_{c5} \right) + TTC\Big|_{\substack{Q_{c3}=0\\Q_{c5}=0}} \tag{8.3}$$

$$TTC(Q_{c3},Q_{c5}) \approx \left.\frac{\partial TTC}{\partial Q_{c3}}\right|_{\substack{Q_{c3}=15\\Q_{c5}=0}} \cdot (Q_{c3}-15) + \frac{1}{2}\left(\left.\frac{\partial^2 TTC}{\partial Q_{c3}^2}\right|_{\substack{Q_{c3}=15\\Q_{c5}=0}} \cdot (Q_{c3}-15)^2 + \left.\frac{\partial^2 TTC}{\partial Q_{c5}^2}\right|_{\substack{Q_{c3}=15\\Q_{c5}=0}} \cdot Q_{c5}^2 \right)$$
$$+ \left.\frac{\partial TTC}{\partial Q_{c5}}\right|_{\substack{Q_{c3}=15\\Q_{c5}=0}} \cdot Q_{c5} + \frac{1}{2}\left(\left.\frac{\partial^2 TTC}{\partial Q_{c3}\partial Q_{c5}}\right|_{\substack{Q_{c3}=15\\Q_{c5}=0}} \cdot (Q_{c3}-15)\cdot Q_{c5} + \left.\frac{\partial^2 TTC}{\partial Q_{c5}\partial Q_{c3}}\right|_{\substack{Q_{c3}=15\\Q_{c5}=0}} \cdot (Q_{c3}-15)\cdot Q_{c5} \right) + TTC\Big|_{\substack{Q_{c3}=15\\Q_{c5}=0}} \tag{8.4}$$

Table 9.1. Taylor series expansion coefficients.

Point coefficients	(0, 0)	(15, 0)
TTC (p.u.)	4.64	4.93
$\partial TTC/\partial Q_{c3}$	1.98×10^{-2}	-2.73×10^{-3}
$\partial TTC/\partial Q_{c5}$	6.28×10^{-3}	-3.22×10^{-3}
$\partial^2 TTC/\partial Q_{c3}^2$	-2.90×10^{-5}	2.39×10^{-5}
$\partial^2 TTC/\partial Q_{c5}^2$	1.69×10^{-6}	2.37×10^{-5}
$\partial^2 TTC/(\partial Q_{c3}\partial Q_{c5})$	-4.19×10^{-6}	2.09×10^{-5}
$\partial^2 TTC/(\partial Q_{c5}\partial Q_{c3})$	-3.46×10^{-6}	2.76×10^{-5}

In (8.3) and (8.4), Q_{c3} and Q_{c5} are variables, $TTC\big|_{\substack{Q_{c3}=a\\Q_{c5}=b}}$ can be calculated directly from TTC OPF GAMS model. The variable marginal cost of Q_{c3} and Q_{c5} can be given by GAMS output, which are exactly the $\partial TTC/\partial Q_{c3}$ and $\partial TTC/\partial Q_{c5}$. Also, $\partial^2 TTC/\partial Q_{c3}^2$, $\partial^2 TTC/(\partial Q_{c3}\partial Q_{c5})$, $\partial^2 TTC/(\partial Q_{c5}\partial Q_{c3})$, and $\partial^2 TTC/\partial Q_{c5}^2$ may be obtained from the slope of $(\partial TTC/\partial Q_{ci})$ versus Q_{cj} curve. The coefficients of Taylor series expansion are shown in Table 8.1.

Substitute the coefficients in Table 8.1 into (8.3) and (8.4), the Taylor series expansions at points (0, 0) and (15, 0) are shown in (8.5) and (8.6) respectively. The two surfaces TTC_1 and TTC_2 are shown in Figure 8.3. The two surfaces in Figure 8.3 cross with each other at the line $TTC_1 = TTC_2$. When $TTC_2 > TTC_1$, TTC_1 is taken as TTC path function; otherwise, TTC_2 is taken.

$$TTC_1(Q_{c3},Q_{c5}) \approx 4.64 + 1.98\times10^{-2}\times Q_{c3} + 6.28\times10^{-3}\times Q_{c5} + 0.5\times(-2.9\times10^{-5}\times Q_{c3}^2 + 1.69\times10^{-6}\times Q_{c5}^2 + (-4.19\times10^{-6} - 3.46\times10^{-6})\times Q_{c3}\times Q_{c5}) \quad (8.5)$$

$$TTC_2(Q_{c3},Q_{c5}) \approx 4.93 - 0.00273\times(Q_{c3}-15) - 3.22\times10^{-3}\times Q_{c5} + 0.5\times(2.39\times10^{-5}\times(Q_{c3}-15)^2 + 2.37\times10^{-5}\times Q_{c5}^2 + (2.09\times10^{-5} + 2.76\times10^{-5})\times(Q_{c3}-15)\times Q_{c5}) \quad (8.6)$$

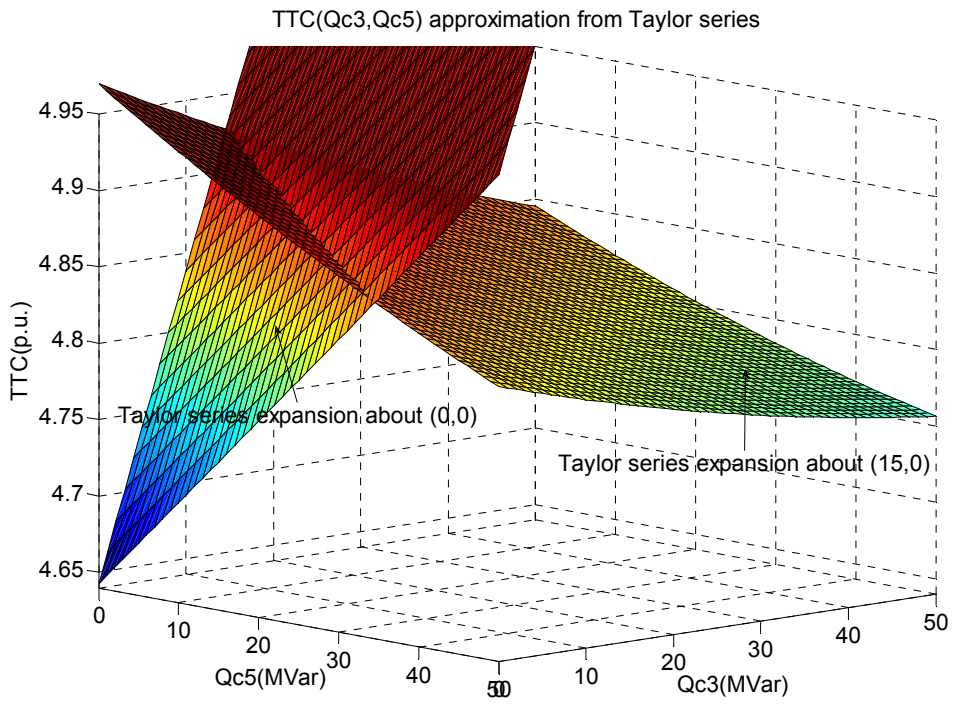

Figure 9.3. Taylor series approximation for TTC function.

Hence, the conditional function *TTC* is equal to TTC_1 when $TTC_1 < TTC_2$, and *TTC* = TTC_2 otherwise. If we use this conditional function into VSCOPF Taylor series approximation model (8.1), the optimal solution is shown in Table 8.2, which is very close to the GAMS output of VSCOPF with two sets of variables model in Table 7.2.

2) Limitation of Taylor series implementation

It is true that Taylor series approach is effective if it is used to estimate TTC at a Var amount that is close to the original point or the reference point. If the new Var amount is quite different from the reference point, large errors may occur. To avoid large error, a piece-wise Taylor series approximation may be needed as shown in the previous discussion. Four difficulties are concluded for piece-wise Taylor series application as follows:

Table 9.2. Variables output from VSCOPF with Taylor series approximation GAMS model.

Objective							
Fuel cost ($/hr)			Var cost ($/hr)			Total cost ($/hr)	
15168.96			24.45			15193.45	
Variables output							
Bus	1	2	3	4	5	6	7
Q_c (MVar)			14.56				
y (binary)			1				
P_{Go} (MW)	85.21			200		300	195.74
Q_{Go} (MVar)	80.85			100		51.64	54.74
P_{Lo}(MW)		100	190	150	200	50	80
Q_{Lo}(MVar)		40	75	50	60	20	40
V_o (V)	1.05	1.01	0.99	1.00	0.97	1.04	1.01
PoC_o(MVA)	369.55						
PoC_*(MVA)	492.73						

- How many points such as (0, 0) and (15, 0) for Taylor series expansion are necessary to reflect the true shape of TTC curve?
- How to locate these points for accurate results?
- Assume n first order Taylor series approximation functions applied to n points with a pre-defined subsection border. Then, TTC function becomes a series of subsection functions as follows:

$$TTC = \begin{cases} f_1(Q_c) & if\ Q_c \in \text{ pre-defined } s\text{ubsection1} \\ f_2(Q_c) & if\ Q_c \in \text{ pre-defined } s\text{ubsection2} \\ \vdots & \\ f_n(Q_c) & if\ Q_c \in \text{ pre-defined } s\text{ubsection}n \end{cases}$$

How to connect these subsection functions continuously? Otherwise these non-continues subsection functions will cause trouble for optimization. Figure 8.4 shows the gap between these subsection functions.

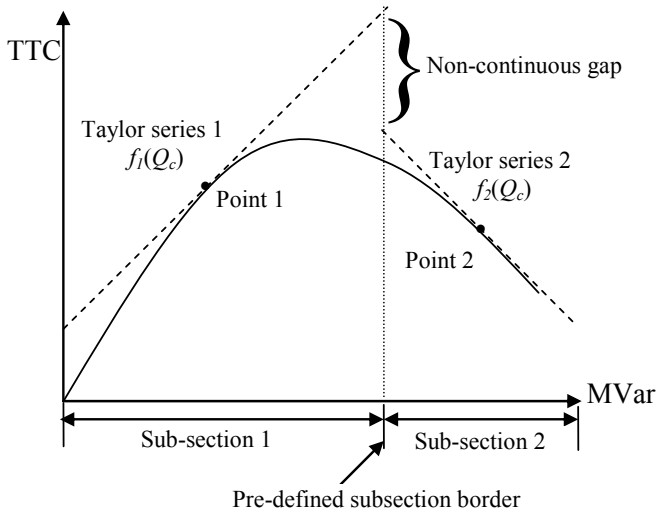

Figure 9.4. Non-continuous Taylor series sub-section functions with pre-defined border

.

- Careful readers may find out that the previous discontinuity problem can be addressed by the following approach: extend each piece of two neighboring Taylor series to find the intersection point; and then use the intersection to find the appropriate subsection for each Taylor approximation series. For instance, f_1 and f_2 in Figure 8.5 can be extended to find the intersection. Then, f_1 is effective for Subsection 1 and f_2 is effective for Subsection 2, as shown in Figure 8.5. Then the TTC function becomes a series of subsection functions as follows:

$$TTC = \begin{cases} f_1(Q_c) & if\ Q_c \in \text{natural cross } s\text{ubsection1} \\ f_2(Q_c) & if\ Q_c \in \text{natural cross } s\text{ubsection2} \\ & \vdots \\ f_n(Q_c) & if\ Q_c \in \text{natural cross } s\text{ubsection}n \end{cases}$$

However, this method will raise a new problem: as shown in Figure 8.5, the intersection of f_2 and f_3 is beyond the normal range of MVar compensation. Thus, it cannot be used to distinguish the subsections suitable for f_2 and f_3, respectively.

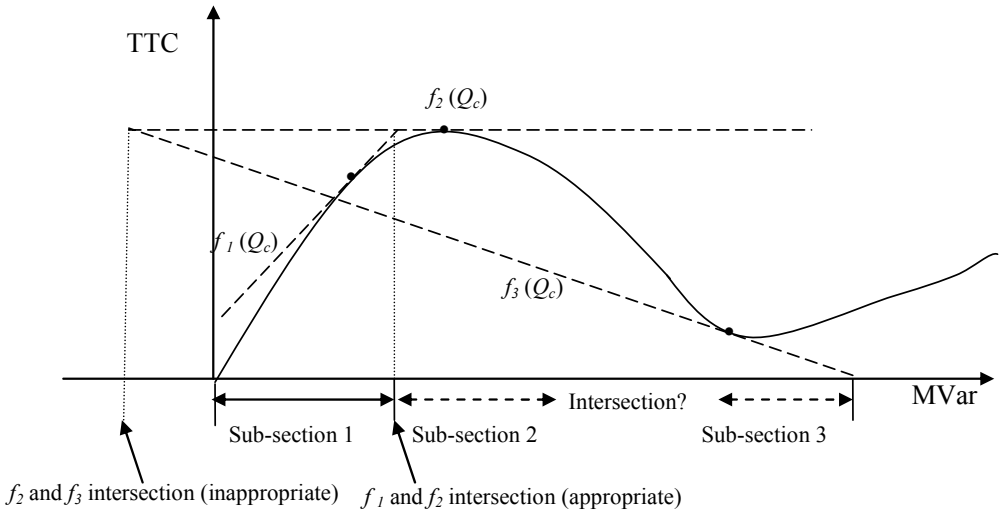

Figure 9.5. Taylor series sub-section functions with natural cross border.

Therefore, additional effort is needed to solve the above difficulties. The next section will propose a new approach based on interpolation.

9.3 Interpolation approximation for TTC function of Var planning

The above two disadvantages essentially limit the application of Taylor series to the TTC function approximation. Interpolation method is proposed in this section to overcome the difficulties raised by Taylor series because of two reasons. (1) Interpolation polynomial can give the whole picture of a function by passing all the sampling points instead of the local image of Taylor series by using the local derivatives. (2) The boundary problem can be easily solved by adopting piecewise interpolation polynomial algorithm.

te interpolation theorem

1) Lagrange Interpolation Formula for One Variable

1. One dimensional interpolation with an example

Assume that there are $m + 1$ data points (x_i, y_i) for $i = 0,\ldots, m$, $y_i = f(x_i)$, and $x_i \neq x_j$ for $i \neq j$. The task of polynomial interpolation is to find an approximate function (*interpolant*) $p(x)$ such that at the nodes x_i: $p(x_i) = y_i$. We define p in the form $p(x) = \sum_{i=0}^{m} L_i(x) y_i$. In order to satisfy the interpolation conditions $p(x_i) = y_i$, it is necessary that $L_i(x_i) = \begin{cases} 1 & for \quad i = j \\ 0 & for \quad i \neq j \end{cases}$, since each of the polynomials $L_0, L_1, \ldots, L_m$ vanishes at all but one of the points x_i. This can be achieved by setting [92]

$$L_i(x) = \frac{(x - x_0)\ldots(x - x_{i-1})(x - x_{i+1})\ldots(x - x_m)}{(x_i - x_0)\ldots(x_i - x_{i-1})(x_i - x_{i+1})\ldots(x_i - x_m)} = \prod_{j \neq i} \left(\frac{x - x_j}{x_i - x_j} \right).$$

Figure 8.6 shows an example [95] for the case $m = 2$, in which $x_0 = 1$, $x_1 = 3$, and $x_2 = 4$. The upper part of the figure shows graphs of the basic functions L_0, L_1, and L_2, each of them is a quadratic polynomial having the value 1 at its associated node and having a zero at each of the other two nodes. Specifically,

$$L_0(x) = \frac{(x-3)(x-4)}{(-2)(-3)}, \; L_1(x) = \frac{(x-1)(x-4)}{(2)(-1)}, \; L_2(x) = \frac{(x-1)(x-3)}{(3)(1)}$$

The lower part of the Figure 8.6 shows the linear combination $p = -1L_0 + (1/2)L_1 + 0L_2$, which is the quadratic polynomial passing through the points $(x_0, y_0) = (1, -1)$, $(x_1, y_1) = (3, 1/2)$, and $(x_2, y_2) = (4, 0)$.

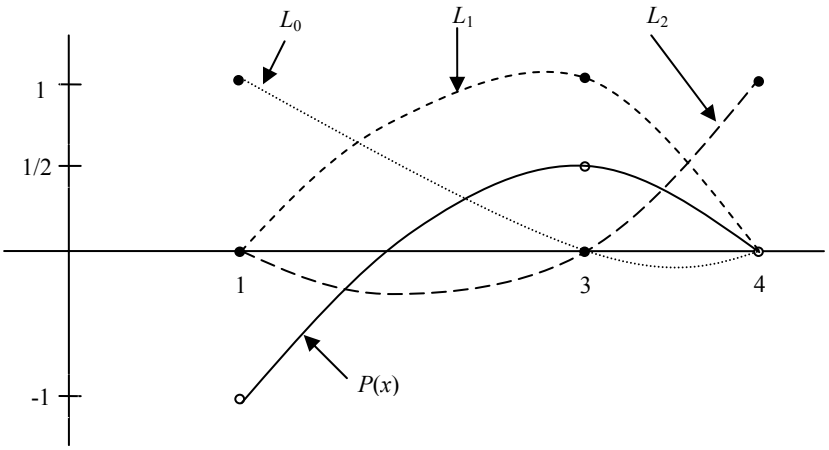

Figure 9.6. Basis functions *Li* and interpolant *p* for a sample problem involving quadratic interpolation.

2. Interpolation error estimation

Theorem 8.1[93] shows how to estimate the distance between the original function and its interpolant.

Theorem 8.1: Let $f(x)$ have an $(n+1)$st derivative, $f^{(n+1)}(x)$, in an interval $[a, b]$. Let $p_n(x)$ interpolate $f(x)$ at the distinct points $x_0, \ldots, x_n$ in the interval $[a, b]$. Then for each $x \in [a, b]$ there exists a point $\xi = \xi(x)$ in the open interval $\min(x_0, \ldots, x_n, x) < \xi < \max(x_0, \ldots, x_n, x)$, such that

$$e_n(x) = f(x) - p_n(x) = \frac{(x-x_0)(x-x_1)\cdots(x-x_n)}{(n+1)!} f^{(n+1)}(\xi) = \frac{\omega_n(x)}{(n+1)!} f^{(n+1)}(\xi) \qquad (8.7)$$

where $e_n(x)$ is the error (also called remainder term), $\omega_n(x) = \prod_{i=0}^{n}(x - x_i)$.

The connection between accuracy and mesh size h is shown as follows. In the case of equidistant nodes $x_{i+1} = x_i + h$ with $x = x_0 + ht$ for $t \in [0, n]$, the error is as follows:

$$e_n(x) = f(x) - p_n(x) = \frac{t(t-1)\cdots(t-n)h^{n+1}}{(n+1)!} f^{(n+1)}(\xi) = \frac{\pi_n(t)h^{n+1}}{(n+1)!} f^{(n+1)}(\xi) \qquad (8.8)$$

where $\pi_n(t) = \prod_{i=0}^{n}(t-i)$.

2) Lagrange Interpolation Formula for Two Independent Variables on a Rectangular Grid

For simplicity, we concentrate on functions of two variables, but extension to more dimensions has no difficulty.

1. Product form

Given n +1 interpolation points $(x_j, y_j, z_j = f(x_j, y_j))$ for the distinct nodes (x_j, y_j), $j = 0, 1, \ldots, n$, we want to find an interpolating algebraic polynomial $p(x, y)$ with $p(x_j, y_j) = f(x_j, y_j)$ for all $j = 0, 1, \ldots, n$. In general, the existence and uniqueness of solution of interpolation for functions in several variables is not certain. Since if all of the points (x_j, y_j) lie on a straight line in x, y, z space, then there are infinitely many planes containing this line [93].

However, if specifically the nodes (x_i, y_j) are $(m + 1)(n + 1)$ distinct points of a rectangular grid for $i = 0, 1, \ldots, m$, $j = 0, 1, \ldots, n$, and $f(x_i, y_j) = f_{ij}$, then this special interpolation problem is solvable uniquely in the product form as follows [92]:

$$p_r(x, y) = \sum_{i=0}^{m} \sum_{j=0}^{n} a_{ij} x^i y^j ,$$

with $(m+1)(n+1)$ coefficients, a_{ij}, to be determined. Here the degree of $p(x, y)$ is defined as $r = \max_{a_{ij} \neq 0} \{i + j\}$. Suppose $m = n$, it can be extended as $p(x, y) = a_{00} + a_{10}x + a_{01}y + a_{20}x^2 + a_{11}xy + a_{02}y^2 + \cdots + a_{m0}x^m + a_{m-1,1}x^{m-1}y + \cdots + a_{0m}y^m$.

2. Blending process

The Lagrange polynomial may be generalized for two variables via the double blending process [94].

For a general function $f(x, y)$, if the value of x is fixed at x_i, then the equation $z = f(x_i, y)$ corresponds to the curve defined by the intersection of the plane $x = x_i$ and the surface $z = f(x, y)$. Assume there are $m + 1$ such curves, corresponding to $x = x_0, x_1, \ldots, x_m$. Then the univariate Lagrange interpolation function can be constructed as follows:

$$\xi(x, y) = \sum_{i=0}^{m} f(x_i, y) L_i(x),$$

where

$$L_i(x) = \prod_{j \neq i} \left(\frac{x - x_j}{x_i - x_j} \right),$$

$\xi(x, y)$ is called a blending function. $\xi(f; x, y)$ is denoted as the blending function dependent on the function f. The blending function $\xi(f; x, y)$ agrees with $f(x, y)$ at all points where the plane $x = x_i$ intersects $z = f(x, y)$, for $0 \leq i \leq m$.

If the roles of x and y are interchanged in the construction of a blending function, an alternative blending function is as follows:

$$\eta(x, y) = \eta(f; x, y) = \sum_{j=0}^{n} f(x, y_j) M_j(y),$$

where

$$M_j(y) = \prod_{k \neq j} \left(\frac{y - y_k}{y_j - y_k} \right),$$

$M_j(y)$ is the fundamental polynomials of the univariate Lagrange interpolation at the

variables $y = y_0, y_1, \ldots, y_n$. The second blending function $\eta(f; x, y)$ agrees with $f(x, y)$ at all points where the plane $y = y_j$ intersects $z = f(x, y)$, for $0 \le j \le n$.

If the second blending process is applied not to $f(x, y)$, but to the first blending function $\xi(x, y)$, the following equation is obtained:

$$p(x,y) = \eta(\xi; x, y) = \sum_{j=0}^{n} \left(\sum_{i=0}^{m} f(x_i, y_j) L_i(x) \right) M_j(y),$$

For $\xi(x, y)$ agrees with $f(x, y)$ along the $m + 1$ curves defined by the intersection of the planes $x = x_i$ with the surface $z = f(x, y)$, for $0 \le i \le m$, and $p(x, y)$ agrees with $\xi(x, y)$ along the $n + 1$ curves defined by the intersection of the planes $y = y_j$ with the surface $z = \xi(x, y)$. Thus $p(x, y)$ agrees with $f(x, y)$ on all points (x_i, y_j) for $i = 0, 1, \ldots, m, j = 0, 1, \ldots, n$.

From another view point, $L_i(x)M_j(y)$ has the value 1 at the point (x_i, y_j), and the value zero at all other points. Thus the required polynomial satisfying $p(x_i, y_j) = f(x_i, y_j)$ can be written as:

$$p(x,y) = \sum_{i=0}^{m} \sum_{j=0}^{n} f(x_i, y_j) L_i(x) M_j(y).$$

3. Cartesian product

Central of the product interpolation is the notion of *Cartesian product* [95]. Denoting the two sets defined above by

$$X = \{ x_0, x_1, \ldots, x_m \} \text{ and } Y = \{ y_0, y_1, \ldots, y_n \},$$

A rectangular grid of $(m + 1) \times (n + 1)$ points can be written as

$$X \times Y = \{ (x_i, y_j) \mid x_i \in X, y_j \in Y \}.$$

$X \times Y$ is called the *Cartesian product* of the two sets X and Y [94].

For example, let $X = Y = \{-1, 1\}$, then the *Cartesian product* of X and Y is the set of points $\{(-1, -1), (-1, 1), (1, -1), (1, 1)\}$. And the interpolating polynomial for a function f defined on these points is given by

$$p(x,y) = f(-1,-1)\cdot\frac{1}{4}(x-1)(y-1) - f(-1,1)\cdot\frac{1}{4}(x-1)(y+1)$$
$$- f(1,-1)\cdot\frac{1}{4}(x+1)(y-1) + f(1,1)\cdot\frac{1}{4}(x+1)(y+1)$$

4. Interpolation error estimation for two variables [93]

If $f(x, y)$ has continuous partial derivatives of orders $m + 1$ and $n + 1$, respectively, in x and y and the appropriate mixed derivative of order $m + n + 2$, then by applying the extension of Theorem 8.1 the error becomes

$$e_n(x,y) = f(x,y) - p_n(x,y) = \frac{\omega_m(x)}{(m+1)!}\frac{\partial^{m+1} f(\xi,y)}{\partial x^{m+1}} + \frac{\omega_n(y)}{(n+1)!}\frac{\partial^{n+1} f(x,\eta)}{\partial y^{n+1}}$$
$$- \frac{\omega_m(x)\omega_n(y)}{(m+1)!(n+1)!}\frac{\partial^{m+n+2} f(\xi',\eta')}{\partial x^{m+1}\partial y^{n+1}} \tag{8.9}$$

In the case of equidistant nodes $x_{i+1} = x_i + h_x$ with $x = x_0 + h_x t_x$ for $t_x \in [0, m]$, and $y_{i+1} = y_i + h_y$ with $y = y_0 + h_y t_y$ for $t_y \in [0, n]$, we can obtain special error forms as follows:

$$e_n(x,y) = f(x,y) - p_n(x,y) = \frac{h_x^{m+1}\pi_m(t_x)}{(m+1)!}\frac{\partial^{m+1} f(\xi,y)}{\partial x^{m+1}} + \frac{h_y^{n+1}\pi_n(t_y)}{(n+1)!}\frac{\partial^{n+1} f(x,\eta)}{\partial y^{n+1}}$$
$$- \frac{h_x^{m+1}h_y^{n+1}\pi_m(t_x)\pi_n(t_y)}{(m+1)!(n+1)!}\frac{\partial^{m+n+2} f(\xi',\eta')}{\partial x^{m+1}\partial y^{n+1}} \tag{8.10}$$

where h_x is equidistant along the x axis; h_y is equidistant along the y axis; $\pi_m(t_x) = \prod_{i=0}^{m}(t_x - i)$; $\pi_n(t_y) = \prod_{i=0}^{n}(t_y - i)$.

Assuming $m = n$, and $h_x = h_y = h$, then (8.10) becomes (8.11):

$$e_n(x,y) = f(x,y) - p_n(x,y) = \frac{h^{n+1}}{(n+1)!}\left(\pi_n(t_x)\frac{\partial^{n+1} f(\xi, y)}{\partial x^{n+1}} + \pi_n(t_y)\frac{\partial^{n+1} f(x,\eta)}{\partial y^{n+1}} \right) - \frac{h^{2(n+1)}\pi_n(t_x)\pi_n(t_y)}{((n+1)!)^2}\frac{\partial^{2(n+1)} f(\xi', \eta')}{\partial x^{n+1}\partial y^{n+1}} \tag{8.11}$$

The partial derivative factor may become big in high degree. Thus high degree polynomial interpolation is risky! The next section will discuss one way to circumvent the use of high degree polynomial interpolation without abandoning the use of fine grids.

5. Piecewise polynomial interpolation [96]

If there are many known interpolation points, the problem of interpolating by a polynomial of "large" degree is met. On one hand, the calculation and evaluation of the interpolating polynomial becomes costly and unreliable as the number of interpolation points becomes large. On the other hand, the use of interpolating polynomials of high degree may increase error. Thus, the interpolating polynomials of high degree can be avoided by partitioning the interval into sufficiently small subintervals and interpolating $f(x)$ in each subinterval by a suitable polynomial. This leads to *piecewise-polynomial interpolation*, which is a way to incorporate many points into the interpolation of a function without using high degree polynomials.

3) Lagrange Interpolation Formula for Multi Independent Variables on a Rectangular Grid

It is obvious to extend all these ideas to boxlike regions in three-dimension. Consider three sets defined by

$$X = \{ x_0, x_1, \ldots , x_m \},\ Y = \{ y_0, y_1, \ldots , y_n \}, \text{ and } Z = \{ z_0, z_1, \ldots , z_l \}.$$

$p(x, y, z)$ interpolates $f(x, y, z)$ on the set defined by Cartesian product $X \times Y \times Z$ as follows:

$$p(x, y, z) = \sum_{i=0}^{m} \sum_{j=0}^{n} \sum_{k=0}^{l} f(x_i, y_j, z_k) L_i(x) M_j(y) N_k(z),$$

where $L_i(x)$, $M_j(y)$, and $N_k(z)$ are fundamental polynomials defined on X, Y, and Z, respectively.

The product interpolation offers the most direct way to use one-dimensional results in multi-dimensional settings. The idea is to use one-dimensional interpolation in each coordinate direction, which allows the products of the interpolating functions to govern variations in directions oblique to the coordinate axes.

The product approach can be extended to the interpolation of functions $f(x_1, x_2, \ldots , x_d)$ of arbitrarily many variables. The main requirement is that the function f is defined on some hypercube $[a_1, b_1] \times [a_2, b_2] \times \cdots \times [a_d, b_d]$ in the d-dimensional Euclidean space. Then a d-dimensional grid $X_1 \times X_2 \times \cdots \times X_d$ can be constructed by using grids in each of the orthogonal coordinate directions x_1, x_2,…, x_d. The product scheme may be automatically applied on the set defined by Cartesian product $X_1 \times X_2 \times \cdots \times X_d$.

ion application procedure

1) Cutting the feasible region into small pieces for piecewise interpolation

The degree of polynomial interpolation is assumed as $m = n = 3$ in order to be easily

solved in optimal power flow model because high order polynomial is expensive to evaluate and calculate in an optimization model. Then, the selection of the mesh size h depends on the error estimation. If it is assumed that the partial derivatives are all less than M, the upper bound of error estimation may be derived from (8.10) as follows:

$$\begin{aligned}
\left|e_n(x,y)\right| &\le \left|\frac{h^{n+1}}{(n+1)!}\left(\pi_n(t_x)\frac{\partial^{n+1}f(\xi,y)}{\partial x^{n+1}}+\pi_n(t_y)\frac{\partial^{n+1}f(x,\eta)}{\partial y^{n+1}}\right)-\frac{h^{2(n+1)}\pi_n(t_x)\pi_n(t_y)}{((n+1)!)^2}\frac{\partial^{2(n+1)}f(\xi',\eta')}{\partial x^{n+1}\partial y^{n+1}}\right| \\
&\le \frac{h^{n+1}}{(n+1)!}\max\left|\pi_n(t)\right|\cdot\left(\left|\frac{\partial^{n+1}f(\xi,y)}{\partial x^{n+1}}\right|+\left|\frac{\partial^{n+1}f(x,\eta)}{\partial y^{n+1}}\right|\right)+\left(\frac{h^{n+1}}{(n+1)!}\max\left|\pi_n(t)\right|\right)^2\cdot\left|\frac{\partial^{2(n+1)}f(\xi',\eta')}{\partial x^{n+1}\partial y^{n+1}}\right| \\
&\le \left[\frac{h^{n+1}}{(n+1)!}\max\left|\pi_n(t)\right|\cdot 2+\left(\frac{h^{n+1}}{(n+1)!}\max\left|\pi_n(t)\right|\right)^2\right]\cdot M
\end{aligned} \tag{8.11}$$

If $n = 3$, $\pi_3(t)$ is equal to $t(t\text{-}1)(t\text{-}2)(t\text{-}3)$ as shown in Figure 8.7. The maximum absolute value of $\pi_3(t)$ is "1" when $t = 0.38$. Substituting $n = 3$ and $\max|\pi_3(t)| = 1$ into (8.11), we have:

$$\left|e_n(x,y)\right| \le \left[\frac{h^{n+1}}{(n+1)!}\max\left|\pi_n(t)\right|\cdot 2+\left(\frac{h^{n+1}}{(n+1)!}\max\left|\pi_n(t)\right|\right)^2\right]\cdot M = \left(\frac{h^4}{12}+\frac{h^8}{24^2}\right)\cdot M \tag{8.12}$$

If $h = 2$ MVar, $|e_n(x, y)| \le 1.78\ M$ (p.u.); if $h = 3$, $|e_n(x, y)| \le 18.14\ M$ (p.u.); and if $h = 4$, $|e_n(x, y)| \le 135.11\ M$ (p.u.). Even though the accurate value of M is hard to approximate, the difference of error level corresponding to mesh size is clearly shown. The guess of M is given as 0.02 based on the data in Table 8.1, hence, mesh size $h = 2$ is preferred in order to keep the maximum error lower than 1% considering the real value of TTC ≈ 5.0 (p.u.).

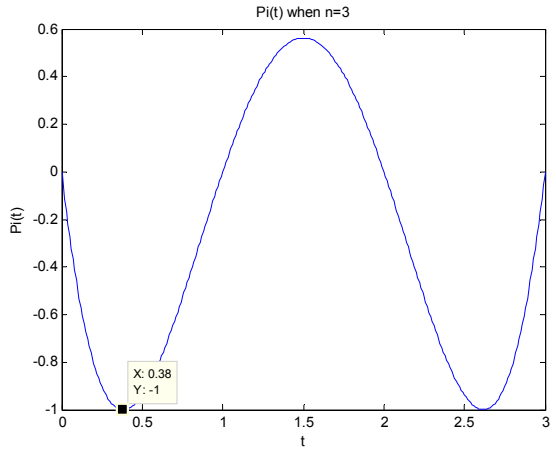

Figure 9.7. Function π3(t).

Assume the feasible region is 0 <= Q_{c3} <= 48 MVar, 0 <= Q_{c5}<= 48 MVar. It can be divided into 64 small pieces by every 6 MVar, as is shown in Table 8.3. The cells in white background show the 6 sub-regions of the 64 ones, which are {0 <= Q_{c3} <= 6, 0 <= Q_{c5}<= 6}, {6 <= Q_{c3} <= 12, 0 <= Q_{c5}<= 6}, {12 <= Q_{c3} <= 18, 0 <= Q_{c5}<= 6}, {0 <= Q_{c3} <= 6, 6 <= Q_{c5}<= 12}, {6 <= Q_{c3} <= 12, 6 <= Q_{c5}<= 12}, and {12 <= Q_{c3} <= 18, 6 <= Q_{c5}<= 12}. The cells in gray background are the common borders of these sub-regions. Interpolation is applied on every sub-region, thus there is an interpolation polynomial function corresponding to each sub-region. The two neighboring interpolation functions will cover all the points on their common borders, thus all the piecewise functions can be connected continuously. This is the fundamental difference from the Taylor series formulation, which presents difficulty in identifying the boundary location.

Table 9.3. Feasible region cutting and sampling point value.

Q_{c5}(MVar) / Q_{c3}	0	2	4	6	8	10	12	…	48
0	4.6424	4.6550	4.6676	4.6802	4.6928	4.7054	4.7180		4.8283
2	4.6819	4.6945	4.7070	4.7196	4.7322	4.7448	4.7574		4.8241
4	4.7213	4.7338	4.7464	4.7589	4.7715	4.7841	4.7967	…	4.8200
6	4.7606	4.7731	4.7856	4.7982	4.8107	4.8233	4.8358		4.8160
8	4.7997	4.8122	4.8247	4.8372	4.8498	4.8623	4.8749		4.8121
10	4.8387	4.8512	4.8637	4.8762	4.8887	4.9013	4.9020	…	4.8083
12	4.8776	4.8901	4.9026	4.9151	4.9089	4.9028	4.8968		4.8047
14	4.9164	4.9224	4.9161	4.9098	4.9037	4.8977	4.8917		4.8011
16	4.9234	4.9170	4.9108	4.9046	4.8986	4.8926	4.8868	…	4.7976
18	4.9180	4.9117	4.9056	4.8995	4.8935	4.8877	4.8819		4.7943
⋮			⋮			⋮		⋱	
48	4.8481	4.8435	4.8390	4.8347	4.8304	4.8261	4.8217		4.7559

2) Piecewise interpolation polynomial functions

The sampling points in Table 8.3 are interpolated based on the following equation, which is concluded in the previous interpolation theorem section.

$$p(x,y)=\sum_{i=0}^{m}\sum_{j=0}^{n} f(x_i,y_j)\cdot\prod_{l\neq i}\left(\frac{x-x_l}{x_i-x_l}\right)\cdot\prod_{k\neq j}\left(\frac{y-y_k}{y_j-y_k}\right)$$

There should be 64 interpolation polynomial functions in total corresponding to the whole feasible region. Here, only 6 functions corresponding to the 6 sub-regions in Table 8.3 are listed as follows for illustration.

$$TTC=\begin{cases} TTC_1(Q_{c3},Q_{c5}) & if\{0<=Q_{c3}<=6,0<=Q_{c5}<=6\} \\ TTC_2(Q_{c3},Q_{c5}) & if\{6<=Q_{c3}<=12,0<=Q_{c5}<=6\} \\ TTC_3(Q_{c3},Q_{c5}) & if\{12<=Q_{c3}<=18,0<=Q_{c5}<=6\} \\ TTC_4(Q_{c3},Q_{c5}) & if\{0<=Q_{c3}<=6,6<=Q_{c5}<=12\} \\ TTC_5(Q_{c3},Q_{c5}) & if\{6<=Q_{c3}<=12,6<=Q_{c5}<=12\} \\ TTC_6(Q_{c3},Q_{c5}) & if\{12<=Q_{c3}<=18,6<=Q_{c5}<=12\} \\ \vdots & \end{cases}$$

Table 9.4. Coefficients of TTC polynomials.

Func.	TTC_1	TTC_2	TTC_3	TTC_4	TTC_5	TTC_6
x(MVar)	[0,6]	[6,12]	[12,18]	[0,6]	[6,12]	[12,18]
y(MVar)	[0,6]	[0,6]	[0,6]	[6,12]	[6,12]	[6,12]
Coefficients of polynomial items						
Const.	4.64	4.64	2.88	4.64	8.35	4.87
x	2×10^{-2}	2×10^{-2}	3.6×10^{-1}	2×10^{-2}	-1.4	1.6×10^{-2}
y	6.3×10^{-3}	6.3×10^{-3}	-1.7	6.3×10^{-3}	-1.6	2.7×10^{-2}
x^2	-1.5×10^{-5}	-1.5×10^{-5}	-2.1×10^{-2}	-1.5×10^{-5}	1.6×10^{-1}	-1.2×10^{-3}
xy			3.4×10^{-1}		5.9×10^{-1}	-5.8×10^{-3}
y^2			6.7×10^{-1}		2.1×10^{-1}	-3.1×10^{-3}
x^3			4.1×10^{-4}		-6.2×10^{-3}	2.5×10^{-5}
x^2y			-2.3×10^{-2}		-7.1×10^{-2}	3.6×10^{-4}
xy^2			-1.3×10^{-1}		-8×10^{-2}	5.9×10^{-4}
y^3			-5.6×10^{-2}		-8.9×10^{-3}	1×10^{-4}
x^3y			5.1×10^{-4}		2.7×10^{-3}	
x^2y^2			8.9×10^{-3}		9.6×10^{-3}	-3.7×10^{-5}
xy^3			1.1×10^{-2}		3.3×10^{-3}	-2×10^{-5}
x^3y^2			-1.9×10^{-4}		-3.7×10^{-4}	
x^2y^3			-7.4×10^{-4}		-4×10^{-4}	
x^3y^3			1.6×10^{-5}		1.5×10^{-5}	

Assume $x = Q_{c3}$ and $y = Q_{c5}$. The coefficients of TTC_i are shown in Table 8.4:

Figure 8.8 demonstrates the combination of these piecewise interpolation functions in the whole feasible region, and the original GAMS TTC result as reference for the comparison purpose. Figure 8.9 shows the error between the above two surfaces. The sampling step is 2 MVar in this case, the maximum error = 0.006 p.u. (≈ 0.1%) is acceptable. The error will become greater with the increase of the sampling step h. As analyzed in (8.12), if $h = 2$, $|e_n(x, y)| \leq 1.78\ M$ (p.u.); if $h = 3$, $|e_n(x, y)| \leq 18.14\ M$ (p.u.); and if $h = 4$, $|e_n(x, y)| \leq 135.11\ M$ (p.u.). The difference of error level corresponding to mesh size is considered before interpolation is applied.

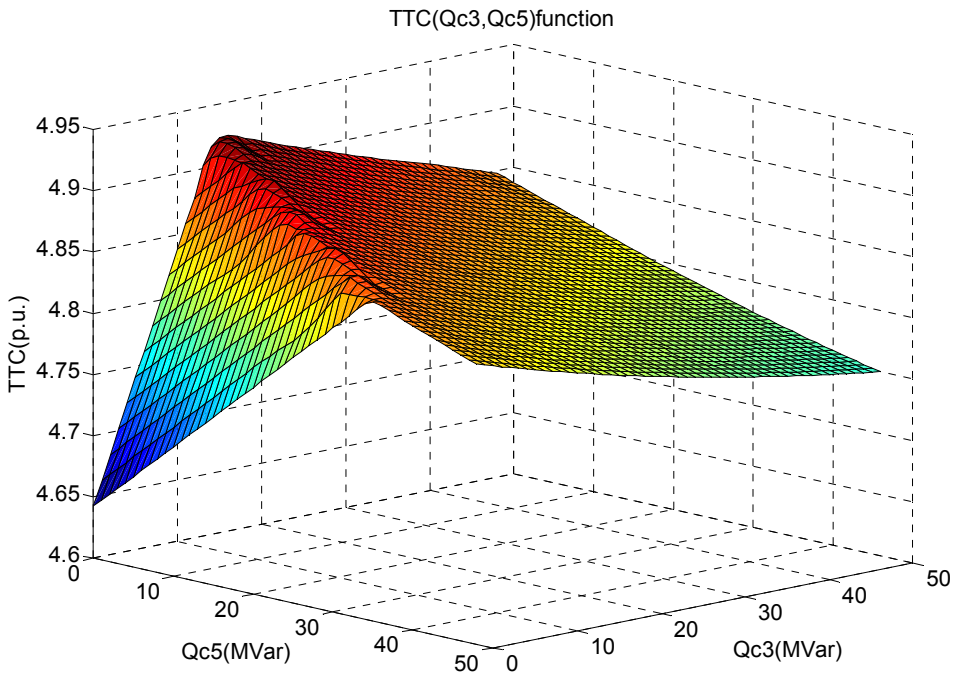

Figure 9.8. Interpolation approximation for TTC function.

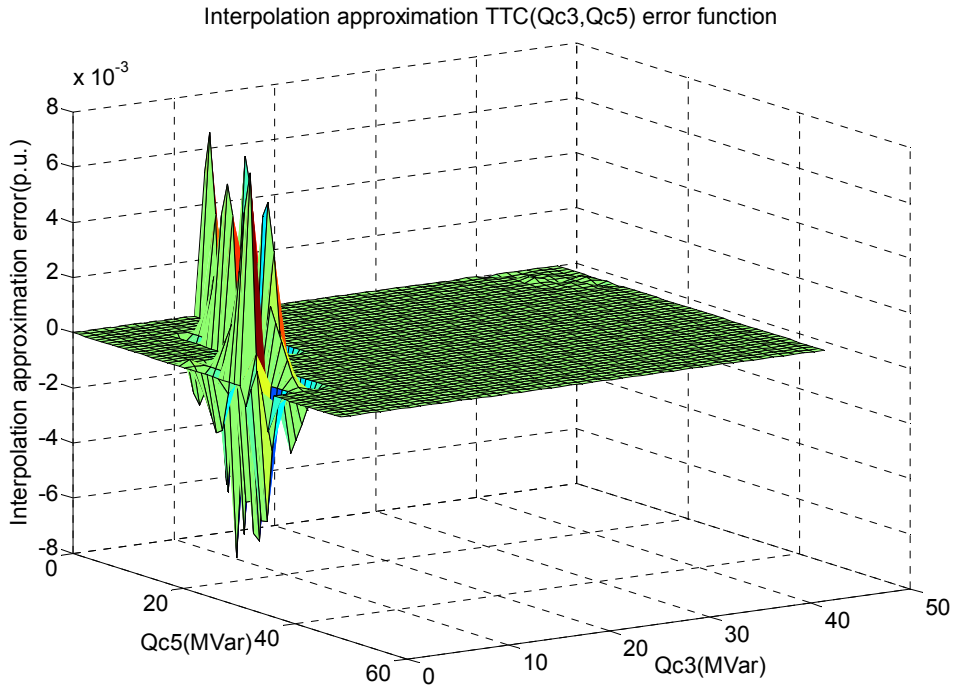

Figure 9.9. Interpolation approximation error function.

Table 9.5. Variables output from VSCOPF with interpolation approximation GAMS model.

Objective							
Fuel cost ($/hr)			Var cost ($/hr)			Total cost ($/hr)	
15170.08			25.26			15195.34	
Variables output							
Bus	1	2	3	4	5	6	7
Q_c (MVar)			15.03				
y (binary)			1				
P_{Go} (MW)	85.46			200.00		300.00	195.47
Q_{Go} (MVar)	80.46			100.00		51.58	54.63
P_{Lo}(MW)		100.00	190.00	150.00	200.00	50.00	80.00
Q_{Lo}(MVar)		40.00	75.00	50.00	60.00	20.00	40.00
V_o (V)	1.05	1.01	0.99	1.00	0.97	1.04	1.01
PoC_o(MVA)	369.25						
PoC_*(MVA)	492.33						

3) GAMS output of the VSCOPF with interpolation approximation model

The piecewise interpolation TTC approximation function is incorporated into GAMS VSCOPF model. The result from VSCOPF with interpolation approximation GAMS model is shown in Table 8.5.

9.4 Comparison of the interpolation approximation, least square ation given in refs. [63], and the two sets of variables method

Reference [63] is one of the very few papers related to voltage stability constrained Var planning OPF model simplification by approximation. This section describes how the approximating accuracy given in [63] can be improved by the interpolation approximation. Reference [63] uses a standard linear/quadratic ordinary least square multi-variate regression model to approximate the locus of TTC in order to obtain the lower computational complexity. The locus of TTC is estimated over various Var compensation scenario/configurations such as increasing the Var support step by step at each individual bus; and various combinations of Var compensation across the buses. The

locus of TTC can be expressed as a function of the bus reactive compensation as:

$$TTC = a + \sum_i b_i Q_{ci} \tag{8.13}$$

$$\text{or} \quad TTC = a + \sum_i b_i Q_{ci} + \sum_i c_i Q_{ci}^2 \tag{8.14}$$

where *TTC* is the maximum MVA loadability for the system with reactive compensation; a, b_i, c_i, are parameters of the locus which may be estimated using the multivariate ordinary least square (OLS) regression method; and Q_{ci} is the reactive compensation from new sources at bus *i*. However, if the number of candidate buses is increased, the procedure will involve evaluating a large number of Var support configurations to capture the interaction of Var compensation at different locations with specified accuracy.

Given the computational advantage, linear and quadratic function forms are selected by [63] to estimate the path of TTC. However, large amount of path of TTC such as the one in 7-bus case as shown in Figure 8.2 will seriously lose the accuracy if approximated by linear or quadratic function as shown in Figure 8.10 - 8.13.

Figure 8.10 shows the TTC approximation using quadratic least square assuming the feasible region is 0-20MVar, and the sampling step size is 1MVar. Figure 8.11 uses 2MVar as step size. The least square quadratic polynomial corresponding to Figure 8.10 is $TTC|_{(0\text{-}20)} = 4.67 - 0.000088 * Q_{c3}^2 + 0.0036 * Q_{c3} - 0.00088 * Q_{c5}^2 + 0.0265 * Q_{c5}$. Figure 8.12 shows the TTC approximation using quadratic least square assuming the feasible region is 0-50MVar. Figure 8.13 uses 2MVar as step size. The least square quadratic polynomial corresponding to Figure 8.12 is $TTC|_{(0\text{-}50)} = 4.84 - 0.000042 * Q_{c3}^2 + 0.00068 * Q_{c3} - 0.000067 * Q_{c5}^2 + 0.0026 * Q_{c5}$. It is shown in Figure 8.10 -13 that the larger assumed feasible region, the results are less accurate.

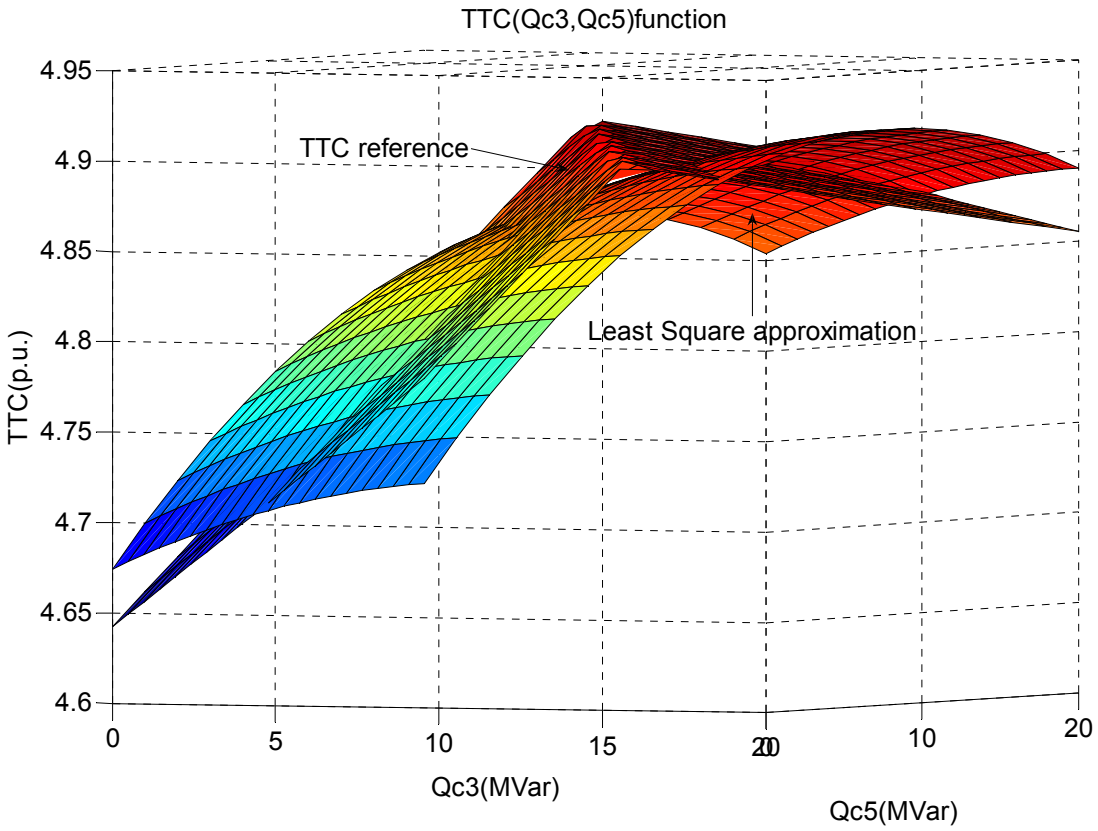

Figure 9.10. TTC approximation error illustration using least square quadratic approximation (feasible region from 0-20MVar, step size = 1MVar).

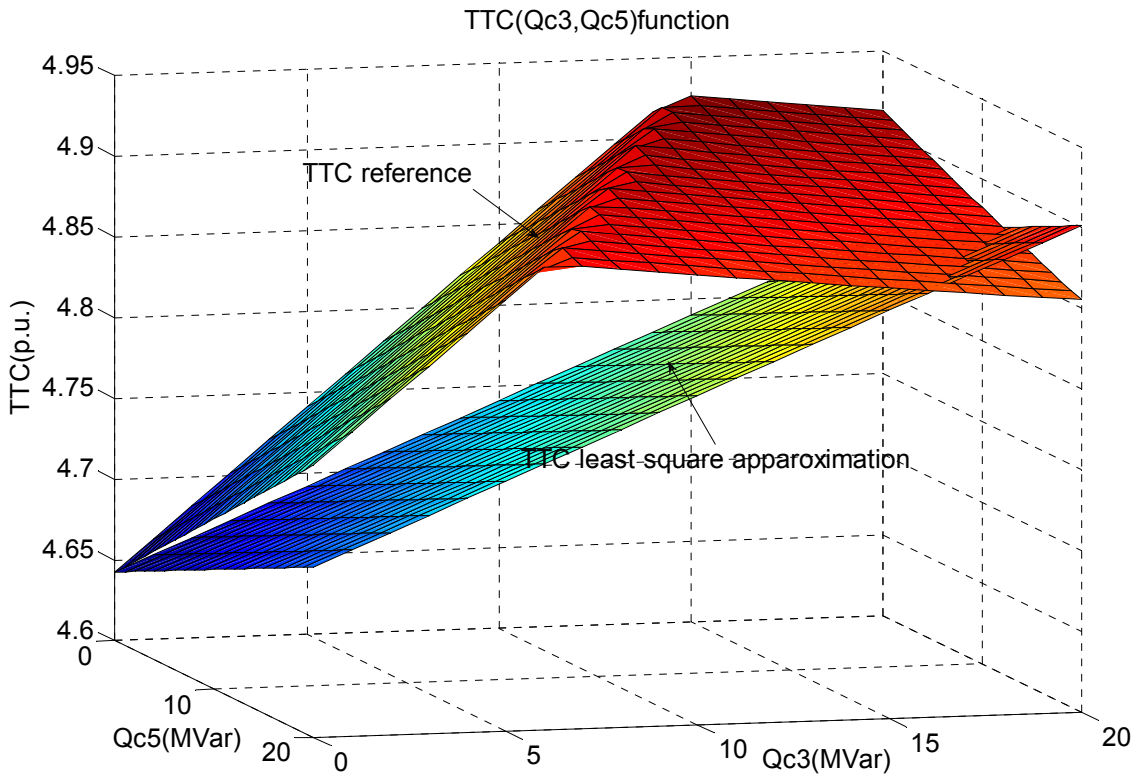

Figure 9.11. TTC approximation error illustration using least square quadratic approximation (feasible region from 0-20MVar, step size = 2MVar).

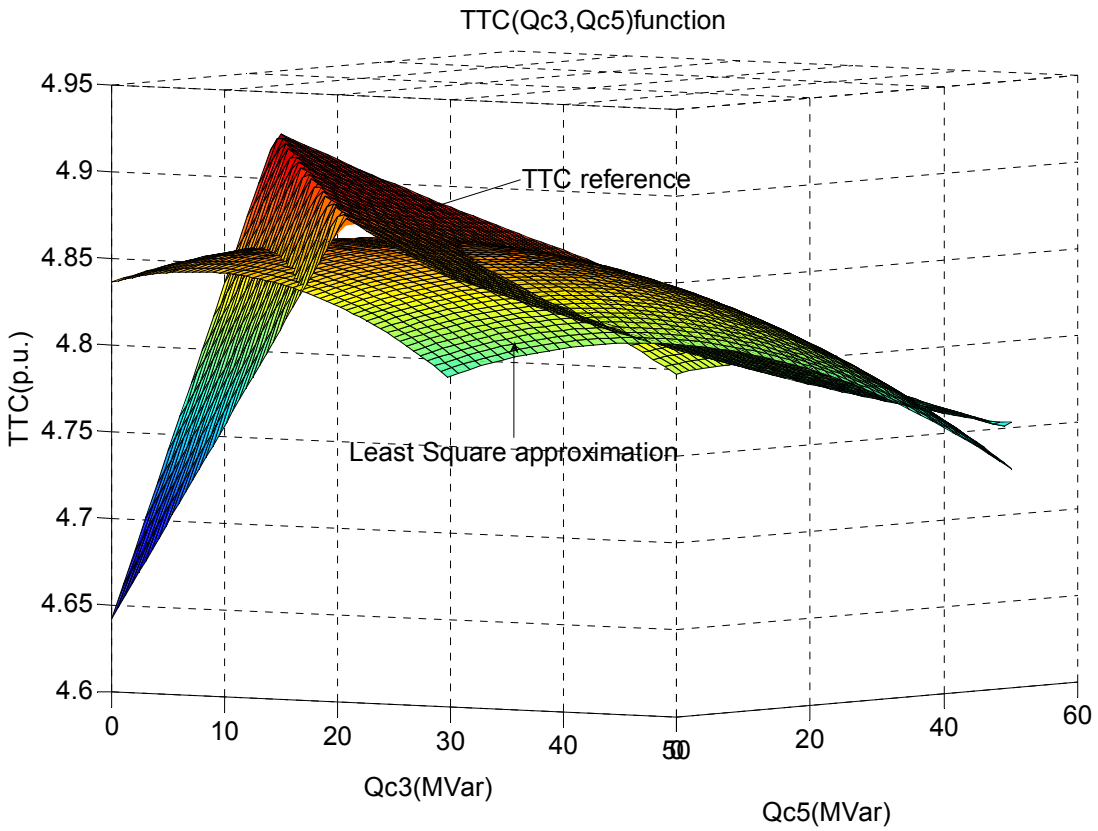

Figure 9.12. TTC approximation error illustration using least square quadratic approximation (feasible region from 0-50MVar, step size = 1MVar).

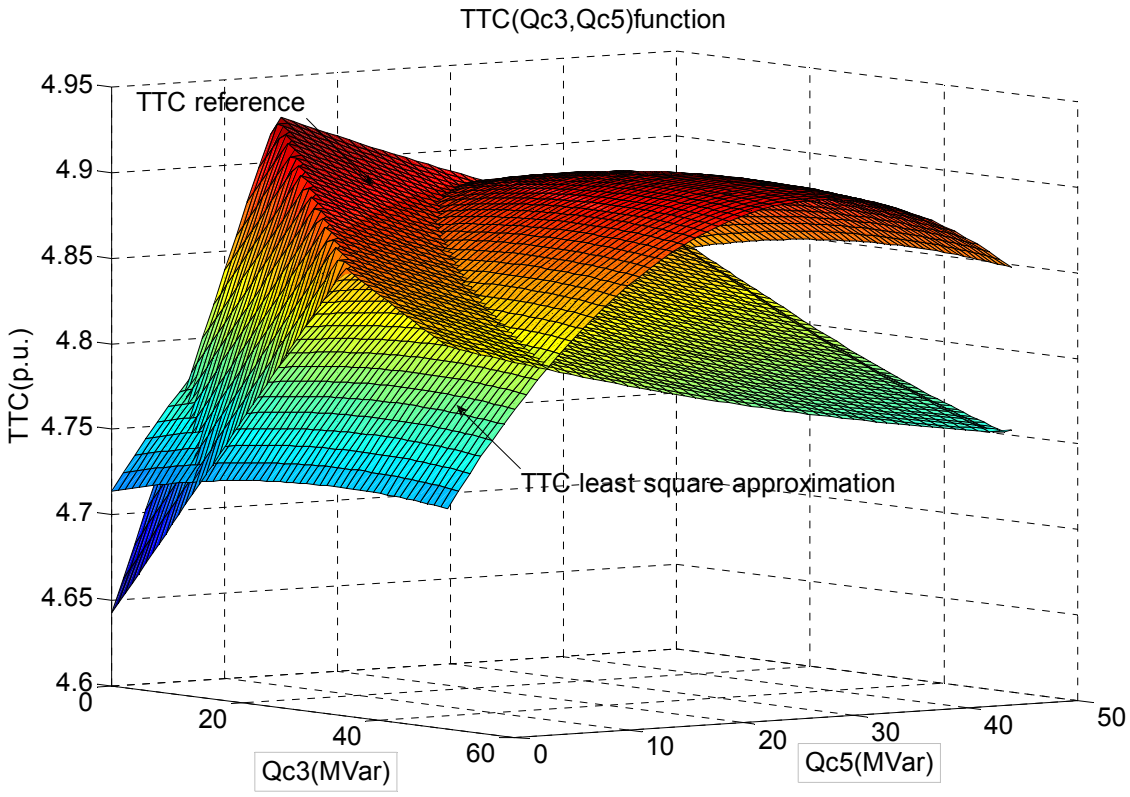

Figure 9.13. Illustration of TTC approximation error using least square quadratic approximation (Feasible region: 0-50MVar; Step size = 2MVar).

As a result, the Var planning model will possibly miss the true optimal solution because linear/quadratic function formulation may not have the capability to capture the turning boundary of the TTC versus Q_c surface in non-linear/non-quadratic cases. Thus, linear or quadratic function, though easier to solve, cannot be used at all in the cases due to losing control of error in a reasonable range. Piecewise interpolation may create the functions suitable for any shape of TTC vs. Q_c curve with reasonable degree of accuracy as analyzed in the previous section.

Usually, interpolation approximation needs less sampling points than least square method under the same accuracy. That is one reason why [63] evaluates large amount of scenarios to obtain many observation points to apply Least Square; the other reason is the linear/quadratic function form proposed in [63] is short of coupling item such as $Q_{ci}*Q_{cj}$ corresponding to the interaction of Var compensation at different locations. Therefore, the coupling effect that should be reflected in the coefficients d_i of the item $Q_{ci}*Q_{cj}$ has to be incorporated into the coefficients b_i and c_i of linear and quadratic items such as Q_{ci} and Q_{ci}^2 in (8.13) and (8.14). This not only implies potentially a large number of Var support configurations to be enumerated in order to get a "coupling item coefficients integrated estimation of b_i and c_i", but also causes less accuracy when the true result is compensation at a single location (a very common case).

The interpolation polynomial has coupling item $Q_{ci}*Q_{cj}$, which can avoid all the trouble brought by the least square polynomial in [63]. Then number of scenarios to be evaluated in the interpolation model depends on the specified degree of accuracy, and does not need to increase the amount of observation points to consider the interaction of Var compensation at different buses.

The main results from 3 models discussed in this dissertation (TSV method I, Interpolation method, and Least Square method) are compared in Table 8.6. The Least Square method totally loses the accuracy on location selection, since it shifts the optimal location from Bus 3 to Bus 5. The Q_c amounts (13.93MVar at Bus 5 for 0-20 feasible region with 1MVar step size, 4.87MVar at Bus 5 for 0-50 feasible region with 1MVar step size) of Least Square method are also very different from the TSV method (14.54MVar) and Interpolation method (15.03 MVar) due to the inaccurate estimation of TTC function as shown in Table 8.6. In the test, the actual TTCs at the Q_c calculated from each method are re-calculated using the accurate TTC OPF model in Section 4.2.2, and then compared with the TTC predicted by each method. The TTC error of the Least Square method (14.36 MVA, 17.41 MVA) is much higher than that of Two Sets of Variable method (0.04MVA) and Interpolation method (0.23MVA). Thus, the objective values of least square method are not precise due to the inaccurate TTC estimation. The actual objective values based on the actual TTC are the real values corresponding to the Var location and size results of every model. If the objective ($15193.56/hr) of TSV model without approximation is treated as the reference, the objective error of interpolation approximation is only $0.98/hr. However, the objective errors of least square approximation are $66.09/hr and $80.56/hr corresponding to 0-20MVar feasible region with 1MVar step size and 0-50 feasible region with 1MVar step size respectively. The least square method makes inaccurate TTC estimation in this case. As a result, it loses the ability to make a sound decision about the Var location and size selection.

Table 8.7 compares the TSV model, Least Square model and Interpolation model at

Table 9.6. Three models' results comparison.

Model type / Main result	VSCOPF with two sets of variables (TSV)	VSCOPF with interpolation approximation (step size 2MVar)	VSCOPF with least square approximation Qc(0-20) MVar (step size 1MVar)	VSCOPF with least square approximation Qc(0-50) MVar (step size 1MVar)	VSCOPF with least square approximation Qc(0-20) MVar (step size 2MVar)	VSCOPF with least square approximation Qc(0-50) MVar (step size 2MVar)
Total NLP seconds	0.219	0.176	0.188	0.172	0.172	0.141
Objective ($/hr)	15193.44	15195.34	15207.65	15210.64	15224.98	15217.25
Qc location	Bus3	Bus3	Bus5	Bus5	Bus5	Bus5
Qc amount (MVar)	14.54	15.03	13.93	4.87	20	25.27
TTC (MVA)	492.73	492.33	487.38	484.72	483.86	487.20
Actual *TTC*	492.69	492.56	473.02	467.31	476.85	480.18
TTC error (MVA & %)	0.04 (0.0081%)	0.23 (0.046%)	14.36 (3.04%)	17.41 (3.73%)	7.01(1.47%)	7.02 (1.46%)
Actual objective based on actual *TTC* ($/hr)	15193.56	15194.54	15259.65	15274.12	15250.35	15242.54
Objective error compared to "two sets of var. model" ($/hr)	0	0.98	66.09	80.56	56.79	48.98

Table 9.7. Comparison of three models.

	Accuracy	Easiness in Computational effort
Two Sets of Variables (TSV) model	***	*
Least Square model in [62]	*	***
Interpolation model	**	**

accuracy and computational time aspects. The more "*" means desired features in Table 8.7. TSV model is the most accurate, but needs the longest computational effort. Least Square model is fastest due to its simple approximation function form, but the least accurate level. Interpolation model proposed in this work is more accurate than Least Square model in [62], and easier to solve than two sets of variables model.

9.5 Conclusion

In this chapter, two approximation methods, Taylor series and Interpolation are presented to simplify the previous VSCOPF with TSV model. The Taylor series has been shown to be incompetitive to the Interpolation method. Then, Interpolation method is compared with the TSV method and another simplified method, the Least Square method proposed in [62]. The test on a seven-bus system shows that very close results are obtained from TSV method and the Interpolation approximation, but the Least Square method shown in literature loses its accuracy on TTC estimation, objective calculation, and Var location and size selection. The conclusions including advantages and disadvantages of every method are compared and summarized as follows:

- The two sets of variables model can be simplified by an approximate method to express TTC as a function of Q_c. This can remove the needs to model all collapse point (PoC) state variables, all PoC state constraints, the power flow constraints, and the bounds in VSCOPF formulation. Thus, the number of variables and constraints would be nearly halved. This is a significant simplification especially for a mixed non-linear optimization problem.
- Taylor series is a series expansion of a function around a point based on its local

derivative information. It is only accurate when it is close to this point. However, challenges arise if the TTC-Q_c curve has a turning point or surface. It is difficult to locate this turning point or surface for an expansion of a multi-dimension function without running a large amount of TTC versus Q_c simulation to obtain such information.

- Interpolation polynomial can give the whole picture of a function by passing all the sampling points instead of local image of Taylor series by using the local derivatives.
- The boundary problem can be easily solved by adopting piecewise interpolation polynomial algorithm. Interpolation is applied on every predefined sub-region, thus there is an interpolation polynomial function corresponding to each sub-region. The two neighboring interpolation functions will cover all the points on their common border, thus all the piecewise functions can be connected continuously, unlike the Taylor series having boundary location problem.
- The shortcoming of interpolation lies in the bigger error at the non-smooth part of the original function than at the smooth part. The above disadvantage can be overcome by decreasing the sampling step width until the maximum error is acceptable.
- Theoretically, piecewise interpolation may create the function form suitable for any shape of TTC vs. Q_c curve with reasonable degree of accuracy, but linear/quadratic functions proposed in least square model in [63] can only obtain acceptable results for linear/quadratic shape TTC curve, not for non-linear/non-quadratic shape TTC curve as the 7-bus case.

- Interpolation polynomial has coupling item such as $Q_{ci}*Q_{cj}$ corresponding to the interaction of Var compensation at different locations, but least square model in [63] does not have this item.
- The Interpolation model is easier to solve than two sets of variables model. At the same time, it is much more accurate than the Least Square model proposed in [63].
- Short term planning or reactive power dispatch is computational-time sensitive and critical; thus, the Interpolation model becomes more attractive in these scenarios.

10 STATIC SYNCHRONOUS COMPENSATOR (STATCOM) MODELING FOR VAR PLANNING

The potential benefits of Flexible AC Transmission System (FACTS) equipment are now widely recognized by the power systems engineering community. Static Var Compensator (SVC) systems are employed for reactive compensation for power transmission lines. There are about 50 SVCs installed in the U.S. Subsequently, with the advent of high power gate turn-off thyristors and transistor devices (GTO, IGBT, etc.), a new generation of power electronic equipment, STATCOM, shows great promise for application in power systems [97]. A STATCOM is specially suited for supplying full compensating current at low AC system voltage and has the ability to compensate for unbalanced voltages and currents. There are several recently completed STATCOMs in the U.S., in the states of Vermont, California, and Texas [98-100]. In addition, there are newly planned STATCOMs in Connecticut [101] and Texas, as well as a small STATCOM (D-VAR) planned for BC Hydro [102] and several other locations. STATCOM planning becomes more and more important in practice in Var planning area.

10.1 A detailed STATCOM model for Var planning

In the previous study, the Var compensator is simply modeled as a special generator only providing reactive power Q_c, as shown in Figure 9.1. Then the type of the compensator can not be differentiated from others such as capacitor, synchronous

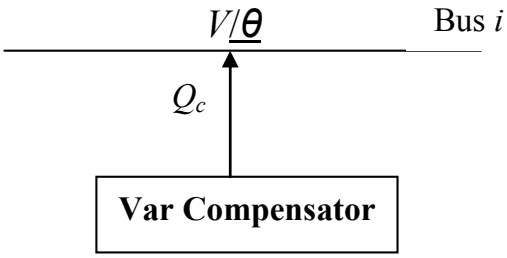

Figure 10.1. Industry used STATCOM model for Var planning study.

condenser, SVC, or STATCOM. All the compensators have a common model, and the special characteristics for different compensators have been ignored in the previous studies [80]. For example, the output of STATCOM is independent of the system voltage, unlike the SVC and capacitor, whose compensating current is dependent on the system voltage. That is a key difference between the SVC and STATCOM. This chapter demonstrates how the STATCOM can be modeled to emphasize its special characteristics.

Variables such as V, θ, and Q_c are already in the industry used STATCOM model. The new variables in the detailed STATCOM model are I_c and V_c. A detailed STATCOM model consists of a voltage source converter (VSC) and a coupling transformer represented by reactance X, as shown in Figure 9.2. This model assumes that the losses in the inverter and the coupling transformer are negligible. Based on the principle of operation, the inverter is then gated such that the output voltage $\vec{V}_c$ is in phase with the system bus voltage $\vec{V}$, which means they have the same phase angle θ. Therefore the output current I_c is a purely reactive current, which is perpendicular to the output voltage. The magnitude of the converter voltage V_c, and thus the reactive output of the converter Q_c, is controllable. The relationship between V_c, V and Q_c is shown in the following

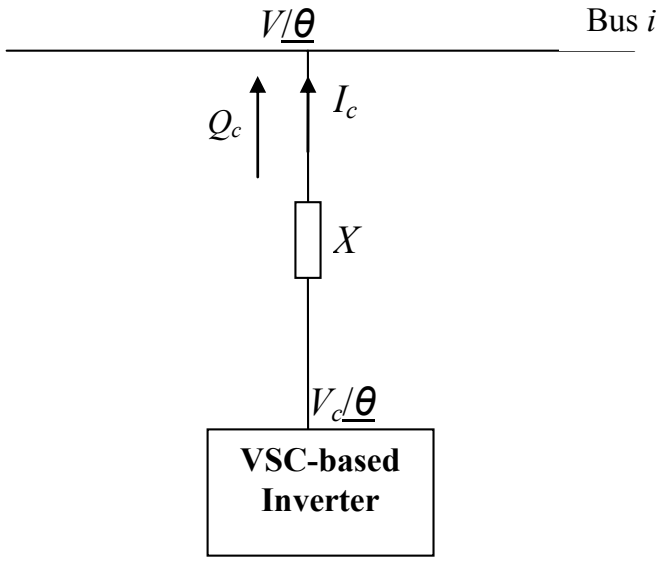

Figure 10.2. Detailed STATCOM model for Var planning study.

equation:

$$Q_c = \frac{V(V_c - V)}{X} \tag{9.1}$$

Equation (9.1) reflects the principle of operation: the STATCOM will absorb reactive power from the AC system if V is greater than the magnitude of the converter voltage V_c,; and it will supply reactive power to the system if V is smaller than V_c. In other words, the reactive power compensation Q_c depends on the voltage magnitude difference $V_c - V$.

Besides the principle of operation, STATCOM has another important characteristic, the steady state V-I characteristic, as shown in Figure 9.3. The steady state V-I characteristic of a STATCOM may be expressed as $V_c = V_{ref} \pm X \bullet I_c$. The current limits in the electronic switches represent the basic control limits on an actual STATCOM in steady state, which is the main limiting factor in VSC-based controllers. Therefore, $I_c^{min} \leq$

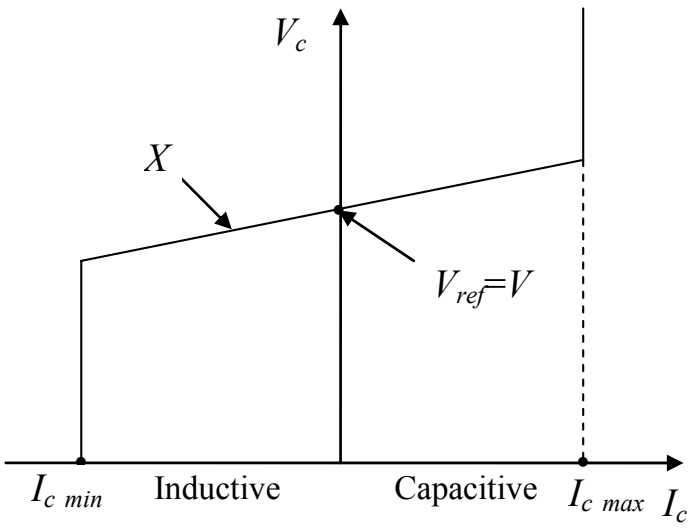

Figure 10.3. Steady state V-I characteristic of a STATCOM.

$I_c \le I_c^{max}$ becomes the main binding limit in the detailed STATCOM model instead of $Q_c^{min} \le Q_c \le Q_c^{max}$ in the industry used STATCOM model.

A complete voltage stability constrained STATCOM planning optimal power flow model is as follows:

$$Min: \sum f_1(P_{Goi}) + \sum f_2(Q_{ci}) \times y_i$$

Subject to:

$$\sum y_i = k \qquad (\textit{Number of Var compensator installations})$$

$$P_{Goi} - P_{Loi} - P(V_o, \theta_o) = 0 \qquad (\textit{Real power balance})$$

$$Q_{Goi} + Q_{ci} - Q_{Loi} - Q(V_o, \theta_o) = 0 \qquad (\textit{Reactive power balance})$$

$$P_{Gi}^{\min} \le P_{Goi} \le P_{Gi}^{\max} \qquad (\textit{Generation real power limits})$$

$$Q_{Gi}^{\min} \le Q_{Goi} \le Q_{Gi}^{\max} \qquad (\textit{Generation reactive power limits})$$

$$V_i^{\min} \le V_{oi} \le V_i^{\max} \qquad (\textit{Voltage limits})$$

$$\left|LF_{lo}\right| \le LF^{\max} \qquad (\textit{Line flow thermal limits})$$

$$SM = \frac{\sum_{l \in Lt} S_{l*} - \sum_{l \in Lt} S_{lo}}{\sum_{l \in Lt} S_{l*}} \qquad (\textit{Tie line MVA transfer capability security margin})$$

$$SM \ge SM_{spec} \qquad (\textit{Security margin limits})$$

$$TTC = \sum_{l \in Lt} S_{l*} \qquad (\textit{Tie line total transfer capability definition})$$

$$TTC = f(Q_{ci}) \qquad (\textit{TTC is not a constant, but a function of Var } Q_{ci})$$

$$Q_{ci} = \frac{V_{oi}(V_{ci} - V_{oi})}{X} \qquad (\textit{STATCOM principle of operation})$$

$$I_{ci} = \frac{(V_{ci} - V_{oi})}{X} \qquad (\textit{STATCOM V-I characteristic})$$

$$I_{ci}^{min} \le I_{ci} \le I_{ci}^{max} \qquad (\textit{STATCOM voltage source converter current limits})$$

The last three equations of the above model may be summarized as one equation: $I_{ci}^{\min} V_{oi} \le Q_{ci} = V_{oi} I_{ci} \le I_{ci}^{\max} V_{oi}$. Usually, Q_c^{max} is derived from $I_c^{max} V_{rated}$ in industry, and V_{rated} is 1 p.u.. Thus, whether the rated voltage such as 1 p.u. or the actual voltage is used to calculate the upper and lower Var compensation limit is the main difference between the detailed STATCOM model and the industry used model.

10.2 Case study

For consistency with the previous chapter, it is still assumed Q_c^{max} is 50MVar, Q_c^{min} is -50MVar, V_{rated} is 1 p.u. (138kV), and X is 0.03 p.u., therefore $I_c^{max} = Q_c^{max} / V_{rated} = 0.5$ p.u. (362.32 A). Then, $I_c^{max} = 0.5$ p.u. is adopted in the detailed STATCOM model. The results from the STATCOM model employed in the industry and the exact STATCOM model proposed here are compared in Table 9.1. They have almost the same results (Point A) in this case, as is illustrated in Figure 9.4 Scenario I, but it is not always so. For example, if the Q_c^{max} is encountered before the objective function reaches its minimum point, as shown in Figure 9.5 Scenario II, then the two results may be different. The result with industrial STATCOM model is point B, and the result with detailed STATCOM model is point C.

Table 10.1. Var planning results comparison of industry used STATCOM model and detailed STATCOM model.

	Var planning using industry used STATCOM model	Var planning using detailed STATCOM model
Objective function (total cost) ($/hr)	15195.34	15195.34
Optimal STATCOM location	Bus 3	Bus 3
Optimal STATCOM size (MVar)	15.03	15.03

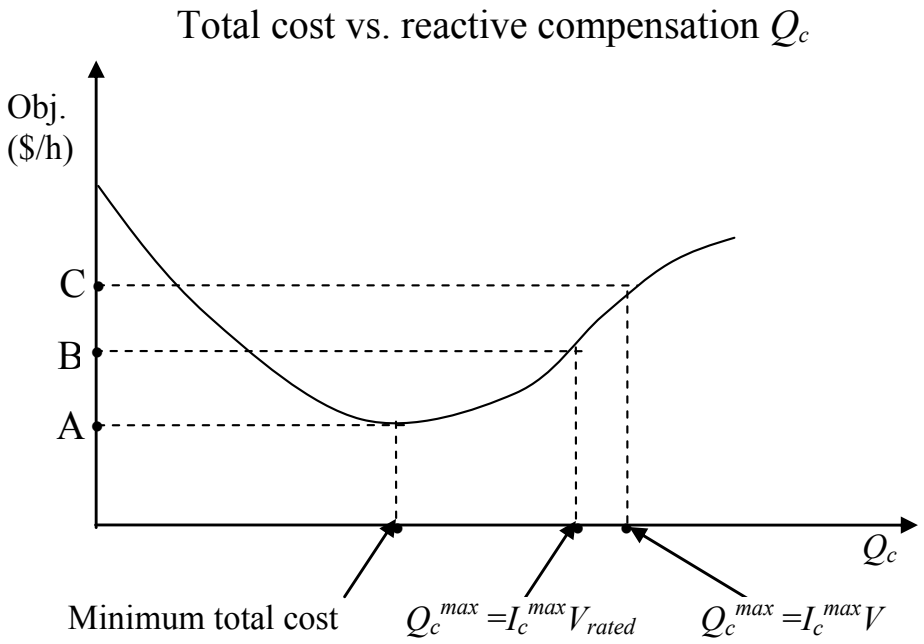

Figure 10.4. Total objective cost vs. reactive compensation Qc in Scenario I.

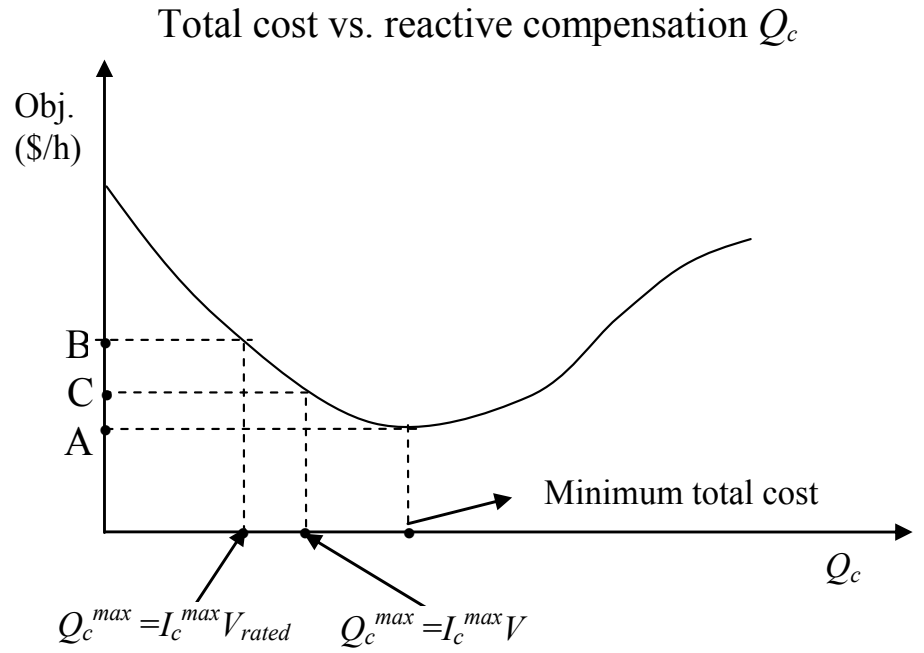

Figure 10.5. Total objective cost vs. reactive compensation Qc in Scenario II.

10.3 Conclusion

A detailed STATCOM model for Var planning is demonstrated in this chapter. Including the variables V, θ, and Q_c in the industrial STATCOM model, the additional new variables in the detailed STATCOM model are voltage source converter current output I_c and voltage output V_c. The additional constraints that connect all these variables are concluded as follows:

- The reactive power flow Q_c between the voltage source converter (VSC) of STATCOM and the AC bus depends on the voltage magnitude difference between voltage source converter and AC bus $V_c - V$: $Q_c = \frac{V(V_c - V)}{X}$.
- Steady state V-I characteristic of a STATCOM: $V_c = V \pm X \bullet I_c$.
- The current limits (I_c^{min}, I_c^{max}) in the voltage source converter (VSC) represent the basic control limits on an actual STATCOM in steady state, which is the main limiting factor in VSC-based controllers: $I_c^{min} \le I_c \le I_c^{max}$

11 CONTRIBUTIONS AND RECOMMENDATIONS

11.1 Contributions

This dissertation has contributed to the existing body of knowledge as follows:

- Demonstrate a possible quantitative approach to assess the "hidden" benefits from Var sources at the demand side including reduced losses, shifting reactive power flow to real power flow, and increased transfer capability.
- Investigate the sensitivity analysis of the economic benefits with respect to the size of the Var compensator and the generator marginal cost.
- The enumeration method based on Var economic benefits is proposed to incorporate voltage stability margin in the reactive power planning. Although this approach may be time-consuming, it does give a full spectrum and insightful information about the benefits under different categories if a Var compensator is installed at a specific location and a specific amount.
- The voltage stability constrained OPF (VSCOPF) with two sets of variables (TSV) model for Var planning can combine 3 models and $1+2mn$ OPF runs in the enumeration method. A new objective function is proposed for the VSCOPF with TSV model in order to maximize the net benefit (equivalent to minimizing the sum of fuel cost and Var cost). The results show that the new objective function may lead to significant difference in the optimal Var location and size.
- In order to circumvent the two sets of variables in the VSCOPF with TSV model,

interpolation method is proposed to approximately estimate the total transfer capability (TTC) path; this would imply a substantial simplification of the TSV model in cases where the TSV model fails to provide any solution due to non-convergence, or it is prone to yield grossly sub-optimal solutions because of its size and complexity.

- A detailed STATCOM model is proposed, which is based on the current limits (the basic control limits on an actual STATCOM in steady state) multiplying real system voltage instead of current limits multiplying rated voltage.

11.2 Recommendations for future work

Future work: Incorporate transient constraints in the present Var planning model. The transient constraints include recovery voltage more than a specified percentage of its initial value; transient voltage more than another specified percentage of its initial value; and oscillations remaining for less than some number of cycles. STATCOM is known for its superior performance in preventing transient voltage stability. Var planning based on steady-state model may not be sufficient to identify the technical benefit of STATCOM. Hence, consideration of the transient constraints may better discover the capability of STATCOM in Var planning.

11.3 Publications

Parts of this dissertation have been published as follows:

- **Wenjuan Zhang**, Fangxing Li, L. M. Tolbert, “A Literature Review of Reactive

Power Planning: Objectives, Constraints and Algorithms," Accepted by *IEEE Transactions on Power Systems* (Journal).

- Fangxing Li, **Wenjuan Zhang**, L. M. Tolbert, J. D. Kueck, D. Tom Rizy, "A Framework to Quantify the Economic Benefit from Local VAR Compensation," Submitted to *Electric Power Systems Research* (*EPSR*) (Journal).
- **Wenjuan Zhang**, Fangxing Li, L. M. Tolbert, "Voltage stability constrained optimal power flow (VSCOPF) for Var planning: Model simplification using interpolation," in preparation for *IEEE Transactions on Power Systems* (Journal).
- **Wenjuan Zhang**, Fangxing Li, L. M. Tolbert, "Voltage Stability Constrained Optimal Power Flow (VSCOPF) with Two Sets of Variables (TSV) for Var Planning," in preparation for *2008 IEEE PES Transmission and Distribution Conference and Exposition,* April 21-24, 2008 in Chicago, Illinois .
- **Wenjuan Zhang**, Fangxing Li, L. M. Tolbert, "Var Compensation Economic Benefits Sensitivity to Generator Marginal Cost," Submitted to *The Third International Conference on Electric Utility Deregulation and Restructuring and Power Technologies (DRPT 2008),* April 6-9, 2008, Nanjing, China.
- **Wenjuan Zhang**, Fangxing Li, L. M. Tolbert, "Analysis of Var Benefits with Application to Var Planning," Accepted by *International Power Engineering Conference (IPEC 2007),* Dec. 03-06, 2007, Singapore.
- **Wenjuan Zhang**, Fangxing Li, L. M. Tolbert, "Optimal Allocation of Shunt Dynamic Var Source SVC and STATCOM: A Survey," *7th IEE International*

Conference on Advances in Power System Control, Operation and Management (APSCOM 2006), Oct. 30 – Nov. 02, 2006, Hong Kong, China.

- Fangxing Li, **Wenjuan Zhang**, L. M. Tolbert, J. D. Kueck, D. Tom Rizy, "Assessment of the Economic Benefits from Reactive Power Compensation," *IEEE Power Engineering Society – 2006 Power System Conference & Exposition (PSCE 2006)*, Oct. 29 – Nov. 01, 2006, Atlanta, GA, pp. 1767-1773.

- Fangxing Li, Rui Bo, **Wenjuan Zhang**, "Comparison of Different LMP Calculations in Power Market Simulation," *2006 International Conference on Power System Technology (PowerCon 2006)*, October 22-26, 2006, Chongqing, China, pp. 1-6.

- Leon M. Tolbert, **Wenjuan Zhang**, et. al., "Power Electronics for Distributed Energy Systems and Transmission and Distribution Applications: Assessing the Technical Needs for Utility Applications," ORNL/TM-2005/230, Oak Ridge National Laboratory, December 2005.

- Hairong Qi, **Wenjuan Zhang**, Leon M. Tolbert, "A Resilient Real-Time Agent - Based System for a Reconfigurable Power Grid," *13th International Conference on Intelligent Systems Application to Power Systems (ISAP 2005)*, November 6-10, 2005, Arlington, Virginia, pp. 43-48.

- **Wenjuan Zhang**, L. M. Tolbert, "Survey of reactive power planning methods," *IEEE Power Engineering Society (PES 2005) General Meeting*, June 12-16, 2005, San Francisco, California, pp. 1580-1590.

References

Chapter 1

[1] J. J. Paserba, "How FACTS benefits AC power systems," *Panel Session on FACTS Fundamentals, Proceedings of the IEEE PES 2004 General Meeting*, Denver, Colorado, June 2004.

[2] N. K. Trehan, R. Saran, "Electric utility deregulation: failure or success," *2004 IEEE Nuclear Science Symposium Conference Record*, vol. 7, 16-22 Oct. 2004, pp. 4614 – 4617.

[3] The Wall Street Journal, "Tansmission flaws boost power costs," December 20, 2001. Original source: FERC

[4] M. Chebbo, M. R. Irving, and M. J. H. Sterling, "Reactive power dispatch incorporating voltage stability," *IEE Proc.,* vol. 139, no. 3, May 1992, pp. 253-260.

[5] U.S.-Canada Power System Outage Task Force, *Final Report on the August 14th Blackout in the United States and Canada*, April 2004.

[6] Oak Ridge National Laboratory, *A Preliminary Analysis of the Economics of Using Distributed Energy as a Source of Reactive Power Supply*, ORNL/DOE Report, April 2006.

[7] C. Schauder, "STATCOM for compensation of large electric arc furnace installations," *Proceedings of the IEEE PES Summer Power Meeting*, Edmonton, Alberta, July 1999, pp. 1109-1112.

[8] D. J. Hanson, C. Horwill, B. D. Gemmell, D. R. Monkhouse, "A STATCOM-Based Relocatable SVC Project in the UK for National Grid," *Proceedings of the IEEE PES Winter Power Meeting*, New York, January 2002.

[9] C. Schauder, E. Stacey, M. Lund, L. Gyugyi, L. Kovalsky, A. Keri, A. Mehraban, A. Edris, "AEP UPFC Project: installation, commissioning and operation of the ±160 MVA STATCOM (Phase I)," *IEEE Transactions on Power Delivery*, vol. 13, no. 4, October 1998, pp. 1530-1535.

[10] B. A. Renz, A. J. F. Keri, A. S. Mehraban, J. P. Kessinger, C. D. Schauder, L. Gyugyi, L. J. Kovalsky, A. A. Edris, "World's first unified power flow controller on the AEP System," CIGRE Paper 14-107, Paris Session, 1998.

[11] B. Fardanesh, M. Henderson, B. Shperling, S. Zelingher, L. Gyugyi, C. Schauder, B. Lam, J. Mountford, R. Adapa, A. Edris, "Convertible static compensator application to the New York transmission System," CIGRE Paper 14-103, Paris Session, 1998.

[12] W. C. Merritt, C. H. Saylor, R. C. Burchett, H. H. Happ, "Security constrained optimization-a case study, " *IEEE Transactions on Power System*, vol 3, no. 3, Aug. 1988, pp. 970 – 977.

[13] W. Qiu, A. J. Flueck, F. Tu, "A new parallel algorithm for security constrained optimal power flow with a nonlinear interior point method," *IEEE Power*

Engineering Society General Meeting, June 12-16, 2005, San Francisco, California, pp. 2422 – 2428.

Chapter 2

[14] W. Zhang, L. M. Tolbert, "Survey of reactive power planning methods," *IEEE Power Engineering Society General Meeting*, June 12-16, 2005, San Francisco, California, pp. 1580-1590.

[15] D. Pudjianto, S. Ahmed, and G. Strbac, "Allocation of VAR support using LP and NLP based optimal power flows," *IEEE Proceedings on Generation, Transmission, and Distribution*, vol. 149, no. 4, 2002, pp. 377-383.

[16] K. Aoki, M. Fan, A. Nishikori, "Optimal Var planning by approximation method for recursive mixed-integer linear programming," *IEEE Trans. on PAS*, vol. 3, no. 4, Nov. 1988, pp. 1741–1747.

[17] J. R. S. Mantovani, A. V. Garcia, "A heuristic method for reactive power planning," *IEEE Tran. on PAS*, vol. 11, no. 1, Feb. 1996, pp. 68–74.

[18] M. Delfanti , G. Granelli, P. Marannino, M. Montagna, "Optimal capacitor placement using deterministic and genetic algorithms," *IEEE Trans. on Power Systems*, vol. 15, no. 3, Aug. 2000, pp. 1041-1046.

[19] C. T. Hsu, Y. H. Yan, C. S. Chen, S. L. Her, "Optimal reactive power planning for distribution systems with nonlinear loads", *IEEE Region 10 International Conference on Computer, Communication, Control and Power Engineering*, Oct. 19-21, 1993, Beijing, China, vol.5, no. 0, pp. 330 – 333.

[20] K. Y. Lee, X. Bai, Y. M. Park, "Optimization method for reactive power planning by using a modified simple genetic algorithm," *IEEE Trans. on Power Systems*, vol. 10, no. 4, Nov. 1995, pp. 1843-1850.

[21] Wen Zhang, Yutian Liu, Yuanqi Liu, "Optimal VAr planning in area power system," *International Conference on Power System Technology*, Oct. 13-17, 2002, vol.4, pp. 2072 – 2075.

[22] K. Iba, H. Suzuki, K. I. Suzuki, K. Suzuki, "Practical reactive power allocation/operation planning using successive linear programming, " *IEEE Trans. on PAS*, vol. 3, no. 2 , May 1988, pp.558–566.

[23] B. Kermanshahi, K. Takahashi, Y. Zhou, "Optimal operation and allocation of reactive power resource considering static voltage stability," *1998 International Conference on Power System Technology (POWERCON '98)*, vol. 2, Aug. 18-21, 1998, pp. 1473–1477.

[24] L. L. Lai, J. T. Ma, "Application of evolutionary programming to reactive power planning-comparison with nonlinear programming approach, " *IEEE Trans. on PAS*, vol. 12, no. 1, Feb. 1997, pp. 198–206.

[25] V. Gopalakrishnan, P. Thirunavukkarasu, R. Prasanna, "Reactive power planning

using hybrid evolutionary programming method," *Power Systems Conference & Exposition*, *2004 IEEE PES*, Oct. 10-13, 2004, New York, vol.3, pp. 1319 – 1323.

[26] J. Urdaneta, J. F. Gomez, E. Sorrentino, L. Flores, R. Diaz, "A hybrid genetic algorithm for optimal reactive power planning based upon successive linear programming," *IEEE Trans. on PAS*, vol. 14, no. 4, Nov. 1999, pp. 1292–1298.

[27] Y. T. Hsiao, C. C. Liu, H. D. Chiang, Y. L. Chen, "A new approach for optimal VAr sources planning in large scale electric power systems," *IEEE Trans. on PAS*, vol. 8 , no. 3, Aug. 1993, pp. 988–996.

[28] Al-Mohammed, A. H. H., I. Elamin, "Capacitor placement in distribution systems using artificial intelligent techniques," *2003 IEEE Power Tech Conference Proceedings*, June 23-26, 2003, Bologna, Italy, vol.4, pp. 7.

[29] R. A. Gallego, A. J. Monticelli, and R. Romero, "Optimal capacitor placement in radial distribution networks," *IEEE Trans. on Power Systems*, vol. 16, no. 4, Nov. 2001 pp. 630 – 637.

[30] F. F. Wu, G. Gross, J. F. Luini, P. M. Look, "A two-stage approach to solving large-scale optimal power flows," *Power Industry Computer Applications Conference, 1979 (PICA-79) IEEE ConferenceProceedings*, May 15-18, 1979, pp. 126–136.

[31] D. Chattopadhyay, K. Bhattacharya, J. Parikh, "Optimal reactive power planning and its spot pricing: An integrated approach," *IEEE Transactions on Power Systems*, vol. 10, no. 4, Nov. 1995, pp. 2014–2020.

[32] K. Y. Lee, F. F. Yang, "Optimal reactive power planning using evolutionary algorithms: a comparative study for evolutionary programming, evolutionary strategy, genetic algorithm, and linear programming," *IEEE Trans. on PAS*, vol. 13, no. 1, Feb. 1998, pp. 101–108.

[33] J. Z. Zhu, C. S. Chang, W. Yan, G. Y. Xu, "Reactive power optimization using an analytic hierarchical process and a nonlinear optimization neural network approach," *IEE Proceedings – Generation, Transmission, and Distribution*, vol. 145, no. 1, Jan. 1998, pp. 89 – 97.

[34] Y. L. Chen, Y. L. Ke, "Multi-objective Var planning for large-scale power systems using projection-based two-layer simulated annealing algorithms," *IEE Proceedings- Generation, Transmission and Distribution*, vol 151, no. 4, July 11, 2004, pp.555 – 560.

[35] W. S. Jwo, C. W. Liu, C. C. Liu, Y. T. Hsiao, "Hybrid expert system and simulated annealing approach to optimal reactive power planning," *IEE Proceedings on Generation, Transmission and Distribution,* vol. 142, no. 4, July, 1995, pp. 381–385.

[36] K. Iba, "Reactive power optimization by genetic algorithm," *Power Industry Computer Application Conference*, May 4-7, 1993, pp. 195–201.

[37] Alsac, and B. Stott, ″Optimal load flow with steady-state security," *IEEE Trans.*

Power App. Syst., vol. PAS-93, May/June 1974, pp. 745-751.

[38] L. G. Dias, M. E. El-Hawary, "Security-constrained OPF: influence of fixed tap transformer fed loads," *IEEE Transactions on Power System*, vol. 6, no. 4, Nov. 1991, pp. 1366-1372.

[39] W. R. Thomas, A. M. Dixon, D. T. Y. Cheng, R. M. Dunnett, G. Schaff, J. D. Thorp, "Optimal reactive planning with security constraints," *IEEE Power Industry Computer Application Conference,* 7-12 May 1995, pp. 79–84.

[40] R. C. Dageneff, W. Neugebauer and C. Saylor, "Security Constrained Optimization: An added dimension in utility systems optimal power flow technology," *IEEE Computer Applications in Power*, October 1988, pp. 26-30.

[41] T. Gomez, I. J. Perez-Arriaga, J. Lumbreras, V. M. Parra, "A security-constrained decomposition approach to optimal reactive power planning, " *IEEE Trans. on PAS*, vol. 6 , no. 3, Aug. 1991, pp. 1069–1076.

[42] B. Cova, et al., "Contingency constrained optimal reactive power flow procedures for voltage control in planning and operation", *IEEE Trans. on Power Systems*, vol. 10, no. 2, May 1995, pp. 602 – 608.

[43] S. Granville, M. V. P. Pereira, A. Monticelli, "An integrated methodology for Var sources planning," *IEEE Transactions on Power Systems*, vol. 3, no. 2, May 1988, pp. 549 – 557.

[44] Y. T. Hsiao, C. C. Liu, H. D. Chiang, Y. L. Chen, "A new approach for optimal Var sources planning in large scale electric power systems," *IEEE Trans. on PAS*, vol. 8 , no. 3, Aug. 1993, pp. 988–996.

[45] V. C. Ramesh, X. Li, "A fuzzy multiobjective approach to contingency constrained OPF," *IEEE Trans. Power Systems*, vol. 12, no.3, Aug. 1997, pp. 1348-1354.

[46] Y. T. Hsiao, H. D. Chiang, C. C. Liu, and Y. L. Chen, "A computer package for optimal multi-objective VAR planning in large scale power systems", *IEEE Trans. on Power Systems*, vol 9, no. 2, May 1994, pp. 668 – 676.

[47] C. Cañizares, "Calculating optimal system parameters to maximize the distance to saddle-node bifurcations," *IEEE Trans. on Circuits and Systems—I: Fundamental Theory and Applications*, vol. 45, no. 3, Mar. 1998, pp. 225–237.

[48] R. Ramos, J. Vallejos, B. Barán, "Multi-objective reactive power compensation with voltage security," *2004 IEEE/PES Transmission and Distribution Conference and Exposition: Latin America*, Nov. 2004, Brazil, pp. 302 – 307.

[49] V. Ajjarapu, P. L. Lau, and S. Battula, "An optimal reactive power planning strategy against voltage collapse," *IEEE Transactions on Power Systems*, vol. 9, no. 2, May 1994, pp. 906-917.

[50] H. Song, B. Lee, S. H. Kwon, V. Ajjarapu, "Reactive reserve-based contingency constrained optimal power flow (RCCOPF) for enhancement of voltage stability

margins," *IEEE Transactions on Power Systems*, vol. 18 , no. 4, Nov. 2003, pp. 1538 – 1546.

[51] C. A. Cañizares, "Applications of optimization to voltage collapse analysis," Panel Session: Optimization Techniques in Voltage Collapse Analysis, *IEEE-PES Summer Meeting*, San Diego, California, July 1998.

[52] V. Ajjarapu, P. L. Lau, and S. Battula, "An optimal reactive power planning strategy against voltage collapse," *IEEE Transactions on Power Systems*, vol. 9, no. 2, May 1994, pp. 906-917.

[53] Y. L. Chen, "Weak bus oriented reactive power planning for system security," *IEE Proceedings on Generation, Transmission and Distribution*, vol 143, no. 6, Nov. 1996, pp. 541 – 545.

[54] T. Van Cutsem, "A method to compute reactive power margins with respect to voltage collapse," *IEEE Transactions on Power Systems*, vol. 6, no. 1, Feb. 1991, pp. 145-156.

[55] Y. L. Chen., C. C. Liu, "Multiobjective Var planning using the goal attainment method," *IEE Proceedings on Generation, Transmission and Distribution*, vol. 141, no. 3, May 1994, pp. 227-232.

[56] Y. L. Chen, "Weighted-norm approach for multiobjective Var planning," *IEE Proceedings on Generation, Transmission and Distribution*, vol 145, no. 4, July 1998, pp.369 – 374.

[57] Y. L. Chen., C. C. Liu, "Interactive fuzzy satisfying method for optimal multi-objective Var planning in power systems," *IEE Proceedings on Generation, Transmission and Distribution*, vol 141, no. 6, Nov. 1994, pp. 554 – 560.

[58] Y. L. Chen., C. C. Liu, "Optimal multi-objective Var planning using an interactive satisfying method," *IEEE Transactions on Power Systems*, vol 10, no. 2, May 1995, pp. 664 – 670.

[59] R. Ramos, J. Vallejos, B. Barán, "Multi-objective reactive power compensation with voltage security," *2004 IEEE/PES Transmission and Distribution Conference and Exposition*: Latin America, Nov. 8-11, 2004, Brazil, pp. 302 – 307.

[60] Obadina, G. J. Berg, "Var planning for power system security," *IEEE Transactions on Power Systems*, vol 4, no. 2, May 1989, pp.677 – 686.

[61] B. B. Chakrabarti, D. Chattopadhyay, C. Krumble, "Voltage stability constrained Var planning-a case study for New Zealand," *2001. LESCOPE '01. 2001 Large Engineering Systems Conference on Power Engineering*, July 11-13, 2001, pp.86 – 91.

[62] D. Chattopadhyay, B. B. Chakrabarti, "Reactive power planning incorporating voltage stability," Int. Journal of Electrical Power and Energy Systems, vol. 24, no. 3, 2002, pp.185-200

[63] D. Chattopadhyay, B. B. Chakrabarti, "Voltage stability constrained Var planning: model simplification using statistical approximation," Int. Journal of Electrical Power and Energy Systems, vol 23, no. 5, 2001, pp.349-358.

[64] E. Vaahedi, J. Tamby, Y. Mansour, W. Li, D. Sun, "Large scale voltage stability constrained optimal Var planning and voltage stability applications using existing OPF/optimal Var planning tools," *IEEE Transactions on Power Systems*, vol. 14, no. 1, Feb. 1999, pp.65 – 74.

Chapter 3

[65] C. A. Cañizares and S. Hranilovic, "Transcritical and Hopf bifurcations in ac/dc systems," *Proc. Bulk Power System Voltage Phenomena III—Voltage Stability and Security,* Fairfax, VA, Aug. 1994, pp. 105–114.

[66] Y. Mansour, W. Xu, F. Alvarado, and C. Rinzin, "SVC placement using critical modes of voltage instability," *IEEE Trans. on Power Systems*, vol. 9, no. 2, May 1994, pp. 757–763.

[67] L. A. S. Pilotto, W. W. Ping, A. R. Carvalho, A. Wey, W. F. Long, C. L. DeMarco, F. L. Alvarado, A. Edris, "Determination of needed FACTS controllers that increase asset utilization of power systems," *IEEE Transactions on Power Delivery*, vol. 12, no. 1, Jan. 1997, pp. 363-371.

[68] M. A. Perez, A. R. Messina, C. R. Fuerte-Esquivel, "Application of FACTS devices to improve steady state voltage stability," *2000 IEEE Power Engineering Society Summer Meeting*, vol. 2, July 2000, pp. 1115 - 1120.

[69] M. K. Verma, S. C. Srivastava, "Optimal placement of SVC for static and dynamic voltage security enhancement," *International Journal of Emerging Electric Power Systems*, vol. 2, no. 2, 2005, Article 1050.

[70] P. Preedavichit and S. C. Srivastava, "Optimal reactive power dispatch considering FACTS devices**,**" *Proceedings of the 4th International Conference on Advances in Power System Control, Operation and Management, APSCOM-97,* Hong Kong, Nov. 1997, pp. 620-625.

[71] P. Bhasaputra, W. Ongsakul, "Optimal power flow with multi-type of FACTS devices by hybrid TS/SA approach," *2002 IEEE International Conference on Industrial Technology*, vol. 1, Dec. 2002, pp. 285 – 290.

[72] C. S. Chang, J. S. Huang, "Optimal SVC placement for voltage stability reinforcement," *Electric Power Systems Research*, vol. 42, no. 3, Sep. 1997, pp. 165-172.

[73] C. S. Chang and J. S. Huang, "Optimal multiobjective SVC planning for voltage stability enhancement," *IEE Proceedings- Generation, Transmission and Distribution*, vol. 145, no. 2, Mar. 1998, pp. 203 – 209.

[74] H. Mori, H. Tani, "Two-staged tabu search for determining optimal allocation of

D-FACTS in radial distribution systems with distributed generation," *2002: Asia Pacific IEEE/PES Transmission and Distribution Conference and Exhibition*, vol. 1, Oct. 2002, pp. 56 – 61.

[75] L. J. Cai, I. Erlich, G. Stamtsis, "Optimal choice and allocation of FACTS devices in deregulated electricity market using genetic algorithms," *2004 IEEE/PES Power Systems Conference and Exposition*, vol. 1, Oct. 2004, pp. 201 - 207.

[76] K. Habur, and D. Oleary, "FACTS – flexible AC transmission systems, for cost effective and reliable transmission of electrical energy," http://www.siemenstd.com/TransSys/pdf/CostEffectiveReliabTrans.pdf.

[77] L. J. Cai, I. Erlich, "Optimal choice and allocation of FACTS devices using genetic algorithms," *ISAP, Intelligent Systems Application to Power Systems, 2003, Lemnos, Greece*, Aug. 31 –Sep. 3, 2003.

[78] R. Palma-Behnke, L. S. Vargas, J. R. Pérez, J. D. Núñez, R. A. Torres, "OPF with SVC and UPFC modeling for longitudinal systems," *IEEE. Trans. Power Systems*, vol. 19, no. 4, Nov. 2004, pp. 1742–1753.

[79] E. E. El-Araby, N. Yorino, H. Sasaki, "A comprehensive approach for FACTS devices optimal allocation to mitigate voltage collapse," *Proc. of IEEE/PES Transmission and Distribution Conference*, vol. 1, Oct. 2002, pp. 62 – 67.

[80] R. Adapa, K. Madajewski, M. Sobierajski, "The study of voltage problems in Polish power system," *2000 IEEE Power Engineering Society Winter Meeting*, vol. 3, pp. 1727–1732.

[81] R. Natesan, G. Radman, "Effects of STATCOM, SSSC and UPFC on voltage stability," *2004 Proceedings of the Thirty-Sixth Southeastern Symposium on System Theory*, 2004, pp. 546 – 550.

[82] H. Yonezawa, T. Shimato, M. Tsukada, K. Matsuno, I. Iyoda, J. J. Paserba, G. F. Reed, "Study of a STATCOM application for voltage stability evaluated by dynamic PV curves and time simulation," *2000 IEEE Power Engineering Society Winter Meeting*, vol. 2, Jan. 2000, pp. 1471 – 1476.

[83] H. G. Sarmiento, G. Pampin, J. D. de Leon, "FACTS solutions for voltage stability problems in a large metropolitan area," *2004 IEEE/PES Power Systems Conference and Exposition*, vol. 1, Oct. 2004, pp. 275 - 282.

[84] G. K. Morison, B. Gao, P. Kundur, "Voltage stability analysis using static and dynamic approaches," *IEEE Transactions on Power Systems*, vol. 8, no. 3, Aug. 1993, pp. 1159 – 1171.

Chapter 4

[85] Z. Huang, Course Documents, http://www.ee.ualberta.ca/~zhuang/.

[86] A.J. Wood and B.F. Wollenberg, *Power Generation Operation and Control*, John Wiley & Sons Inc, 1996

[87] Powerworld Website, http://www.powerworld.com.

Chapter 7

[88] C. Canizares, W. Rosehart, A. Berizzi, C. Bovo, "Comparison of voltage security constrained optimal power flow techniques," *2001 IEEE Power Engineering Society Summer Meeting*, vol. 3, July 15-19, 2001, pp. 1680-1685.

[89] GAMS solver manual

[90] D. P. Bertsekas, *Nonlinear Programming*, Athena Scientific, 2003

Chapter 8

[91] http://en.wikipedia.org/wiki/Taylor%27s_theorem

[92] Gisela Engeln-Mullges and Frank Uhlig, *Numerical Algorithms with C*, Springer Inc., 1996.

[93] Eugene Isaacson and Herbert Bishop Keller, *Analysis of Numerical Methods*, John Wiley & Sons Inc., 1966.

[94] George M. Phillips, *Interpolation and Approximation by Polynomials*, Springer Inc., 2003.

[95] Myron B. Allen and Eli L. Isaacson, *Numerical Analysis for Applied Science*, John Wiley & Sons Inc., 1998.

[96] S. D. Conte and Carl de Boor, *Elementary Numerical Analysis*: *an Algorithmic Approach*, McGraw-Hill, 1972

Chapter 9

[97] M. Noroozian, A. N. Petersson, B. Thorvaldson, B. A. Nilsson, C. W. Taylor, "Benefits of SVC and STATCOM for electric utility application" *2003 IEEE PES Transmission and Distribution Conference and Exposition*, Sep.7-12, 2003, vol 3, pp. 1192 – 1199.

[98] G. Reed, J. Paserba, T. Croasdaile, M. Takeda, Y. Hamasaki, T. Aritsuka, N. Morishima, S. Jochi, I. Iyoda, M. Nambu, N. Toki, L. Thomas, G. Smith, D. LaForest, W. Allard, D. Haas, "The VELCO STATCOM-Based Transmission System Project," Proceedings of the 2001 IEEE PES Winter Power Meeting, Columbus, OH, January/February 2001.

[99] G. Reed, J. Paserba, T. Croasdaile, M. Takeda, N. Morishima, Y. Hamasaki, L. Thomas, W. Allard, "STATCOM Application at VELCO Essex Substation," Panel Session on FACTS Applications to Improve Power System Dynamic Performance, Proceedings of the IEEE PES T&D Conference and Exposition, Atlanta, Georgia, October/November 2001.

[100] G. Reed, J. Paserba, T. Croasdaile, R. Westover, S. Jochi, N. Morishima, M. Takeda, T. Sugiyama, Y. Hamazaki, T. Snow, A. Abed, "SDG&E Talega STATCOM Project - System Analysis, Design, and Configuration," Panel Session on FACTS Technologies: Experiences of the Past Decade and Developments for the 21st Century in Asia and the World, Proceedings of the IEEE PES T&D-Asia Conference and Exposition, Yokahama, Japan, October 2002.

[101] A. Scarfone, B. Oberlin, J. Di Luca Jr., D. Hanson, C. Horwill, M. Allen, "Dynamic Performance Studies for a ±150 Mvar STATCOM for Northeast Utilities," Panel Session on FACTS Applications to Improve Power System Dynamic Performance, Proceedings of the IEEE PES T&D Conference and Exposition, Dallas, Texas, September 2003.

[102] N. Reddy, H. Iosfin, "BC Hydro Experience Using a Small STATCOM to Address Utility Voltage Problems," Panel Session on FACTS Applications to Improve Power System Dynamic Performance, Proceedings of the IEEE PES T&D Conference and Exposition, Dallas, Texas, September 2003.

Vita

Wenjuan Zhang received her B.E. in electrical engineering from Hebei University of Technology, China, in 1999 and an M.S. in electrical engineering from Huazhong University of Science and Technology, Wuhan, China, in 2003. She worked at the Beijing Coherence Prudence Development Company for one year on power distribution related projects.

Wenjuan Zhang started her Ph.D. program at the Department of Electrical and Computer Engineering, The University of Tennessee in August 2003. At the same time, she joined the Power Electronics Laboratory at The University of Tennessee as a graduate research assistant, working on reactive power planning including STATCOM planning issues. She has worked at Oak Ridge National Laboratory since 2005 by joining a reactive power project in the Reactive Power Laboratory. She graduated with a Doctor of Philosophy degree in Electrical Engineering from The University of Tennessee in September 2007.

Wenjuan Zhang is a member of IEEE. She has received academic scholarship awards for her B.E. program from Hebei University of Technology in China, and for her M.S. from Huazhong University of Science and Technology in China.